

Hot spot formation in trickle bed reactors

Hot spot formation in trickle bed reactors

PROEFSCHRIFT

ter verkrijging van de graad van doctor
aan de Technische Universiteit Delft,
op gezag van de Rector Magnificus Prof. ir. K.C.A.M. Luyben,
voorzitter van het College voor Promoties,
in het openbaar te verdedigen
op dinsdag 22 oktober 2013 om 15:00 uur
door

Farzad MOUSAZADEH

Master of Science in Chemical Engineering
Amirkabir University of Technology (Tehran Polytechnic)

geboren te Ardebil, Iran

Dit proefschrift is goedgekeurd door de promotoren:

Prof. dr. R. F. Mudde

Prof. dr. ir. H. E. A. van den Akker

Samenstelling promotiecommissie:

Rector Magnificus,

Prof. dr. R. F. Mudde,

Prof. dr. ir. H. E. A. van den Akker,

Prof. dr. ir. J. Derksen,

Prof. dr. ir. S. Sundaresan,

Dr. B.I.M. ten. Bosch,

Prof. dr. D. J. E. M. Roekaerts,

Prof. dr. ir. M. T. Kreutzer,

voorzitter

Technische Universiteit Delft, promotor

Technische Universiteit Delft, promotor

University of Aberdeen

Princeton University

Shell Global Solutions B.V

Technische Universiteit Delft

Technische Universiteit Delft

© 2013, Farzad Mousazadeh

All rights reserved. No part of this book may be reproduced, stored in a retrieval system, or transmitted, in any form or by any means, without prior permission from the copyright owner.

ISBN 978-94-6186-216-7

Keywords: Trickle bed reactor, Hot spot formation, CFD simulation

The research described in this thesis was performed in Transport Phenomena Group, Department of Chemical Engineering, Delft University of Technology, Delft, the Netherlands.

Printed in the Netherlands

*In the memory of my grandmother
To my father and mother
To Nasim*

Contents

Summary	ix
Samenvatting	xv
1 Introduction	1
1.1 Trickle bed reactors	1
1.2 Hot spot formation	2
1.3 Modeling approaches	7
1.4 Thesis outline	8
1.5 Acknowledgement	9
1.6 Bibliography	10
2 Multi-phase flow concepts	13
2.1 Introduction	13
2.2 Types of multi-phase flows	14
2.3 Modeling concepts of multi-phase flows	15
2.4 Modeling dispersed multi-phase flows	17
2.5 Flow in porous media	22
2.6 Summary	23
2.7 Bibliography	26
3 The Ansys Fluent model	31
3.1 Introduction	31
3.2 Transport equations in Ansys Fluent	32
3.3 Volume fraction equation	34
3.4 Interphase momentum exchange coefficients	34
3.5 Heat transfer	35
3.6 Mass transfer	35

3.7	Bibliography	39
4	CFD-based analysis of fluid flow in a 2-D packed bed reactor with random particle distribution	41
4.1	Introduction	42
4.2	Geometry and meshing	42
4.3	Model description (CFD approach)	44
4.4	Pressure drop	45
4.5	Results and discussion	46
4.6	Grid independency	52
4.7	CONCLUSIONS	53
4.8	Bibliography	56
5	Direct numerical simulation of an exothermic gas-phase reaction in a packed bed with random particle distribution	59
5.1	Introduction	60
5.2	Geometry and meshing	61
5.3	Model description	62
5.4	Results and discussion	66
5.5	CONCLUSIONS	74
5.6	Bibliography	77
6	Eulerian simulation of heat transfer in a trickle bed reactor with constant wall temperature	79
6.1	Introduction	80
6.2	Modeling	81
6.3	Experimental set-up	90
6.4	Results and discussion	90
6.5	CONCLUSIONS	99
6.6	Bibliography	102
7	Normal operation and hot spots formation in a trickle bed reactor	107
7.1	Introduction	108
7.2	Geometry and setup	109
7.3	Model description	111
7.4	Results and discussion	118
7.5	CONCLUSIONS	129
7.6	Bibliography	134

8	Normal operation and evaporation in a trickle bed	137
8.1	Introduction	138
8.2	Geometry and setup	139
8.3	Model description	140
8.4	Results and discussion	147
8.5	CONCLUSIONS	152
8.6	Bibliography	156
9	Conclusion	159
9.1	Review of the work	159
9.2	Recommendations for future work	164
	List of Publications	167
	Acknowledgement	169
	Curriculum Vitae	171

Summary

Trickle bed reactors (TBRs) are multi-phase flow reactors consisting of a packed bed of catalyst with co-current or counter-current flow of gas and liquid. They are used for hydro-treating, hydro-desulfurization, hydrogenation and oxidation applications in refining or chemical industry. In trickle bed reactors, reactions take place at the surface of the catalyst. The presence of the particles causes a plug flow of the gas and liquid inside trickle beds. This makes them preferred over other three-phase reactors in which the catalyst is not stationary. However, the disadvantages of trickle bed reactors are their impracticality for reactions with fast deactivating catalysts (such as in heavy oil hydro-treating processes) and the possibility of liquid mal-distribution, which may cause hot spots and reactor runaways. When these hot spots exceed some critical value it may cause an increase in the rate of reactions (desired or undesired). These hot spots may deactivate the catalyst. In addition, these hot zones may lead to severe safety problems specially when they exist near the wall of the reactor.

We have two different reactors in this research and both of them are 2-D. The first one is a two-phase (gas and solid) packed bed reactor with the length of 240 mm and width of 38 mm . The diameter of particles is 2.9 mm . We have a gas-phase reaction in the system. The second one is a three-phase (gas, liquid and solid) trickle bed reactor with the length of 160 cm and width of 30 cm . The diameter of particles in this reactor is 2.9 mm . There is a mass transfer from gas to the liquid phase and the reaction occurs in the liquid phase.

There are three possible mechanisms which can cause hot spots in trickle beds: local mal-distribution in the reactor, evaporation or evaporation-condensation process in the reactor and reaction mechanisms and effects of temperature on that. We investigated the first and second mechanism of hot spots formation using Computational Fluid Dynamics (CFD). We performed CFD simulations to investigate radial convection, effects of mal-distribution and evaporation on the performance of trickle beds for this purpose.

There are two different numerical approaches to describe transport properties and hydrodynamics of trickle beds. In the first method, three-phase trickle beds are treated as a pseudo-homogeneous media. The Navier-Stokes equations are applied in conjunction with the closure relations to account for the fluid-solid and fluid-fluid interaction. This approach is called Eulerian-Eulerian. In the second approach, two-phase packed beds are simulated based on the consideration of the real geometry. In this method, the Navier-Stokes equations are applied to the void between the particles. This yields a detailed description of the fluid flow and other transport properties between the particles. This approach is called Direct Numerical Simulation (DNS). In this research we used both the Eulerian-Eulerian and DNS approaches. The Eulerian-Eulerian approach was used for two-phase and three-phase flow (gas-solid and gas-liquid-solid) simulations and DNS approach for two-phase flow (gas and stationary solids) simulations.

The objective of this research is to develop a three-phase trickle bed model (as fundamental as possible) to handle thermodynamics, heat and mass transfer and reaction engineering in trickle beds using Computational Fluid Dynamics (CFD). The final goal of the project is to investigate hot spots formation in trickle bed reactors in the presence of mal-distribution and investigate the effects of evaporation on the thermal performance of a trickle bed reactor.

Fluid flow and its effect on the radial heat transfer (or radial convection) is very important in the investigation of hot spots formation in trickle bed reactors. So, as the first step, we performed simulations to better understand the radial heat transfer and fluid flow in packed beds.

We performed Direct Numerical Simulation (DNS) of fluid flow in 2-D packed bed reactors with two different configurations of particles. We investigated the effects of particle distribution on the flow field and radial convection. In addition, effects of walls on the pressure drop were investigated. The velocity distribution is a function of the voidage and arrangement of particles. In the area with small porosity the velocity can be smaller than the inlet velocity and in the area with high porosity the velocity can be 2-10 times larger than the inlet velocity. Channeling was observed in both linear and more random distribution of particles in packed beds. Channeling mostly happens when the particles are distributed in a line along the reactor. The maximum length of the channels in (almost) linear and more random configuration of particles are about 70-80% and 20-30% of the length of the reactor, respectively. Random distribution of particles reduces the length of the channels in the reactor, considerably. On the other hand, it increases radial convection. Walls have a significant effect on the pressure drop and should be taken into account in the design of packed beds. For our cases, if the walls are taken into account in the

calculation of the pressure drop, the calculated pressure drop is 20-25% more than the case without considering wall effects.

We also performed Direct Numerical Simulation of an exothermic gas-phase reaction in a 2-D packed bed with real geometry. We investigated the effects of the velocity field on the heat transfer in the radial direction. In the modeled packed bed reactor in a small region in the reactor the temperature difference between the walls and the bulk of the reactor is about 100 K. This large temperature difference in a small length (the width of the reactor is about 38 mm) shows that convection in the radial direction is small in the modeled reactor. If the particles are arranged randomly, the radial convection is much more than in the linear arrangement of particles.

The most important part of the Direct Numerical Simulations are the mesh generation and computation time. The real geometry of a packed bed is very complicated. So, the generation of the mesh is also very complicated and time consuming. In the reactor modeled with this method, making connection between the structured mesh around each particle and unstructured mesh of the bulk of the packed bed is very important. The size of the two different type of meshing in one geometry (structured and unstructured part) should be optimized to make it easy to get to a converged solution, otherwise it is impossible to get a converged solution and the results are not accurate. In addition, the time scale of the reaction is much smaller than that of the flow. Since the flow time scale is relatively large many small time steps are required to reach to the final steady-state solution. It makes the above simulations computationally very expensive.

We also used the Eulerian-Eulerian approach to investigate radial heat transfer in three phase trickle beds. For the investigation of radial heat transfer in trickle beds, we calculated the effective radial bed conductivity in a trickle bed reactor with constant wall temperature. The concept of the effective radial bed conductivity is based on the assumption that on a macroscale, the bed can be described as a continuum. The effective radial bed conductivity increases if we increase the mass flux of gas or liquid but the effect of liquid mass flux is much more significant than the gas mass flux because of the higher conductivity of the liquid in comparison with the gas. In the Eulerian-Eulerian approach average mass, flow and energy equation are solved. There is not a high radial convection in the packed beds modeled with this method because of the plug flow regime in the reactor. To account for the convective heat transfer in the radial direction we considered the effective conductivity of the flowing fluids (both gas and liquid) as a linear function of the Reynolds and Prandtl number according to the equation $k_{fluid} = k_f + 0.10k_f Re_p Pr_f$. In the trickle flow regime the effective radial conductivity is 2-5 times higher than for the dry gas flow.

To reach our final goal, a trickle bed reactor with mass transfer, exothermic reaction, heat transfer between the phases, etc under normal flow condition was modeled. Then we added a local mal-distribution to the system to investigate the effect of mal-distribution on the performance of a trickle bed reactor. For this purpose we used the Eulerian-Eulerian multi-phase approach.

A hot spot is observed in the trickle flow reactor with a local blockage which prevents fluid from flowing downstream the reactor. The size of the hot spot is about the size of several particles. The results show that trickle bed reactors have the potential of hot spots formation in the case of local blockage against flow. From the simulation results the temperature difference between the hot spot and surrounding area is about $120K$. We conclude that liquid needs to be trapped to form a hot spot in trickle beds. When the liquid cannot convect in the radial or axial direction hot spots form in trickle beds.

Finally, we used the full model (mass transfer, exothermic reaction, heat transfer between the phases, etc) with evaporation to investigate the effects of evaporation on the performance of a trickle bed reactor. The Eulerian-Eulerian multi-phase approach is used in this part of the research.

Evaporation affects the temperature and volume fraction profiles along the reactor. The effect of evaporation on the temperature profile is very important in the investigation of hot spots formation in trickle bed reactors. Evaporation is an endothermic process and can prevent hot spots formation due to the consumption of heat of reaction. Evaporation affects the production rate of desired or undesired species due to the effect of temperature on reaction rate. In addition, when the volume fraction changes due to the evaporation, the concentration of species in the liquid and gas phase will change. These changes can also affect the production rate of desired and undesired species. According to the simulation results of the reactor with evaporation, the temperature of the reactor at the outlet is $50K$ less than the reactor without evaporation. The evaporation has a significant effect on the temperature profile even at a low rate of evaporation like the case that we have in this research.

One of the important issues of the Eulerian-Eulerian simulations are the closure relations (such as drag coefficient, heat transfer coefficient, etc) and validity of these relations for a trickle bed. There are a lot of closure relations regarding to the drag coefficient of solid-fluid or fluid-fluid, the mass transfer between the phases, the heat transfer between the phases, evaporation-condensation, etc available in literature and CFD tools. But some of the available closure relations are not suitable for the trickle bed reactors that we have and other relations should be used to have more realistic results. In that case, the desired closure relations should be

implemented in the main code using User Defined Functions (UDF). This implementation causes a longer computation time. The simulations are very complex and there is a coupling between different parameters (for example, velocity and pressure or density and temperature, etc) in trickle beds. In addition, due to the difference between the time scale of the reaction and flow the simulations should be performed with small time steps which makes them computationally very expensive.

In trickle bed reactors with a local blockage which traps the fluid from flowing downstream the reactor hot spots can form. A hot spot is not observed in the other case of mal-distributed reactor (diagonal barrier against flow) because of convection in the radial and axial direction. So, if the flow can convect in the axial and radial direction a hot spot cannot be formed in trickle beds even in the case of local mal-distribution.

Samenvatting

Een trickle-bed reactor (TBR) is een meerfasen-reactor die bestaat uit een gepakt bed van katalysatordeeltjes, waar gas en vloeistof in mee- of tegenstroom doorheen stromen. TBRs worden gebruikt voor oxidatiereacties en de zuivering en ontsulfurering onder invloed van waterstofgas tijdens olieraffinage en in de chemische industrie. In een trickle-bed reactor vinden chemische reacties plaats aan het oppervlak van de katalysatordeeltjes. Door de aanwezigheid van deze deeltjes ontstaat er een propstroom van gas en vloeistof in het trickle-bed. Door deze eigenschap hebben TBRs de voorkeur boven andere drie-fasen reactoren waarin de katalysatordeeltjes niet stil staan. Een nadeel van trickle-bed reactoren is dat ze slecht geschikt zijn voor reacties met katalysatoren die snel gedeactiveerd worden (zoals het geval is bij de zuivering van zware olie onder invloed van waterstofgas). Bovendien zijn ze gevoelig voor een onevenwichtige verdeling van de vloeistoffase in de reactor. Deze onevenwichtige verdeling kan leiden tot de vorming van gebieden met een zeer hoge temperatuur ('hot-spots') en gepaard gaan met oncontroleerbaar oplopende reactiesnelheden. Indien een bepaalde kritische temperatuur in de hot-spots overschreden wordt, kan dit leiden tot een verhoging van de reactiesnelheid van zowel gewenste als ongewenste reacties. Bovendien kunnen in hot-spots katalysatordeeltjes gedeactiveerd worden. Ook kan de temperatuur in een hot-spot zo hoog oplopen dat dit ernstige veiligheidsrisico's met zich meebrengt, met name als de hot-spot zich dicht bij de wanden van de reactor bevindt.

In dit onderzoek beschouwen we twee typen tweedimensionale reactoren. De eerste reactor bestaat uit een twee-fase gepakt bed (gas en vaste stof) met een lengte van 240 *mm* en een breedte van 38 *mm*. De diameter van de katalysatordeeltjes is in dit geval gelijk aan 2.9 *mm* en in dit systeem vinden de reacties plaats in de gasfase. Het tweede type reactor dat beschouwd wordt is een drie-fase (gas, vloeistof en vaste stof) trickle-bed reactor, met een lengte van 160 *cm* en een breedte van 30 *cm*. De diameter van de deeltjes in deze reactor is ook 2.9 *mm*. In deze reactor beschouwen we massatransport van de gas- naar de vloeistoffase en vindt

de reactie plaats in de vloeistoffase.

Er zijn drie verschillende verschijnselen die ten grondslag kunnen liggen aan het ontstaan van een hot-spot in een trickle-bed reactor. Ten eerste kunnen hot-spots worden veroorzaakt door een onevenwichtige lokale distributie van de vloeistof in de reactor, ten tweede door verdamping of door verdamping/condensatie, en tenslotte door een temperatuurstijging die wordt veroorzaakt door de chemische reactie zelf. Om onderzoek te doen naar de eerste twee verschijnselen hebben wij gebruik gemaakt van Computational Fluid Dynamics (CFD). Er zijn CFD simulaties uitgevoerd om de invloed van radiale convectie, verdamping en onevenwichtige vloeistof-distributie op de prestaties van trickle-bed reactoren te onderzoeken.

Er bestaan twee verschillende methoden om de transportverschijnselen en hydrodynamica in een trickle-bed in een numeriek model te beschrijven. In de eerste methode wordt het drie-fasen trickle-bed beschreven als een pseudo-homogeen medium. In dit geval worden de Navier-Stokes vergelijkingen gecombineerd met sluitingsrelaties om de interacties tussen de vloeistof en de vaste stof en tussen de vloeistof onderling te modelleren. Deze aanpak staat bekend als de Euler-Euler methode. In de tweede methode wordt het twee-fasen gepakte bed gesimuleerd door de daadwerkelijke geometrie van het bed in ogenschouw te nemen. In deze methode worden de Navier-Stokes vergelijkingen opgelost in de vrije ruimte tussen de deeltjes. Dit is de Direct Numerical Simulation (DNS) methode en deze aanpak resulteert in een gedetailleerde beschrijving van de vloeistofstroming en andere transportverschijnselen tussen de deeltjes. In dit onderzoek passen we zowel de Euler-Euler als de DNS aanpak toe. De Euler-Euler methode is gebruikt voor de simulaties van twee-fasen en drie-fasen stroming (gas/vaste stof en gas/vloeistof/vaste stof) en de DNS methode is gebruikt voor de één-fase simulaties, waarin gas en stilstaande vaste stof is meegenomen.

De doelstelling van dit onderzoek is het ontwikkelen van een zo fundamenteel mogelijk drie-fasen trickle-bed model, dat thermodynamica, warmte- en massaoverdracht en proceskunde in beschouwing neemt, en gebruik maakt van CFD. Het uiteindelijke doel van dit project is het onderzoeken van de vorming van hot-spots in een trickle-bed reactor ten gevolge van een onevenwichtige vloeistof-distributie en het onderzoeken van de invloed van verdamping op de thermische prestaties van de reactor.

Vloeistofstroming en haar invloed op de radiale warmteoverdracht (of radiale convectie) is een zeer belangrijk aspect bij het onderzoeken bij de vorming van hot-spots in trickle-bed reactoren. Als eerste stap hebben wij daarom simulaties uitgevoerd om een beter inzicht te verkrijgen in het radiale warmtetransport en de vloeistofstroming in een gepakt deeltjesbed.

Wij hebben DNS simulaties van de stroming in tweedimensionale gepaktbedreactoren uitgevoerd voor twee verschillende deeltjesconfiguraties. Hierbij hebben wij de invloed van de deeltjesverdeling op het stromingsveld en de radiale convectie onderzocht. Bovendien is de invloed van de wanden op de drukval bestudeerd. De snelheid van de vloeistof is een functie van de open ruimte tussen en de schikking van de deeltjes. In gebieden waar de porositeit klein is, kan de vloeistofsnelheid kleiner zijn dan de snelheid waarmee de vloeistof de reactor instroomt, terwijl in gebieden met een hoge porositeit de snelheid een factor vijf tot tien keer groter kan zijn dan de instroomsnelheid. Zowel voor een lineaire alsook een meer willekeurige verdeling van de deeltjes in het gepakte bed wordt de vorming van kanalen waargenomen. Deze kanalen ontstaan voornamelijk als de deeltjes lijnpatronen in de reactor vormen. De maximale lengte van de kanalen die gevonden wordt voor een (bijna) lineaire en een meer willekeurige verdeling van deeltjes is respectievelijk ongeveer 70-80% en 20-30% van de lengte van de reactor. Een willekeurige verdeling van deeltjes in de reactor vermindert de lengte van de kanalen aanzienlijk; daarentegen vergroot het de radiale convectie. De wanden hebben een significant effect op de drukval in de reactor en dienen dus meegenomen te worden in het ontwerp van het gepakte bed. In onze simulaties vinden we een 20-25% grotere drukval indien de wanden worden meegenomen ten opzichte van de situatie waarin de wanden niet worden meegenomen.

We hebben ook DNS simulaties uitgevoerd aan een exotherme gasfase reactie in een tweedimensionaal gepakt bed met een realistische geometrie. Hierbij hebben wij het effect van het stromingsveld op de warmteoverdracht in de radiale richting bestudeerd. In de gemodelleerde reactor ontstaat er in een kleine regio een temperatuurverschil van 100 K tussen de wand en de bulk van de reactor. Dit grote temperatuurverschil over een kleine afstand (de breedte van de reactor is ongeveer 38 mm) toont aan dat de radiale convectie klein is in deze reactor. Als de deeltjes willekeurige verdeeld zijn in de reactor leidt dit tot een veel grotere radiale convectie dan gevonden wordt bij een lineaire deeltjesverdeling.

De meest belangrijke aspecten van de DNS simulaties zijn het opbouwen van het numerieke rooster en de rekentijd die nodig is om de simulaties uit te voeren. Een realistische geometrie van een gepakt bed is zeer complex, waardoor het opbouwen van een numeriek rooster zeer ingewikkeld en tijdrovend is. In een reactor die op deze wijze gemodelleerd wordt, is het zeer belangrijk om een goede overgang te maken tussen het gestructureerde rooster dat gebruikt wordt rond ieder deeltje en het ongestructureerde rooster in de bulk van de reactor. De groottes van het gestructureerde en het ongestructureerde deel van het rooster dienen te worden geoptimaliseerd, zodat gemakkelijk een geconvergeerde oplossing gevonden kan worden. Bij

onjuiste roostergroottes kan er geen geconvergeerde oplossing gevonden worden en zijn de resultaten niet nauwkeurig. Bovendien is de tijdschaal van de chemische reacties veel kleiner dan die van de stroming. Aangezien de karakteristieke tijdschaal van de stroming relatief groot is, zijn er veel tijdstappen nodig om de uiteindelijke stationaire oplossing te vinden. Hierdoor zijn deze simulaties zeer tijdrovend.

Wij hebben ook de Euler-Euler methode gebruikt om het radiale warmtetransport in een drie-fase trickle-bed reactor te onderzoeken. Hiertoe hebben we de effectieve radiale geleidbaarheid in een trickle-bed reactor met een constante wandtemperatuur berekend. Het concept van de effectieve radiale geleidbaarheid is gerechtvaardigd door de aanname dat het trickle-bed op de macroschaal als een continuüm beschreven kan worden. De effectieve radiale geleidbaarheid van het bed neemt toe als we het debiet van het gas of van de vloeistof verhogen. Hierbij is de invloed van het vloeistofdebiet veel groter dan die van het gasdebiet, omdat de geleidbaarheid van de vloeistof veel groter is dan die van het gas. In de Euler-Euler aanpak worden vergelijkingen voor de gemiddelde massa, snelheid en energie opgelost. In gepakte bedden die op deze manier gemodelleerd worden is sprake van een kleine radiale convectie, vanwege het propstromingsregime dat in de reactor optreedt. Om het convectieve warmtetransport in de radiale richting toch in beschouwing te nemen, modelleren we de effectieve conductiviteit van de stromende fluïda (zowel gas en vloeistof) als een lineaire functie van het Reynolds en Prandtl nummer: $k_{\text{fluid}} = k_f + 0.10k_f Re_p Pr_f$. In het trickle-stromingsregime is de radiale geleiding twee tot vijf keer groter dan in een droge gasstroom.

Om ons uiteindelijke doel te bereiken hebben we een trickle-bed reactor met onder andere massatransport, exothermische reacties en warmteoverdracht tussen de fasen gemodelleerd. Daarnaast hebben we een lokale verstoring van de vloeistof-distributie in het systeem geïntroduceerd om de effecten hiervan op de prestaties van de TBR te onderzoeken. Hiervoor hebben we de Euler-Euler aanpak gebruikt. Als er een lokale blokkade in de trickle-bed reactor aanwezig is die de vloeistof-doorstroming in de reactor verhindert, nemen we de vorming van een hot-spot waar. De grootte van deze hot-spot correspondeert ruwweg met de diameter van enkele deeltjes. De temperatuur in de hot-spot is ongeveer 120 K hoger dan in het omringende gebied van de reactor. Deze resultaten tonen aan dat in trickle-bed reactoren mogelijk hot-spots gevormd kunnen worden als er sprake is van een lokale stromingsobstructie. Hieruit concluderen wij dat hot-spots in trickle-bed reactoren alleen gevormd kunnen worden als vloeistof ingesloten wordt, zodat radiale of axiale convectie van de vloeistof niet langer mogelijk is.

Tenslotte hebben we het complete model (waarin massatransport, exothermische

reacties, warmteoverdracht tussen de fasen en verdamping worden meegenomen) gebruikt om de effecten van verdamping op de prestaties van de te onderzoeken. Ook voor dit gedeelte van het onderzoek is gebruik gemaakt van de Euler-Euler aanpak.

Verdamping beïnvloedt het profiel van de temperatuur en de volumefracties in de reactor. De invloed van verdamping op het temperatuurprofiel is van zeer groot belang bij het onderzoeken van de vorming van hot-spots in trickle-bed reactoren. Aangezien verdamping een endothermisch proces is, kan het de vorming van hot-spots verhinderen doordat het reactiewarmte aan de reactor onttrekt. Aangezien de reactiesnelheid van chemische reacties temperatuur afhankelijk is, beïnvloedt verdamping ook de snelheid waarmee zowel gewenste als ongewenste reactieproducten gevormd worden. Bovendien heeft verdamping zijn weerslag op de concentratie van stoffen in de vloeistof- en gasfase, doordat het een verandering in de volumefracties met zich meebrengt. Ook door deze concentratiewijzigingen kan de productie van zowel gewenste als ongewenste reactieproducten beïnvloedt worden. In onze simulaties is de temperatuur aan de uitgang van de reactor 50 K lager wanneer er verdamping wordt meegenomen in het reactormodel, vergeleken met de situatie waarin verdamping wordt verwaarloosd. Verdamping heeft een significante invloed op het temperatuurprofiel, zelfs als de verdampingssnelheid relatief laag is, zoals het geval is in dit onderzoek.

Een belangrijk aspect van de Euler-Euler simulaties zijn de gebruikte sluitingsrelaties (zoals voor de wrijvingscoëfficiënt of de warmteoverdrachtscoëfficiënt) en de toepasbaarheid van deze relaties op een trickle-bed. Zowel in de literatuur als in CFD-applicaties zijn vele sluitingsrelaties beschikbaar, bijvoorbeeld voor de wrijvingscoëfficiënt, zowel tussen vaste stoffen en vloeistoffen als tussen vloeistoffen onderling, alsook voor de overdracht van massa en warmte tussen verschillende fasen en voor verdamping en condensatie. Omdat sommige van deze sluitingsrelaties niet toepasbaar zijn op de trickle-bed reactoren die wij onderzoeken, zijn er andere sluitingsrelaties nodig om realistische resultaten te verkrijgen. Deze sluitingsrelaties dienen zelf geïmplementeerd moeten worden in de code door gebruik te maken van User Defined Functions (UDFs). De implementatie van UDFs vergroot echter de benodigde rekentijd. De simulaties zijn erg complex en in een trickle-bed zijn verschillende parameters (bijvoorbeeld: de snelheid, de druk, de dichtheid en de temperatuur) onderling afhankelijk. Het grote verschil tussen de karakteristieke tijdschalen van de chemische reacties en de vloeistofstroming vereist bovendien dat er een zeer kleine tijdstap wordt gebruikt in de simulaties. Dientengevolge is de benodigde rekentijd zeer groot.

In een trickle-bed reactor kunnen hot-spots gevormd worden wanneer een lokale

ophoping van deeltjes verhindert dat de vloeistoffase door de reactor heen kan stromen. In andere onevenwichtige deeltjesverdelingen die in dit werk beschouwd zijn, waarin sprake is van diagonale stromingsbarrières en convectie in de radiale en axiale richting nog wel mogelijk is, wordt geen hot-spot gevormd. Wij concluderen daarom dat er geen hot-spots kunnen worden gevormd worden in een trickle-bed reactor zolang er convectie plaats kan vinden in de radiale en axiale richting, zelfs als er sprake is van een lokale verstoring van de evenwichtsverdeling.

INTRODUCTION

1.1 Trickle bed reactors

Multi-phase flow reactors are reactors with more than one phase. All catalytic reactors are multi-phase reactors. Trickle bed reactors (TBRs) are multi-phase reactors with a three-phase trickling flow regime in them. Trickle bed reactors have a fixed-bed of solid catalysts in which liquid and gas flow co-current or counter current through the bed and reaction takes place on the surface of the catalyst [1]. These reactors operate continuously and are used in petroleum, petrochemical and chemical industries such as:

- Hydrogenation of Hydrocarbons
- Hydrodesulphurization
- Hydro-finishing of lubricating oils

The economic impact of how well these reactors operate is considerable since in the petroleum industry annual processing capacity of various hydro-treatments is estimated at capacity of 1.6 billion metric tones [2].

Because of stationary catalyst particles inside the reactor, the fluid flow regime is plug flow in trickle bed reactors, so TBRs are preferred to other three-phase reactors where the catalyst is either slurried or fluidized. For instance, high catalyst loading per unit volume of the liquid in trickle bed reactors make them preferable to slurry reactors. However, the disadvantages of trickle bed reactors are their impracticality for reactions with fast deactivating catalysts such as in heavy oil hydro-treating processes and the possibility of liquid mal-distribution, which may cause hot spots

and reactor runaways [3].

Most commercial trickle bed reactors normally operate adiabatically at high temperatures and high pressures and generally involve hydrogen and liquids with superficial gas and liquid velocities up to 30 and 1 cm/s , respectively. Kinetics and thermodynamics of reactions conducted in trickle bed reactors require high temperatures, which in return increase gas expansion and impede the gaseous reactant from dissolving sufficiently into the liquid. Therefore, high pressures (up to 60 MPa) are necessary to improve the gas solubility and mass and heat transfer rates to handle large gas volumes at less capital expense and to slow down the catalyst deactivation [1]. Figure 1.1 shows a schematic of a trickle bed reactor.

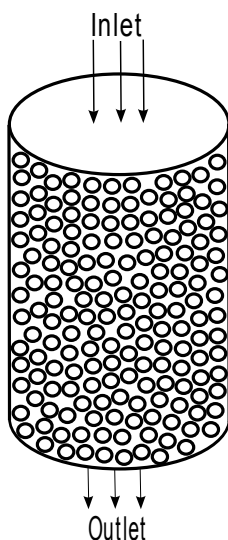


Figure 1.1: Schematic of a trickle bed reactor.

1.2 Hot spot formation

Hydro-processing trickle bed reactors have the potential of developing runaways, which may ultimately result in vessel failure, due to excessive pressure and excessive temperature of the vessel wall. One of the main problems of trickle bed reactors is formation of hot spots. The temperature profile of a trickle bed reactor in which

an exothermic reaction occurs, attains a local maximum, which is referred to as a hot spot [4].

When these hot spots exceed some critical value it may lead to a reactor runaway caused by an increase in the rate of the desired or undesired reaction, which has a negligible rate under normal operating conditions. Some literature exist on this subject, reviewed recently by Varma, Morbidelli and Wu [5]. The formation of hot zones may have a harmful impact on the yield of the desired product (or products) and it may deactivate the catalyst. When a hot zone exists next to the walls of a reactor, it may decrease the mechanical strength of the wall. Thus, a hot zone may lead to severe safety problems. The formation of these hot zones is of both practical importance and of intrinsic academic interest.

Several researchers tried to explain and predict the formation of hot spots in commercial trickle bed reactors. For example, Jaffe [6] showed that internal obstruction might cause hot spot formation in trickle bed reactors. Boreskov et al. [7] showed that non-uniform catalyst (the same shape of catalyst but different sizes) particles of the bed could generate local hot zones. Subramanian and Balakotaiah [8] showed that at rather low feed rates, the temperature dependence of the fluid properties might generate spatiotemporal flow and temperature patterns in trickle bed reactors [9].

Some important issues which can play a role in the formation of hot spots in trickle bed reactors is discussed below briefly.

1.2.1 Flow regimes

There are four different flow regimes in three phase packed bed reactors. At low liquid and gas flow rates, the liquid trickles over the particles in the form of a thin film with a thickness of the order of one-tenth of a millimeter and the gas phase is the continuous phase filling the voids inside the reactor. This regime is called trickle flow or gas-continuous flow regime. At low liquid and high gas flow rates, the spray or mist-flow regime appears. The liquid film is broken into fine droplets entrained by the gas phase. The pulse-flow regime can be observed at higher liquid and high gas loads. The liquid periodically blocks the small channels between catalyst particles and forms liquid plugs that prevent the flow of gas. If the velocity of liquid is increased then the liquid becomes continuous phase, whereas gas flows as a uniform bubble dispersion downward through bed [10]. Figure 1.2 shows flow patterns in a co-current three-phase packed bed reactor. Hot spots are observed in

1. Introduction

the trickle flow regime. So, knowledge of the flow regimes inside the packed beds is important in the investigation of hot spots formation.

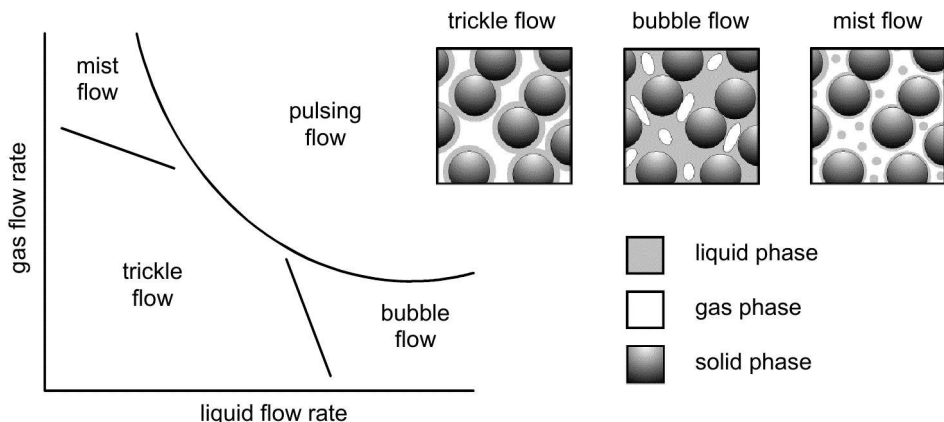


Figure 1.2: Different flow regimes in three phase packed beds as a function of flow rate of gas and liquid [10].

1.2.2 Wetting efficiency

External catalyst wetting efficiency is an important parameter in trickle bed reactors. Internal wetting efficiency is less important than the external wetting efficiency in trickle bed reactors because the internal wetting efficiency is almost one due to the capillary effects and external wetting efficiency is less than one. Part of the liquid is more or less stagnant and makes a high or low resistance to mass transfer (depending on the thickness of the liquid layer on the catalyst surface), which leads to non-uniform reactant concentration around the catalyst, in case of high intrinsic reaction rates. Another phenomenon, which can reduce reactor efficiency, is incomplete wetting of the catalyst particles. In principle, incomplete wetting can take place on a reactor scale as well as on a particle scale. Normally, incomplete wetting of large catalyst zones can be one of the reasons for the formation of hot spots in trickle bed reactors [1].

1.2.3 Heat transfer

One of the important phenomena in the investigation of hot spots formation in trickle bed reactors is heat transfer in the reactor. There is both axial and lateral (radial and tangential) heat transfer in trickle bed reactors.

As mentioned before, reactions carried out in trickle bed reactors such as hydrogenation can be highly exothermic. A good knowledge of heat transfer in trickle beds is necessary for the design of the reactor and heat removal system. Although quite a lot of studies were done in the last thirty years in the field of trickle bed reactors, relatively few deal with the heat transfer. Furthermore, major part of heat transfer studies in trickle bed reactors have been carried out with water and air (or nitrogen) [11].

1.2.4 Mal-distribution

In trickle bed reactors, the liquid is in the form of films, rivulets and liquid pockets at particle level. Under complete wetting condition, catalyst particles are fully covered by liquid films while the gas travels in the interstitial void space. If the liquid rate decreased, complete films would break up into partial films and rivulets. Internal wetting, however, is usually considered to be complete due to strong capillary effects [12]. Spatial distribution of the liquid influences the rate of heat and mass transfer and the rate of reaction. If distribution is not complete, some parts of catalyst will be dry. When reaction takes place in these parts, we will observe a temperature rise because there is no liquid to transfer heat of reaction out of the bed. According to kinetic theories when the temperature is increasing, some undesired reactions would take place or the rate of reaction will be very high and it will be very difficult to control the reactor [12].

In a trickle bed reactor, as the gas and liquid flow downward, the liquid has a tendency to move towards the reactor wall, which is undesirable since the wall is not catalytically active. This tendency is attributed to the lower resistance to flow due to high void fraction near the wall. Normally reactor interiors are necessary to take care of any mal-distribution that has a bearing on a pressure drop across the reactor. Sundaresan [13] reported that in a trickle bed reactor, the startup procedure is important for uniform wetting. Niu et al. [14] used a sheet of convex hemispheres in a staggered arrangement to line the inside of a tube to eliminate wall effects in a trickle bed reactor. He noticed that the lining was effective in reducing the void

fraction adjacent to the reactor wall, which led to improved liquid distribution. Moller et al. [15] suggested using a large-particle top layer to improve liquid distribution. Lutran et al. [16] also studied the liquid distribution in trickle beds by using computer-assisted tomography. They observed that the flow pattern depends strongly on whether the bed had been pre-wetted by flooding the column with liquid or were initially dry [17].

Wall flow depends on the ratio of the reactor diameter to the catalyst particle diameter, physical and chemical properties of the liquid (density, viscosity and surface tension), liquid and gas flow rates, porosity, shape and orientation of the catalyst particles. Compared to the other hydrodynamic parameters of trickle bed reactors, relatively few studies have been reported on the radial liquid distribution. Reactor to particle size ratio (D/d_p) has a significant effect on the radial flow distribution.

1.2.5 Evaporation-condensation

Some researchers believe that critical phenomena such as formation of hot spots in trickle beds, multiplicity of steady state regimes and hysteresis phenomena are generated by liquid evaporation and transition of the reaction to the gas-phase mode [18].

When evaporation occurs, the reactants and products will be present in both vapor and liquid phases. Consequently, the liquid residence time will increase and the concentration of the reacting species in the liquid phase will increase because of decrease of the volume of liquid (due to evaporation). Moreover, as the reactant in the liquid phase is consumed, part of the reactant in the vapor phase will condense back to the liquid phase. Obviously, this evaporation-condensation process will have strong influence on the extent of reaction. This process may affect product selectivity and may form hot spots in the reactor [19].

The factors promoting transition of the reaction to the gas phase are as follows: heat production of the reaction, existence of dry and partially wetted catalyst particles, non-uniform liquid distribution in the reactor and non-equilibrium phase in trickle bed reactors [18].

1.3 Modeling approaches

We performed numerical simulations to understand more about formation of hot spots in trickle bed reactors using Computational Fluid Dynamics (CFD). In Computational Fluid Dynamics, numerical methods and algorithms are used to solve and analyse the problems that involve fluid flows. Two different numerical approaches can be found in literature to describe hydrodynamics and transport properties of trickle bed reactors.

1.3.1 Actual trickle bed geometry

In this approach, trickle beds are simulated based on the consideration of the actual trickle bed geometry. This yields a detailed description of the fluid flow and species distribution between the particles. In this method, no additional empirical correlations are required for the porosity distribution. To solve the fluid flow between particles, two different methods are used. The first method is the Lattice Boltzman Method (LBM). Freund et al. [20] calculated the local velocity and the pressure drop in irregular arrangements of spheres in cylindrical containers with the Lattice Boltzman Method and the simulation results were in a good agreement with the experimental data. In the second method, the Navier-Stokes equations are applied to the void between the spheres. In the work of Calis et al. [21], the local velocity field in both regular and irregular configuration of spheres was studied in rectangular containers for the tube to particle diameter ratio up to four. Furthermore, Dixon and Nijemeisland [22] investigated the relationship between the local flow field and the local wall heat flux in a packed bed of spheres. Kloker et al. [23] studied the mass transfer phenomena for the different flow rates in the spherical geometries.

1.3.2 Pseudo-homogeneous model

In the second approach, trickle beds are treated as a pseudo-homogeneous medium, where modified Navier-Stokes equations are applied in conjunction with the Ergun pressure drop calculation to account for the fluid-solid interaction [24], [25], [26], [27]. To govern local phenomena, overall averaged quantities are replaced by functions describing the radial change of these quantities. For example, to account

for the radial porosity variation, the overall averaged porosity of the whole packed bed reactor is replaced with a function accounting for the porosity distribution in the radial direction.

1.4 Thesis outline

In this thesis we performed simulations of two phase packed bed and three phase trickle flow reactors. We used both Direct Numerical Simulations (DNS) and Pseudo-homogeneous model to investigate hot spots formation. This thesis organized in the following chapters.

Chapter 2 describes multi-phase flow concepts. In this chapter we discuss various types of multi-phase flow and modeling concepts. In addition, different modeling approaches will be discussed briefly.

Chapter 3 describes the Ansys Fluent Model. In this chapter, all equations which were solved in multi-phase trickle bed reactor simulations will be discussed.

In chapter 4 we investigate the effects of particle distribution on the flow field and radial convection in packed beds. In addition, effects of the wall on the pressure drop and velocity distribution was investigated. We used two different configurations of packed beds for this purpose.

In chapter 5 we performed Direct Numerical Simulation (DNS) of an exothermic gas-phase reaction under laminar flow condition in a packed bed reactor with random distribution of particles. The reaction used in this work is of Arrhenius type between Ethylene and Oxygen with Ethylene Oxide as product. This chapter provides useful data on the flow field and radial convection in packed beds which may be used for the improvement and further optimization of the design and operation of packed bed reactors.

Chapter 6 describes heat transfer in trickle bed reactors which reports a study of steady-state heat transfer of gas and liquid flowing through a trickle bed with constant wall temperature. The effect of gas and liquid flow rates on heat transfer in packed beds are discussed. In this investigation the Eulerian-Eulerian multi-phase approach is used to solve the average mass, flow and energy equations for each phase separately.

Chapter 7 describes a three-phase trickle bed reactor with mass transfer from gas to the liquid phase, heat transfer between three phases (gas, liquid and solid) and an exothermic reaction in the liquid phase. In addition, we discuss the effects of

mal-distribution on the thermal performance of a trickle bed reactor and formation of hot spots. For this investigation we also used the Eulerian-Eulerian multi-phase approach.

In chapter 8 we discuss the evaporation phenomena and its effect on the performance of a trickle bed reactor and formation of hot spots.

Finally, chapter 9 summarizes the relevant and important conclusions and also discusses recommendations for possible future works.

1.5 Acknowledgement

This project was funded by Shell Global Solutions International B.V, Amsterdam. During this work, the author was a member of OSPT (OnderzoekSchool Process Technologie), the Netherlands research School in Process Technology.

The author gratefully acknowledges interest, inspiration and useful discussions and valuable contributions by Dr. Benoit Witkamp, Dr. Sami Sapmaz, Dr. Ed Ouwerkerk and Dr. B.I.M. ten Bosch.

1.6 Bibliography

- [1] Muthanna, H. Al-Dahhan, Faical Larachi, Milorad P. Dudukovic, and Andre Laurent. High pressure trickle bed reactors : A review. *Ind. Eng. Chem. Res.*, 36:3292–3314, 1997.
- [2] P. Trambouze. Multi-phase catalytic reactors in the oil industry, an introduction. *Rev. Inst. Fr. Pet.*, 46:433, 1991.
- [3] Mc Manus, R.K. Funk, G.A. Harold M.P, and Ng K.M. Experimental study of reaction in trickle bed reactors with liquid mal-distribution. *Ind. Eng. Chem. Res.*, 32:570, 1993.
- [4] Giuseppe Biardi and Giancarlo Baldi. Three-phase catalytic reactors. *Catalysis Today*, 52:223–234, 1999.
- [5] Varma, Morbidelli, and Wu. Parametric sensitivity in fixed-bed catalytic reactors with reverse flow operation. *Chemical Engineering Science*, 54:4579–4588, 1999.
- [6] Stephen B. Jaffe. Hot spot simulation in commercial hydrogenation processes. *Industrial and Engineering Chemistry Process Design and Development*, 15 (3):410–416, 1976.
- [7] Boreskov GK, Matros YuSh, Klenov OP, Logovkoi VI, and Lakhmostov VS. Local nonuniformities in a catalyst bed. *Doklady Akademii Nauk SSSR*, 258:1418–1420, 1981.
- [8] Subramanian S and Balakotaiah V. Analysis and classification of reaction driven stationary convective patterns in a porous medium. *Phys of Fluids*, 9:1674–1695, 1997.
- [9] Ganesh A. Viswanathan and Dan Luss. Model prediction of hot spots formation in shallow adiabatic packed-bed reactors. *AIChE Journal*, 52:1533–1538, 2006.
- [10] K. Roel Westerterp and Wino J.A. Wammes. *Three-phase trickle-bed reactors*. 2005.
- [11] A.S. Lamine, L. Gerth, H.L. E Gall, and G. wild. Heat transfer in a packed bed reactor with co-current down flow of a gas and a liquid. *Chemical engineering Science*, 52:3813–3827, 1996.

-
- [12] S.P. Zimmerman and K.M. Ng. Liquid distribution in trickling flow trickle-bed reactors. *Chemical engineering Science*, 41:861–866, 1986.
- [13] Sundaresan S. Liquid distribution in trickle bed reactors. *Energy and Fuels*, 8:531, 1994.
- [14] Niu M, T. Akiyama, R. Takahashi, and J. Yagi. Reduction of the wall effect in a packed bed by a hemispherical lining. *AIChE J*, 42:1181, 1996.
- [15] Moller L.B, C. Halken, A. Hansen, and J. Bartholdy. Liquid and gas distribution in trickle bed reactors. *Ind. Eng. Chem. Res.*, 35:926, 1996.
- [16] Lutran P.G, K. M. Ng, and E. P. Delikat. Liquid distribution in trickle beds, an experimental study using computer-assisted tomography. *Ind. Eng. Chem. Res.*, 30:1270, 1991.
- [17] Anil K. Saroha, K.D.P. Nigam, Alok K. Saxena, and V. K. Kapoor. Liquid distribution in trickle bed reactors. *AIChE Journal*, 44:2044–2052, 1998.
- [18] Valery A. Kirillov and Igor V. Koptug. Critical phenomena in trickle bed reactors. *Ind. Eng. Chem*, 44:9727–9738, 2005.
- [19] G.R. Kocis and T.C. HO. Effects of liquid evaporation on the performance of trickle bed reactors. *Chemical Engineering Research and Design*, 64a:288–291, 1986.
- [20] H. Freund, T. Zeiser, F. Huber, E. Klemm, G. Brenner, F. Durst, and G. Emig. Numerical simulations of single phase reacting flows in randomly packed fixed-bed reactors and experimental validation. *Chemical Engineering Science*, 58:903–910, 2003.
- [21] H.P. A. Calis, J. Nijenhuis, B.C. Paikert, F.M. Dautzenberg, and C.M. van den Bleek. CFD modeling and experimental validation of pressure drop and flow profile in a novel structured catalytic reactor packing. *Chemical Engineering Science*, 56:1713–1720, 2001.
- [22] A.G. Dixon and M. Nijemeisland. CFD as a design tool for fixed-bed reactors. *Ind. Eng. Chem. Res*, 40:5246–5254, 2001.
- [23] M. Kloker, E.Y. Kenig, R. Piechota, S. Burghoff, and Y. Egorov. CFD-based study on hydrodynamics and mass transfer in fixed catalyst beds. *Chem. Eng. Technol*, 28:31–36, 2005.

- [24] J.N. Papageorgiou and G.F. Froment. Simulation models accounting for radial voidage profiles in fixed-bed reactors. *Chemical Engineering Science*, 56:3043–3056, 1995.
- [25] O. Bey and G. Eigenberger. Fluid flow through catalyst filled tubes. *Chemical Engineering Science*, 52:1365–1376, 1997.
- [26] M.K. Rottschafer and D. Vortmeyer. Measured and modeled superficial flow profiles in packed beds with liquid flow. *AIChE Journal*, 44:484–490, 1998.
- [27] M. Winterberg and E. Tsotsas. Impact of tube-to-particle-diameter ratio on pressure drop in packed beds. *AIChE Journal*, 46:1084–1088, 2000.

CHAPTER 2

MULTI-PHASE FLOW CONCEPTS

The purpose of this chapter is to explain briefly the concepts of multi-phase flow and its application in chemical reactor engineering. Types of multi-phase flow, concepts and multi-phase flow modeling approaches will be discussed in this chapter.

2.1 Introduction

Multi-phase flow is a type of fluid flow which consists of more than one phase. The phase here means the thermodynamic state of the fluids, i.e, gas, liquid or solid. Multi-phase flows encompass a wide range of fluid flows such as gas-liquid, liquid-liquid, gas-solid, liquid-solid or gas-liquid-solid flows. There are a lot of examples of multi-phase flow in industry such as gas-solid flow in cyclones, gas-liquid flow in pipelines, gas-solid or gas-liquid-solid flow in chemical reactors, etc. Multi-phase flow regimes depend on the geometry, the velocities and properties of the flowing fluids. For example, in multi-phase flow reactors such as three-phase packed bed reactors there are four different flow regimes called trickle flow, bubble flow, mist flow and pulsating flow. The main difference between these flow regimes are the velocity of the gas and liquid phases. Multi-phase reactors are used in different industries e.g, in the production of oil and gas, in the food processing, or in water treatment plants, etc. So, it is important to know more about these reactors. In addition, with understanding more about these reactors we will be able to design

more effective and high performance multi-phase reactors and improve the performance of the existing multi-phase reactors in industry.

2.2 Types of multi-phase flows

When two or more phases flow together in a reactor, pipeline or canal a lot of different flow regimes can be seen. It is possible to classify these flow regimes in different ways. The first way is the classification of the flow regime with the thermodynamic state of the phases, for example, gas-liquid, liquid-solid, gas-solid, gas-liquid-solid, etc. In addition, if the properties of two liquids are different and they do not mix very well (immiscible liquids) we can also have a liquid-liquid two-phase flow. For example, mixtures of oil and water can be classified as two-phase liquid-liquid flow. Broadly, multi-phase flow regimes can be divided in dispersed flows, separated flows and mixed flows [1]. Dispersed flow is a kind of multi-phase flow with all phases dispersed except for one that is continuous. In this sort of flow all dispersed phases flow through the continuous phase. Fluid flow in bubble column reactors, trickle bed reactors and cyclones are examples of dispersed flow regime. Separated flows are flows in which none of the phases is dispersed and all phases are continuous or semi-continuous. The examples of these kind of flow are film flow and annular flow. Mixed flow is a combination of dispersed flow and separated flow. So, in mixed flow we have both dispersed and separated phases. The example of this sort of multi-phase flow can be bubbly annular flow and slug flow. In three-phase reactors such as packed bed reactors we can have both separated and mixed flow regimes. For example, in these reactors in the trickling flow regime the gas phase is the continuous phase and the liquid phase is the dispersed phase. Depending on the superficial velocity of gas and liquid, the continuous and dispersed phases the flow regime can change in trickle bed reactors.

In two-phase gas-solid reactors where the solid phase is not moving (fixed bed reactors) it is possible to consider the solid phase as a porous medium. In a porous medium, gas flows over the surface of the solid phase as well as in/through the pores of the solid phase. In this case, the size of the pores, the properties of solid particles and distribution of the gas phase can have an effect on the flow of gas. There are applications for this kind of reactor in industry such as the Ethylene Oxide reactor.

There are other kind of gas-solid reactors in which both gas and solid phases are

moving. They are called fluidized bed reactors. In these reactors, the gas phase is the continuous phase and the solid phase is the dispersed phase. It is also possible to have some other sub-regimes in these reactors. The sub-regimes can be the dense bed regime, the turbulent bed or the fast fluidized bed regime depending on the velocity of gas and solid phases.

For gas-liquid-solid reactors, such as packed bed reactors, in the trickling flow regime, the liquid phase is the dispersed phase and the gas phase is the continuous phase. We have discussed the flow regimes of trickle bed reactors in chapter 1. In the three-phase bubble column reactors the gas and solid phases are the dispersed phase and the liquid phase is the continuous phase. In bubble column reactors depending on the operating condition, property of the phases and velocity of the phases, other sub-regimes such as turbulent flow and slug flow are also possible .

2.3 Modeling concepts of multi-phase flows

Computational methods for multi-phase flows were pioneered by Harlow and Welch [2], Hirt [3], Amsden and Harlow [4], [5], Nichols and Hirt [6], [7], [8]. Development of these methods was based on finite difference discretization of the continuity and Navier-Stokes equations. The initial idea was based on using velocity and pressure as the initial variables. An other group also worked on computational methods with introducing the basic principles of the finite volume method [9]. The first commercial CFD code (PHOENICS) for solving multi-phase flow problems was produced by Spalding [10], [11], [12], [13], [14]. A review on models and numerical methods for multi-phase flow has been presented by Stewart and Wendroff [15] and Crowe [16] and Crowe et al. [17], [18].

As mentioned before multi-phase flows can be classified as separated flows and dispersed flows. This classification is important from a computational point of view as well as a physical point of view. For the modeling of dispersed flow systems such as most multi-phase flow reactors three main issues need to be addressed:

- Definition of phase, flow regime and required resolution
- Formulation of governing equations
- Solution of governing equations

As mentioned before the first classification of the multi-phase flows is based on the thermodynamic state (gas, liquid or solid). It is also possible to define different dispersed phases based on the particle size. For example, particles with size A as

phase a and size B as phase b . Both a and b phases can be gas, liquid or solid. In addition it is also possible to define two different thermodynamic states as one phase. For example, a mixture of liquid and solid as slurry phase in three-phase (gas, liquid and solid) bubble column reactors. So, in three-phase bubble column reactors there will be two phases: gas and slurry (liquid-solid). The first steps in selection of the best multi-phase model are the definition of the phases and flow regime. Depending on the flow regime and properties of phases, different modeling approaches can be used.

There are three different approaches for the modeling of multi-phase flows:

- (i) Volume of fluid (VOF) approach
- (ii) Eulerian-Lagrangian approach
- (iii) Eulerian-Eulerian approach

The first method (VOF) is conceptually the simplest method of multi-phase flow modeling. In this method, all phases (two or more) are considered as non interpenetrating continuum. In this method a single set of momentum equations is solved and the volume of each phase is tracked in the computational domain. The interfaces between the phases are tracked by the solution of a continuity equation for the volume fraction of the phases. This method is suitable for the modeling of multi-phase systems in a small domain. This method is also suitable for the multi-phase flow systems for which the behavior of the interface is a point of interest. This method is not suitable for the modeling of large scale systems because it is computationally very expensive.

The Eulerian-Lagrangian approach is more complicated than the volume of fluid approach. In this method the fluid phase is considered as continuum and Navier-Stokes equations are solved for the continuous phases while the dispersed phases are solved by tracking the particles (bubbles or droplets) through the calculated flow field. The dispersed phases exchange momentum, mass and energy with the continuous phase. This method is suitable for the modeling of multi-phase flow systems with low volume fraction of dispersed phases (less than 10%). This model is an appropriate model for e.g. liquid fuel combustion and spray dryers.

The Eulerian-Eulerian multi-phase approach is based on the assumption of each phase as interpenetrating continuum. The phases can be solid, liquid or gas and any combination of these three phases. In this method any number of secondary or dispersed phase is possible. The number of phases is only limited by memory requirements and convergence issues. In this method, a single pressure is shared by all phases. The continuity, momentum, energy and species transfer equations are solved for each phase separately. This method is suitable for multi-phase flow modeling with a range of volume fraction between 0 and 1. As there is no limitation

in the volume fraction or number of phases in this method, this method is a suitable approach for the simulation of multi-phase reactors with more than one dispersed phase in the system. For all these methods the number of phases are limited only by the computation time and availability of memory.

It is not a priori clear which of these methods is the best for the simulation of multi-phase systems. The appropriate method should be chosen based on the complexity of the dispersed phase, the size of the equipment and the parameters which we are interested in. For more understanding of multi-phase flows for some cases it is possible to model a problem with two of these approaches.

2.4 Modeling dispersed multi-phase flows

Dispersed multi-phase flow is present in a number of multi-phase flow reactors such as fluidized beds, bubble columns and trickle beds. The modeling of three-phase reactors is very complex due to the quite complex phenomena which occur in three-phase reactors. The reactor engineer has to deal with a lot of phenomena such as flow, species transport, heat transfer, mass transfer, chemical reaction, evaporation, condensation, etc. In addition, the dispersed phase will have an effect on the continuous phase flow specially when the volume fraction of the dispersed phase is increasing.

For selection of the most suitable model for the simulation of multi-phase flow reactors it is very important to have a detailed look at the coupling issues between the continuous and dispersed phases [19]. After this step and considering computation time it will be possible to choose the best approach. Governing equations and more details of three modeling approaches are discussed below.

2.4.1 Volume of fluid (VOF) approach

In this approach, a single set of conservation equations is shared between the fluids. The governing equations can be written as follows:

$$\frac{\partial(\rho)}{\partial t} + \nabla \cdot (\rho \vec{v}) = \sum_{q=1}^n (S_q) \quad (2.1)$$

2. Multi-phase flow concepts

$$\frac{\partial(\rho \vec{v})}{\partial t} + \nabla \cdot (\rho \vec{v} \vec{v}) = -\nabla P + \rho \vec{g} + \vec{F} \quad (2.2)$$

where ρ is the density, \vec{v} is the velocity vector, S is the mass source, P is the pressure, \vec{g} is the gravity acceleration vector and \vec{F} is the force vector.

The equations 2.1 and 2.2 are the same equation which we use in single-phase flow problems. For multi-phase flows it is also possible to use these equations with the desired boundary conditions at the interface of different phases. But the important issue is that density, viscosity and other physical properties should be changed at the interface for the calculations. The other important issue is that when the volume fractions are changing the interface is also changing.

In the volume of fluid approach the movement of all phases is simulated and not the motion of the interface. The movement of the interface is inferred indirectly through the movement of different phases separated by an interface. Motion of the different phases is tracked by solving an advection equation of a phase volume fraction. If the control volume is occupied by one phase, the properties of that phase are used in the calculations but if a control volume is not entirely occupied by one phase, mixture properties are used while solving governing equations 2.1 and 2.2. The properties appearing in equations 2.1 and 2.2 are related to the volume fraction of the q^{th} phase as follows:

$$\rho = \sum_{q=1}^n \alpha_q \rho_q \quad (2.3)$$

$$\mu = \sum_{q=1}^n \frac{\alpha_q \rho_q \mu_q}{\alpha_q \rho_q} \quad (2.4)$$

The volume fraction of each fluid, α_q , is calculated by tracking the interface between different phases throughout the solution domain. Tracking of the interfaces between n different phases is accomplished by solving continuity equations for $n - 1$ phases. For the q^{th} phase, this equation has the following form:

$$\frac{\partial \alpha_q}{\partial t} + (v_q \cdot \nabla) \alpha_q = S_{\alpha q} \quad (2.5)$$

Some techniques were proposed for the tracking of the interface by Rider [20] and Rudman [21].

The volume of fluid method is computationally very expensive. This is the main disadvantage of this method. So, it is very difficult to use this method for dispersed multi-phase flows with a lot of particles in dispersed phase. Therefore, this method

is not very effective in the modeling of large scale systems, however, it can be helpful for understanding of the local phenomena of dispersed multi-phase flows.

2.4.2 Eulerian-Lagrangian approach

In the Eulerian-Lagrangian approach, the particles of the dispersed phase are considered as rigid spheres which do not deform. The motion of a particle is governed by the Lagrangian form of the Newton's second law [22], [23], [24], [18]:

$$\frac{d(m_p v_p)}{dt} = f_{hp} + f_p + f_E + f_G + f_D + f_V + f_L + f_B \quad (2.6)$$

where $m_p = \rho_p V_p$ is the mass of the particle. As mentioned, the dispersed phase is assumed to be rigid spheres, so m_p , ρ_p and V_p are constant in time. The forces in the equation 2.6 are surface and body forces acting on a particle. f_{hp} is the force due to the hydrostatic pressure, f_p is the force due to any external pressure gradients, f_E is any external body force except the gravity, f_G is the body force due to the gravity, f_D is the steady drag force, f_V is the virtual mass force, f_L is the lift force and f_B is the Basset force.

The particle trajectory is calculated from the definition of the translational velocity of the center of mass of the particle:

$$\frac{dr_p(t)}{dt} = v_p(t, r_p(t)) \quad (2.7)$$

In a one way coupled system, any effect of the dispersed phase on the continuous phase is neglected. So, the local velocity of the dispersed phase has no effect on the continuous phase but the local velocity of the continuous phase has an impact on the dispersed phase. This is only true for systems with small volume fraction of the dispersed phase. For a system with higher volume fraction the effects of the dispersed phase on the continuous phase cannot be neglected. So, for denser systems, it is necessary to consider particle-particle interaction and also its effects on the continuous phase. Hence, four-way coupling is recommended.

The dispersed phase volume fraction and the number of particles of dispersed phase are the main issues in the coupling between the phases in the Eulerian-Lagrangian method. For very dilute systems ($\alpha_p < 10^{-6}$) a simple one-way coupling between dispersed and continuous phase is sufficient for considering the interaction between these two phases. For denser dispersed phases ($10^{-6} < \alpha_p < 10^{-3}$)

two-way coupling is considered enough and reasonable. Finally, for the phases which $\alpha_p > 10^{-3}$ four-way coupling is recommended [25], [26]. In the Eulerian-Lagrangian simulations the computational time should be taken into account. For the flows with a number of not more than 10^6 particles it is possible to solve Lagrangian equations for each element. But, if the number of particles are more than 10^4 particles a statistical approach is more useful and practical.

For simulations with two and four way coupling the continuous phase is described by modified single phase momentum equations [27], [28], [29], [30], [31], [32]. The momentum equations are solved considering the interaction terms between particles. These interaction terms are taken into account based on Newtons' third law (action=re-action).

The main advantage of the Eulerian-Lagrangian approach in comparison with the Eulerian-Eulerian approach is its flexibility with respect to the incorporation of the microscopic transport phenomena. The Eulerian-Lagrangian approach is computationally more expensive than the Eulerian-Eulerian approach. This is the main disadvantage of the Eulerian-Lagrangian approach.

In general, multi-phase flow reactors are dense systems. So, it is very expensive to track a high number of dispersed particles [33]. Therefore, averaged methods should be used for the modeling. For this purpose appropriate closure laws are needed for the interfacial transport of momentum. It is worth mentioning that these closures are not complete and they are still under development.

2.4.3 Eulerian-Eulerian approach

In the Eulerian-Eulerian approach all phases (dispersed and continuous) are taken as interpenetrating continuum. This method is the most suitable method for the modeling of multi-phase flow reactors such as fluidized bed reactors, bubble column reactors and trickle bed reactors with high volume fraction of dispersed phases ($> 10\%$). The coupling between the phases should be implemented via suitable interphase transport models. It is not easy to model complex phenomena (such as reaction, evaporation, condensation, mass transfer, etc) at the particle level with the Eulerian-Eulerian approach.

For single-phase flows, basic transport equations are given in the form of mass, momentum and energy conservation. For multi-phase flows such equations should be solved with averaging. Several different averaging methods can be used for this purpose. For example, Ishii [1] and Drew [34] used time averaging while Harlow

and Amsden [2], Rietema and van den Akker [35] and Ahmed [36] used a volume averaging method.

In this section, we present a general form of the governing equations for the Eulerian-Eulerian multi-phase flows. With this approach, it is assumed that the sum of volume fraction of phases is equal to 1.0. If there are n phases in total, this gives:

$$\sum_{q=1}^n \alpha_q = 1.0 \quad (2.8)$$

For the Eulerian-Eulerian multi-phase approach the averaged conservation equations for mass and momentum for each phase are given by:

$$\frac{\partial(\alpha_q \rho_q)}{\partial t} + \nabla \cdot (\alpha_q \rho_q \vec{v}_q) = \Gamma_q \quad (2.9)$$

and

$$\frac{\partial(\alpha_q \rho_q \vec{v}_q)}{\partial t} + \nabla \cdot (\alpha_q \rho_q \vec{v}_q \vec{v}_q) = -\alpha_q \nabla P + \nabla \cdot (\alpha_q \sigma_q) + M_{q,l} + \Gamma_q \vec{v}_l + S_q + \alpha_q \rho_q \vec{g} \quad (2.10)$$

where ρ_q , \vec{v}_q , α_q and σ_q are respectively the density, velocity, volume fraction and viscous stress tensor of the q^{th} phase, P is the pressure, Γ_q is a source term of mass, $M_{q,l}$ is the interface momentum exchange between phase q and phase l , \vec{v}_l is the relative velocity and S_q is a momentum source term of phase q due to external forces other than the gravity.

The advantage of the Eulerian-Eulerian multi-phase model is that if closures for the coupling are available it is possible to model any multi-phase flow regime. In addition, the Eulerian-Eulerian approach is computationally less expensive in comparison to the Eulerian-Lagrangian approach as an alternative. The main disadvantage of the Eulerian-Eulerian multi-phase approach is the need for closures for the exchange between the phases. Unfortunately, these closure relations are not available for all case of fluid-fluid or fluid-solid systems and they are not very accurate. So, the accuracy of this model is less than the Eulerian-Lagrangian model [37], [38], [39], [40], [41], [24].

Considering all advantages and disadvantages of the Eulerian-Eulerian and the Eulerian-Lagrangian multi-phase approaches such as accuracy, computation time, etc for dense multi-phase flows such as multi-phase flow reactors the Eulerian-Eulerian method is the best choice for the modeling [42].

2.5 Flow in porous media

2.5.1 One-phase flow in porous media

As mentioned before, packed bed reactors which contain stationary particles are an example of one-phase or multi-phase flow in porous media. Prediction of fluid flow, heat transfer, mass transfer and other transport phenomena are really important tasks of a chemical reactor designer. For the modeling of multi-phase flow reactors using the porous medium approach two approaches exist. The first one is a lumped parameter approach and the second one is rigorous modeling which takes into account the complex geometry of the porous medium. It is obvious that the second approach is computationally much more expensive than the first one. In the first approach the packing or porous medium is represented by some source or sink term in the conservation equations. For example, the resistance against flow caused by a porous medium can be represented by a sink term which for a single-phase is:

$$\nabla P = -\frac{\mu}{\beta}U - C\left(\frac{1}{2}\rho U|U|\right) \quad (2.11)$$

In the equation 2.11, μ is the molecular viscosity, ρ is the density, U is the velocity, β is the permeability, and C is the inertial resistance of the porous media. The Ergun equation can be used for the calculation of C and β for packed beds.

The governing equations for the porous medium approach and the Eulerian-Eulerian approach for modeling of multi-phase flow reactors are not similar. The volume fraction of the solid phase (porous media) in the porous medium approach is not a variable. In the energy equation it is possible to implement the effect of a porous medium on heat transfer by using an effective thermal conductivity, k_{eff} which is:

$$k_{eff} = \varepsilon k_f + (1 - \varepsilon)k_s \quad (2.12)$$

where ε is the porosity and k is the conductivity.

The rigorous modeling of porous media is very difficult, expensive and challenging in comparison to the lumped model. In this approach a real porous medium including complicated flow paths is considered. So, the geometry of the system in this method including solid regions and open regions is considered. Therefore, the geometry and grid generation is really difficult and complicated. In addition, this method is computationally very expensive [43] but it gives very detailed information about the flow, heat transfer, etc of the multi-phase flow systems such

as multi-phase flow reactors. This information can be very useful in design and improvement of the multi-phase flow reactors.

2.5.2 Multi-phase flow in porous media

It is also possible to model multi-phase flows with the porous medium approach. In this case the open spaces in a porous medium are filled with two or more phases. Trickle bed reactors are good examples of this case. Trickle flow regime is known as separated flow regime in porous medium. Depending on the velocity of the gas and liquid phase in a porous medium, other sub-regimes such as annular flow may exist. In the annular flow regime in a porous medium the liquid phase flows in the form of an annular film attached to the conduit walls and gas flows through the central core. In the modeling of multi-phase flow systems using the porous medium approach the interface between the separated phases (gas and liquid) is very important. So, the volume of fluid approach can be a very useful modeling approach for these cases. The separated multi-phase model in a porous medium is very demanding but it is a very useful learning tool in the modeling of multi-phase systems such as multi-phase flow reactors.

2.6 Summary

Modeling and simulation of multi-phase flow systems is very complex, challenging and computationally expensive. Modeling approaches, closure relations, etc are still a developing subject both in academy and industry. There are different methods for modeling of multi-phase flow systems. Choosing the most suitable model is a very important issue. Multi-phase flow modeling is a difficult job but it is a very useful tool to understand more about these flows.

NOMENCLATURE

ρ	density	kg/m^3
t	time	s
\vec{v}	velocity vector	m/s
S	mass source	$\text{kg/m}^3\text{s}$
P	pressure	Pa
\vec{g}	gravity acceleration vector	m/s^2
\vec{F}	force vector	N
α	volume fraction	—
m_p	mass of particle	kg
f_{hp}	force due to hydrostatic pressure	N
f_p	force due to the external pressure gradient	N
f_E	force due to an external body force	N
f_G	force due to the gravity	N
f_D	drag force	N
f_V	virtual mass force	N
f_L	lift force	N
f_B	Basset force	N
$\frac{dr_p}{dt}$	translational velocity	m/s
Γ	source term of mass	$\text{kg/m}^3\text{s}$
S_q	momentum source term	$\text{kg/m}^2\text{s}^2$
$M_{q,l}$	interface momentum exchange	—
σ_q	viscous stress tensor	N/m^2
μ	molecular viscosity	kg/ms
β	permeability	m^2
C	initial resistance	$1/\text{m}^2$
U	velocity	m/s
ε	porosity	—
k	thermal conductivity	W/mK
v_I	relative velocity	m/s
r	radius	m
V	volume	m^3
n	number of phases	—

INDICES

q	phase q
f	fluid phase (gas or liquid)
s	solid phase
eff	effective
hp	hydrostatic pressure
\mathbf{p}	external pressure gradient
G	gravity
E	external
D	drag
V	virtual mass
L	lift force
B	Basset force
p	particle

2.7 Bibliography

- [1] M. Ishii. *Thermo-Fluid Dynamic theory of Two Phase Flow*. 1975.
- [2] F.H. Harlow and J.E. Welch. Numerical calculation of time-dependent viscous incompressible flow of fluid with free surface. *Physics of Fluids*, 8:2182–2189, 1965.
- [3] C.W. Hirt. Heuristic stability theory for finite difference equations. *Journal of Computational Physics*, 2:339–355, 1968.
- [4] A.A. Amsden and F.H. Harlow. A simplified MAC technique for incompressible fluid flow calculations. *Journal of Computational Physics*, 6:322–325, 1970.
- [5] F.H. Harlow and A.A. Amsden. Numerical calculation of multi-phase fluid flow. *Journal of Computational Physics*, 17:19–52, 1975.
- [6] B.D. Nichols and C.W. Hirt. Method for calculating multi-dimensional transient free surface flows past bodies. *International conference NumShip Hydrodynamics*, 1975.
- [7] C.W. Hirt and B.D. Nichols. Volume of fluid (VOF) method for the dynamics of free boundaries. *Journal of Computational Physics*, 39:201–225, 1981.
- [8] C.W. Hirt and B.D. Nichols. Adding limited compressibility to incompressible hydrocodes. *Journal of Computational Physics*, 34:300–390, 1980.
- [9] A.D. Gosman, W.M. Pun, A.K. Runchal, D.B. Spalding, and M. Wolfshein. *Heat and mass transfer in recirculating flows*. 1969.
- [10] D.B. Spalding. The calculation of free-convection phenomena in gas-liquid mixtures. *Turbulent Buoyant Convection*, ICHMT Seminar:569–586, 1977.
- [11] D.B. Spalding. Numerical computation of multi-phase fluid flow and heat transfer. In *Taylor C. et al. recent advances in numerical methods in fluids*, pages 139–167, 1980.
- [12] D.B. Spalding. Mathematical methods in nuclear reactor thermal hydraulics. *ANS meeting on nuclear reactor thermal hydraulics*, pages 1979–2023, 1980.
- [13] D.B. Spalding. New developments and computed results. *Thesis*, Imperial College of Science and Technology, London, 1981.

-
- [14] D.B. Spalding. Computer simulation of two-phase flows with special reference to nuclear reactor systems. *Computational techniques in heat transfer*, pages 1–44, 1985.
 - [15] H.B. Stewart and B. Wendroff. Two-phase flow: Models and methods. *Journal of Computational Physics*, 56:363–409, 1984.
 - [16] C.T. Crowe. Review: Numerical models for dilute gas particle flows. *Journal of Fluid Engineering*, 104:297–303, 1982.
 - [17] C.T. Crowe and T.R. Troutt. Numerical models for two-phase turbulent flows. *Annual Review of fluid mechanics*, 28:11–43, 1996.
 - [18] C.T. Crowe, M. Sommerfeld, and Y. Tsuji. *Multi-phase flows with droplets and particles*. 1998.
 - [19] S.E. Elghobashi. Particle-laden turbulent flows: Direct simulation and closure models. *Appl. Sci. Res*, 48:301–314, 1991.
 - [20] W.J. Rider and D.B. Kothe. Stretching and rearing interface tracking methods. *Los Alamos National Laboratory*, 1995.
 - [21] M. Rudman. Volume tracking methods for interfacial flow calculations. *International Journal of Numerical Methods*, 24:671, 1997.
 - [22] G.M. Hidy and J.R. Broch. *The dynamics of aerocolloidal system*. 1970.
 - [23] M.R. Maxey and J.J. Riley. Equation of motion for a small rigid sphere in a non-uniform flow. *Physics of Fluids*, 26:883–889, 1983.
 - [24] H.A. Jakobsen, B.H. Sannaes, S. Grevskott, and H.F. Svendsen. Modeling of vertical bubble driven flows. *Ind Eng Chem Res*, 36:4052–4074, 1997.
 - [25] I. Dybkjaer. Tubular reforming and autothermal reforming of natural gas-an overview of available processes. *Fuel Proc Techn*, 42:42–107, 1995.
 - [26] J.V. Villadsen and W.E. Stewart. Solution of boundary-value problems by orthogonal collocation. *Chem Eng Sci*, 22:1483–1501, 1967.
 - [27] M.J. Prather. Numerical advection by conservation of second order moments. *Journal of Geophysical Research*, 91:6671–6681, 1986.
 - [28] S.S. Rao. *Applied numerical methods for engineers and scientists*. 2002.

- [29] M.C. Melaaen. Calculation of fluid flows with staggered and nonstaggered curvilinear nonorthogonal grids-the theory. *Numerical Heat Transfer*, 21:1–19, 1992.
- [30] M.C. Donald. Accuracy of multiply-stream, semi-lagrangian advective schemes ii. *Mon Wea Rev*, 115:1146–1450, 1987.
- [31] J.H. Ferziger and M. Peric. *Computational methods for fluid dynamics*. 1996.
- [32] J.H. Ferziger. *Numerical methods for engineering applications*. 1998.
- [33] R.W. Mac Cormack. The effect of viscosity in hypervelocity impact cratering. *AIAA*, 69:354, 1969.
- [34] D.A. Drew. Mathematical modeling of two-phase flow. *Ann. Rev. Fluid Mech*, 15:261, 1983.
- [35] K. Rietema and H.E.A van den Akker. On momentum equations in dispersed two phase system. *Int. J. Multiphase Flow*, 9:21, 1983.
- [36] G. Ahmedi. On the mechanics of incompressible multi-phase suspensions. *Adv. Water Res*, 10:32, 1987.
- [37] I. Celik. Numerical uncertainty in fluid flow calculations: Needs for future research. *ASME Jou Fluids Engineering*, 115:194–195, 1993.
- [38] J. Freitas. Editorial. Transactions of the ASME, journal of fluids engineering. *American Society of Mechanical Engineers*, 115:339–340, 1993.
- [39] B.P. Leonard and J.E. Drummond. Why you should not use hybrid, power-law or related exponential schemes for convective modeling-there are much better alternatives. *Int Jou for Numerical Methods in Fluids*, 20:421–442, 1995.
- [40] A. Sokolichin, G. Eigenberger, A. Lapin, and A. Lubbert. Dynamic numerical simulations of gas-liquid two-phase flows. Euler/Euler versus Euler/Lagrange. *Chem Eng Sci*, 52(4):611–626, 1997.
- [41] A. Sokolichin and G. Eigenberger. Applicability of the standard $k - \varepsilon$ turbulence model to the dynamic simulation of bubble columns: Part i. detailed numerical simulations. *Chem Eng Sci*, 54:2273–2284, 1999.
- [42] H.A. Jakobsen, B.H. Sannaes, S. Grevskott, and H.F. Svendsen. Modeling of vertical bubble driven flows. *Ind Eng Chem*, 36(10):4052–4074, 1997.

- [43] S.A. Logtenberg, M. Nijemeisland, and A.G. Dixon. Computational fluid dynamics simulations of fluid flow and heat transfer at the wall particle contact points in a fixed bed reactor. *Chem. Eng. Sci.*, 54:2433–2440, 1999.

THE ANSYS FLUENT MODEL

For the research presented in this thesis, Ansys Fluent is used to perform Computational Fluid Dynamics (CFD) simulations of three-phase (gas, liquid and solid) trickle bed reactors and Direct Numerical Simulation (DNS) of a two-phase (gas-solid) packed bed reactor.

In this chapter the background of the Ansys Fluent model is briefly discussed based on the documents published in the open literature.

3.1 Introduction

Ansys Fluent contains broad physical modeling capabilities for the modeling of flow, heat transfer, mass transfer, reaction and turbulence for industrial applications. These applications can be air flow over an aircraft wing, combustion, multi-phase flow reactors such as bubble column reactors, semiconductors, etc. It is possible to model one phase as well as multi-phase flows with Ansys Fluent. So, Ansys Fluent is capable of modeling three-phase trickle bed reactors as multi-phase flow reactors with all phenomena which may occur inside these reactors such as chemical reactions, heat transfer, mass transfer, evaporation, condensation, etc. Three different multi-phase approaches are available in Ansys Fluent which are: Volume of fluid (VOF) model, Eulerian-Lagrangian model and Eulerian-Eulerian model. For the modeling of a trickle bed reactor we use the Eulerian-Eulerian approach. More

details about different multi-phase approaches and their applications can be found in chapter 2.

3.2 Transport equations in Ansys Fluent

In this part, multi-phase flow equations solved by Ansys Fluent are discussed. The equations are discussed for a general case of n phase flow.

3.2.1 Conservation of mass

The conservation of mass in the Eulerian-Eulerian multi-phase approach for each phase q is:

$$\frac{1}{\rho_{rq}} \left(\frac{\partial(\alpha_q \rho_q)}{\partial t} + \nabla \cdot (\alpha_q \rho_q \vec{v}_q) \right) = \frac{1}{\rho_{rq}} \sum_{p=1}^n (\dot{m}_{pq} - \dot{m}_{qp}) \quad (3.1)$$

In the equation 3.1, ρ_{rq} is the phase reference density or the volume averaged density of the q^{th} phase in the solution domain, α_q is the volume fraction of phase q , ρ_q is the density of phase q , \vec{v}_q is the velocity of phase q , t is the time, \dot{m}_{pq} is the mass transfer from the p^{th} to the q^{th} phase, \dot{m}_{qp} is the mass transfer from the q^{th} to the p^{th} phase and n is the number of phases [1].

3.2.2 Conservation of momentum

The conservation of momentum in the Eulerian-Eulerian multi-phase approach for each phase q is:

$$\begin{aligned} \frac{\partial(\alpha_q \rho_q \vec{v}_q)}{\partial t} + \nabla \cdot (\alpha_q \rho_q \vec{v}_q \vec{v}_q) = & -\alpha_q \nabla P + \nabla \cdot \vec{\tau}_q + \alpha_q \rho_q \vec{g} + \\ & \sum_{p=1}^n (K_{pq}(\vec{v}_p - \vec{v}_q) + \dot{m}_{pq} \vec{v}_{pq} - \dot{m}_{qp} \vec{v}_{qp}) + (\vec{F}_q + \vec{F}_{lift,q} + \vec{F}_{vm,q}) \end{aligned} \quad (3.2)$$

In the equation 3.2, P is the pressure, $\vec{\tau}_q$ is the stress strain tensor of phase q , \vec{g} is the gravity vector, K_{pq} is the momentum exchange coefficient between two fluids or a fluid and solid, \vec{v}_{pq} is the interphase velocity, \dot{m}_{pq} is the mass transfer from the p^{th} to the q^{th} phase, \dot{m}_{qp} is the mass transfer from the q^{th} to the p^{th} phase, \vec{F}_q includes all external body forces except gravity, $\vec{F}_{lift,q}$ is the lift force and $\vec{F}_{vm,q}$ is the virtual mass force [1].

3.2.3 Conservation of energy

The conservation of energy in the Eulerian-Eulerian multi-phase model for the q^{th} phase is:

$$\begin{aligned} \frac{\partial(\alpha_q \rho_q h_q)}{\partial t} + \nabla \cdot (\alpha_q \rho_q \vec{v}_q h_q) = & -\alpha_q \frac{\partial p_q}{\partial t} + \vec{\tau}_q : \nabla \vec{v}_q - \nabla \cdot \vec{q}_q + S_q + \\ & \sum_{p=1}^n (Q_{pq} + \dot{m}_{pq} h_{pq} - \dot{m}_{qp} h_{qp}) \end{aligned} \quad (3.3)$$

In the equation 3.3, h_q is the specific enthalpy of the q^{th} phase, \vec{q}_q is the heat flux, S_q is a source term which includes sources of enthalpy (for example chemical reaction), Q_{pq} is the heat transfer between the phases p and q and h_{pq} is the interphase enthalpy [1]. All details of the energy equation are discussed in chapter 6.

3.2.4 Conservation of species

It is possible to solve the conservation equations of chemical species in the multi-phase Eulerian-Eulerian approach using Ansys Fluent. The local mass fraction of each species Y_i^q can be calculated by solving a convection-diffusion equation for the i^{th} species. The conservation of species in the Eulerian-Eulerian multi-phase model for the q^{th} phase is:

$$\begin{aligned} \frac{\partial(\rho^q \alpha^q Y_i^q)}{\partial t} + \nabla \cdot (\rho^q \alpha^q \vec{v}^q Y_i^q) = & -\nabla \cdot (\alpha^q \vec{J}_i^q) + \alpha^q R_i^q + \alpha^q S_i^q + \\ & \sum_{p=1}^n (\dot{m}_{p^i q^j} - \dot{m}_{q^j p^i}) + \mathbb{R} \end{aligned} \quad (3.4)$$

In the equation 3.4, R_i^q is the net rate of production of homogeneous species i by chemical reaction for phase q , \dot{m}_{qjpi} is the mass transfer source between species i and j from the phase q to the phase p and \mathbb{R} is the heterogeneous reaction rate. In addition, α^q is the volume fraction for phase q and S_i^q is the rate of creation by addition from a dispersed phase to a continuous phase and \vec{J}_i^q is the diffusion flux of species i , which arises due to gradients of concentration and temperature [1].

3.3 Volume fraction equation

As mentioned before, when we consider multi-phase flows as interpenetrating continua (the Eulerian-Eulerian approach) we introduce phase volume fractions, denoted here by α_q . Volume fractions represent the space occupied by each phase. The laws of conservation of mass and momentum are satisfied by each phase individually [2], [3]. The volume fraction equation for a n phase flow can be written as:

$$\sum_{q=1}^n \alpha_q = 1 \quad (3.5)$$

3.4 Interphase momentum exchange coefficients

The momentum exchange coefficient is divided in two parts which are the fluid-fluid and fluid-solid exchange coefficients. The pressure profile in multi-phase flow systems such as trickle bed reactors is calculated from the momentum conservation equation based on these exchange coefficients. Exchange coefficients should be defined as interaction force between the phases in Ansys Fluent. In the Eulerian-Eulerian dispersed multi-phase approach, each secondary phase is assumed in the form of particles (droplets or bubbles). In multi-phase flows, if there are unequal amounts of two phases (volume fractions of two phases are not equal) the predominant fluid is recommended to be modeled as a primary phase. There are relations available in literature for the calculation of the fluid-fluid and fluid-solid exchange coefficients for multi-phase systems.

3.5 Heat transfer

In Ansys Fluent the energy for each phase q is defined via:

$$H_q = \int c_{p,q} dT_q \quad (3.6)$$

In the equation 3.6, H_q is the enthalpy of phase q , $c_{p,q}$ is the specific heat of phase q at constant pressure and T_q is the temperature of phase q .

The rate of heat transfer between two phases is a function of the temperature difference between the phases:

$$Q_{pq} = h_{c,pq}(T_p - T_q) \quad (3.7)$$

In the equation 3.7, $h_{c,pq}(=h_{c,qp})$ is the heat transfer coefficient between the p^{th} and q^{th} phases. The heat transfer coefficient is calculated based on the Nusselt number, Nu_p by:

$$h_{c,pq} = \frac{6k_p\alpha_p\alpha_qNu_p}{d_p} \quad (3.8)$$

where k_p is the thermal conductivity of the p^{th} phase. There are some correlations in literature which we can use for the calculation of the Nusselt number in different multi-phase systems. The detailed description of the calculation of the Nusselt number for both fluid-fluid and fluid-solid systems will be discussed in chapter 6.

3.6 Mass transfer

Mass transfer models available in Ansys Fluent are constant rate mass transfer, evaporation-condensation and cavitation. Any other model can be defined via user-defined functions (UDF). In the Eulerian-Eulerian approach in Ansys Fluent contributions due to the mass transfer are added to the mass, momentum, species and energy equations.

3.6.1 Constant rate mass transfer

The constant rate mass transfer model defines a positive mass flow rate per unit volume from phase p to phase q :

$$\dot{m}_{pq} = \max[0, \lambda_{pq}] - \max[0, -\lambda_{pq}] \quad (3.9)$$

where

$$\lambda_{pq} = \dot{r} \alpha_p \rho_q \quad (3.10)$$

and \dot{r} is a constant mass transfer rate.

For a phase p which includes a mixture material, constant rate mass transfer for species i of phase p is:

$$\lambda_{pq} = \dot{r} \alpha_p Y_{p,i} \rho_q \quad (3.11)$$

where $Y_{p,i}$ is the mass fraction of species i in the phase p .

3.6.2 Evaporation-condensation model

The evaporation-condensation model of Ansys Fluent is a model with a physical basis [4]. The mass transfer due to the evaporation and/or condensation can be described as follows based on the temperature regimes.

If $T > T_{sat}$:

$$\dot{m}_{e \rightarrow v} = \text{coeff} * \alpha_l \rho_l \frac{(T - T_{sat})}{T_{sat}} \quad (3.12)$$

If $T < T_{sat}$:

$$\dot{m}_{e \rightarrow v} = \text{coeff} * \alpha_v \rho_v \frac{(T - T_{sat})}{T_{sat}} \quad (3.13)$$

In the above equation $\dot{m}_{e \rightarrow v}$ represents the rate of mass transfer from the liquid phase to the vapor phase, with unit of $kg/s/m^3$. coeff is a coefficient that needs to be fine tuned. α and ρ are the phase volume fraction and density, respectively.

NOMENCLATURE

ρ	density	kg/m^3
t	time	s
\vec{v}	velocity vector	m/s
P	pressure	Pa
$\vec{\tau}_q$	the stress strain tensor of phase q	N/m^2
\vec{g}	gravity acceleration vector	m/s^2
h	enthalpy	J/kg
k	conductivity	W/mK
c_p	specific heat	J/kgK
S_q	heat source	$\text{J/m}^3\text{s}$
Y_i	mass fraction of species i	—
\vec{J}_i	diffusion flux of species i	$\text{kg/m}^2\text{s}$
R_i	reaction rate of production	$\text{kg/m}^3\text{s}$
S_i	rate of creation by other sources	$\text{kg/m}^3\text{s}$
\dot{m}	mass transfer rate	$\text{kg/m}^3\text{s}$
K	interphase momentum exchange coefficient	Ns/m
α	volume fraction	—
T_{sat}	saturation temperature	K
Q_{pq}	energy transfer between the phases	$\text{J/m}^3\text{s}$
\vec{v}_{pq}	interphase velocity	m/s
λ_{pq}	mass transfer rate	$\text{kg/m}^3\text{s}$
\dot{r}	mass transfer rate	$\text{kg/m}^3\text{s}$
$Y_{p,i}$	mass fraction of species i in phase p	—
d_p	fluid particle diameter	m
$h_{c,pq}$	heat transfer coefficient	$\text{W/m}^2\text{K}$
ρ_{rp}	mixture density	kg/m^3
H	enthalpy	J/kg
\vec{q}_q	heat flux	$\text{W/m}^2\text{s}$
\mathbb{R}	heterogeneous reaction rate	$\text{mol/m}^3\text{s}$
T	temperature	K
$\dot{m}_{e \rightarrow v}$	evaporation rate	$\text{kg/m}^3\text{s}$
Nu	Nusselt number	—
\vec{F}	force	N

INDICES

<i>i</i>	species <i>i</i>
<i>j</i>	species <i>j</i>
<i>p</i>	phase <i>p</i>
<i>q</i>	phase <i>q</i>
<i>v</i>	vapor phase
<i>l</i>	liquid phase
<i>lift</i>	lift force
<i>vm</i>	virtual mass force
<i>coeff</i>	coefficient
<i>max</i>	maximum
<i>sat</i>	saturation
<i>pq</i>	interaction between phase <i>p</i> and <i>q</i>
<i>n</i>	number of phases

3.7 Bibliography

- [1] FLUENT Incorporate, M.A Natick. *Fluent 12.06.016 Theory Guide*, 2009.
- [2] T.B. Anderson and R. Jackson. A fluid mechanical description of fluidized beds. *I and EC Fundam*, 6:527–534, 1967.
- [3] R.M. Bowen. *Theory of mixtures*. 1976.
- [4] W.H. Lee. A pressure iteration scheme for two-phase modeling. *Technical Report, Los Alamos Scientific Laboratory, Los Alamos, New Mexico*, 79:975, 1979.

CFD-BASED ANALYSIS OF FLUID FLOW IN A 2-D PACKED BED REACTOR WITH RANDOM PARTICLE DISTRIBUTION

Abstract

We performed Direct Numerical Simulation (DNS) of fluid flow in 2-D packed bed reactors with cylindrical particles of 2.9 mm and no slip wall condition. We investigated the effects of particle distribution on the flow field and radial convection in packed beds. In addition effects of the wall on the pressure drop and velocity distribution was investigated. Two different random configuration of particles are used for the simulations. The results show that walls have a significant effect on the pressure drop and for the pressure drop calculations they should be taken into account. Channeling was observed in packed beds near walls as well as in the bulk, depending on the arrangement of the particles and the porosity distribution. The axial velocity profile inside the packed bed shows that the velocity distribution is a function of the porosity and arrangement of particles. In addition the results show that in packed beds with more random distribution of particles the radial convection is higher. CFD simulations provide useful data on the flow field, channeling and pressure drop inside packed beds which can be used for improvement and further optimization of the design and operation of packed beds.

4.1 Introduction

Packed bed reactors have been widely used in numerous industrial applications for more than 70 years. They are applied in different chemical processes such as gas absorption, stripping and catalytic conversion. Although new structured catalysts and reactors have been developed, packed bed reactors will most probably be in use in the forthcoming decades, mainly because of their low costs. Hydrodynamics are very important for the design and operation of the packed bed reactors [1]. Two different numerical approaches can be found in literature to describe hydrodynamic and transport properties of packed beds.

In the first method, packed beds are treated as pseudo-homogeneous media. Modified Navier-Stokes equations are applied in conjunction with the Ergun pressure drop relation to account for the fluid-solid interaction [2], [3], [4], [5]. To govern local phenomena, overall averaged quantities are replaced by functions describing the radial change of these quantities. For example, to account for the radial porosity variation, the overall averaged porosity of the whole packed bed reactor is replaced by a function accounting for the porosity distribution along the reactor radius [4], [6], [7].

In the second approach, packed beds are simulated based on the actual packed bed geometry. This yields a detailed description of the fluid flow between the particles. In this method, no additional empirical correlation is required for the porosity distribution and interaction force between fluid and solid. In this method, the Navier-Stokes equations are applied to the void between the spheres.

The main objective of this work is to investigate the effect of particle distribution on the flow field and on the radial convection in packed beds. In addition, the other goal is understanding of the effects of the wall on the velocity field and the pressure drop in packed beds. In this research we used the second approach.

4.2 Geometry and meshing

In this work a two-dimensional packed bed of non-overlapping cylindrical particles arranged on a regular square lattice with random position perturbation was used. To provide reference for predicting the flow in a packed bed the geometry shown in Figure 4.1 is used. The packed bed contains 60×10 cylindrical particles with a diameter of $d_p = 2.9 \text{ mm}$. The two-dimensional computational domain has been

made based on the stream wise length $L_x=60d_p$ and a transverse length $L_y=10d_p$ plus the space between the particles for both directions. The average distance between the particles in streamwise and transverse directions are about 1.09 mm and 0.8 mm respectively. We make this mesh by arranging 10 particles on a square lattice spanning the width of the reactor. Next the position of each particle is randomly perturbed such that the particle stays within its square. We put 60 of these configurations next to each other in the axial direction to make the whole packed bed. The length of the reactor is 240.6 mm and the width of the reactor is 38.3 mm . The reactor consists of 600 cylindrical particles of 2.9 mm diameter. There are 70 grid nodes on the surface of each particle and the boundary layer around each particle is made of a layer of 15 cells (Figure 4.1). We use a structured mesh on the surface of the particles and an unstructured mesh in the bulk of the reactor. The number of grid nodes along the wall of the reactor is 3000 and along the inlet and outlet it is 500.

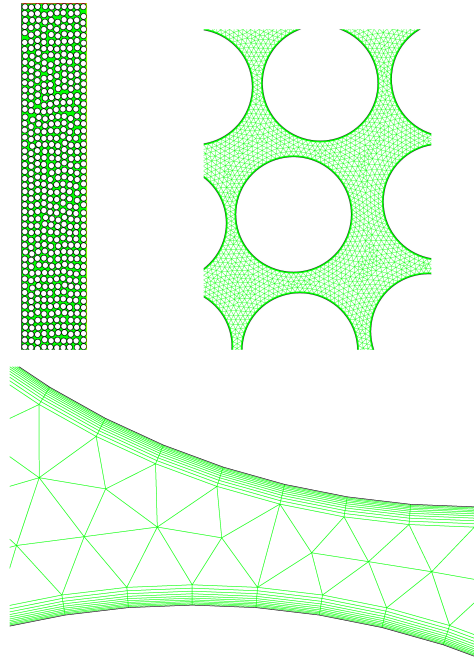


Figure 4.1: The geometry and meshing of the modeled packed bed.

4. CFD-based analysis of fluid flow in a 2-D packed bed reactor with random particle distribution

In total the whole domain consists of 1.8×10^6 grid cells. In addition, we have made two other meshes with 8×10^5 and 2.7×10^6 grid cells. We have used another configuration that was made with the same method as the first one but with only 420 particles. In this configuration we distributed the particles more randomly than the first configuration. Figure 4.1 shows the geometry of the modelled packed bed.

4.3 Model description (CFD approach)

In Computational Fluid Dynamics (CFD), numerical methods and algorithms are used to solve and analyse the fluid flow problems. To describe the 2-D flow field between the particles inside the packed bed reactor the mass and momentum conservation equations were solved. The flow through the packed bed was considered incompressible. The solid particles do not move and the void between them remains constant.

The simulations were performed under laminar flow condition [8]. Conservation of mass and momentum can be written as follows.

Mass conservation equation:

$$\frac{\partial \rho}{\partial t} + \nabla \cdot (\rho \vec{v}) = 0 \quad (4.1)$$

Equation 4.1 is the general form of the mass conservation equation and is valid for the incompressible as well as the compressible flows. In equation 4.1, ρ is the density of fluid, \vec{v} is the velocity of fluid and t is the time.

Momentum conservation equation:

$$\frac{\partial (\rho \vec{v})}{\partial t} + \nabla \cdot (\rho \vec{v} \vec{v}) = -\nabla P + \nabla \cdot \tau + \rho \vec{g} + \vec{F} \quad (4.2)$$

In equation 4.2, P is the static pressure, τ is the stress tensor, \vec{g} is the acceleration of gravity and \vec{F} includes all external body forces of the system. The stress tensor is defined as:

$$\tau = -\mu[(\nabla \vec{v} + \nabla \vec{v}^T)] - \frac{2}{3}\mu \nabla \cdot \vec{v} I \quad (4.3)$$

where μ is the molecular viscosity, I is the unit tensor and the second term on the right hand side is the effect of volume dilation [9].

The equations 4.1 and 4.2 are subject to the following boundary conditions. At the inlet of the reactor we use a velocity inlet boundary condition with constant velocity. At the outlet of the reactor we use a pressure outlet boundary condition with zero gauge pressure. We have stationary walls with no slip boundary condition. All particles are modelled as structured walls with no slip boundary condition.

All simulations have been performed with the CFD code FLUENT version 12.0.16. Meshing of the two-dimensional computational domain was performed in Gambit version 2.4.6. The governing equations were discretised by the finite volume approach. The second-order UPWIND differencing method was used for discretization of the convection terms and the SIMPLE method was applied for simultaneous solution for the pressure velocity coupled equations. Mass and momentum equations were solved in two-dimensional transient formulations. Convergence limits of the sum of the absolute residuals for all the equations were set to 10^{-5} . Unsteady simulations with a time step of 0.01 second were continued until steady state in the outlet velocity was reached. In all simulations normal Hexene (n-hexene, C_6H_{12}) at $20^\circ C$ is used as the fluid medium.

4.4 Pressure drop

Packed bed reactors have a complex geometry. A number of studies have been conducted on the flow through packed beds. For most practical problems simple and semi-empirical relationships between the pressure drop and fluid velocity have been developed [5]. The most widely used correlation which relates the pressure drop to the fluid velocity is the Ergun equation. The Ergun equation states that the pressure drop for the flow through a bed of particles with uniform size is the result of kinetics and viscous losses. Considering the packing as a series of parallel channels formed between the spheres the following expression was achieved [10]:

$$\frac{\Delta P}{L} = \frac{A_E(1-\epsilon)^2 \rho \mu v}{\epsilon^3 d_p^2} + \frac{B_E(1-\epsilon) \rho v^2}{\epsilon^3 d_p^2} \quad (4.4)$$

In equation 4.4, ΔP is the pressure drop, L is the bed length, v is the superficial fluid velocity (i.e. the volumetric flow rate divided by the cross-sectional area of the bed), ρ is the density of the fluid, μ is the viscosity of the fluid, d_p is the particle

4. CFD-based analysis of fluid flow in a 2-D packed bed reactor with random particle distribution

diameter, ε is the average porosity and A_E and B_E are the Ergun constants. The Ergun equation with the original Ergun constants ($A_E=150$ and $B_E=1.75$) applies only for packed beds with negligible wall effects. Wall effects on the pressure drop in packed beds have not received much attention. In comparison a great deal of studies has been conducted for the flow through the packing.

In all flow regimes, the pressure drop will increase due to the wall friction. So, for the calculation of the pressure drop considering wall effects the original Ergun constants ($A_E=150$ and $B_E=1.75$) are small and they should be modified. Table 4.1 provides the average values of the modified Ergun constants for cylindrical particles of different aspect ratio (length/diameter) as fitted from experimental data obtained from different sources [11], [12], [13], [14], [15].

h_p/d_p	ε	A_E	B_E	Source
0.37	0.418-0.50	280	4.6	Pahl (1975)
0.72	0.323-0.490	190	2.7	Pahl (1975)
0.91	0.336-0.588	200	2.5	Pahl (1975)
1.00	0.363	200	2.0	Reichelt (1972)
1.00	0.35	180	2.0	England (1970)
1.33	0.368-0.420	210	1.9	Damjan (2005)
1.91	0.334-0.682	210	2.5	Pahl (1975)
2.94	0.437	240	2.4	Damjan (2005)
3.81	0.402-0.492	230	2.5	Pahl (1975)
5.77	0.484-0.526	250	2.5	Damjan (2005)

Table 4.1: Ergun constants for packed beds with cylindrical particles with various aspect ration.

4.5 Results and discussion

4.5.1 Validation of the CFD simulations

The CFD simulations were validated with calculation of the pressure drop using the Ergun equation [10]. The Ergun equation with the Ergun constants of 150 and 1.75 applies only for packed beds with negligible wall effects. In packed beds the pressure drop will increase due to the additional wall friction. Therefore, for

validation of the CFD simulations considering wall effects we used a modified Ergun equation with higher Ergun constants of 210 and 2.5 respectively (Table 4.1). Validation was done for the simulations with the Reynolds number between 3 and 75 based on the particle diameter and superficial velocity of the fluid in the packed bed. The pressure drop calculated from the Ergun equation and CFD simulations are in agreement. Figure 4.2 shows the results of the pressure drop versus superficial velocity based on CFD simulations and the Ergun equation.

Pressure drops from CFD simulations are larger than the pressure drops calculated based on the Ergun equation. If the wall effects are considered in the calculation of the pressure drop the range of A_E and B_E should be between 180 to 280 and 1.9 to 4.6 respectively [11]. We fixed $A_E=210$ and $B_E=2.5$ for our calculations. The differences between the results of CFD simulations and the Ergun equation is because of rather small Ergun equation constants which we used for the validation [11].

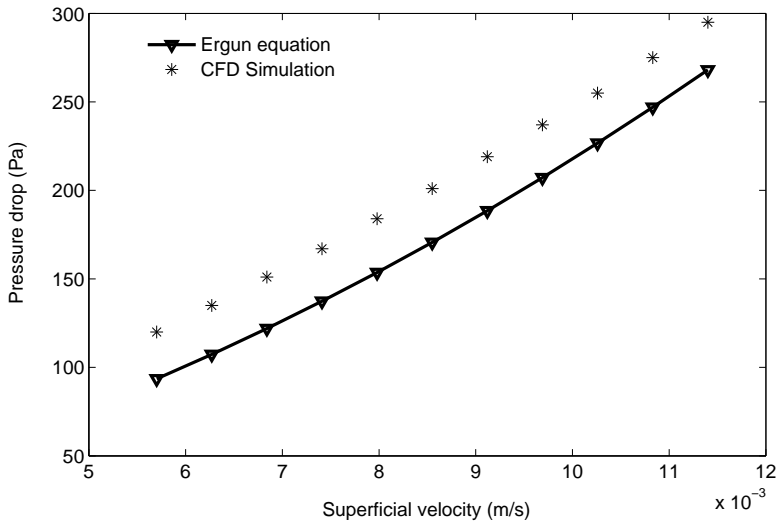


Figure 4.2: Pressure drop versus superficial fluid velocity for the modeled packed bed.

4.5.2 Velocity profile in packed beds

When fluid flows into the reactor and the fluid parcels encounter the particles they start moving in the radial direction. Radial convection inside the packed bed increases the radial mixing. The velocity profile is influenced by the walls and porosity profile. Figure 4.3 shows the axial velocity vectors inside the packed bed reactor. The velocity on the surface of the particles is zero and there is a velocity profile around each particle. Local velocities between the particles are approximately 2-8 times higher than the superficial or inlet velocity. It is clear that for our first particle arrangement the fluid tends to flow predominantly in the channels between the particles.

Figure 4.4 shows the axial velocity vectors around and between the particles in

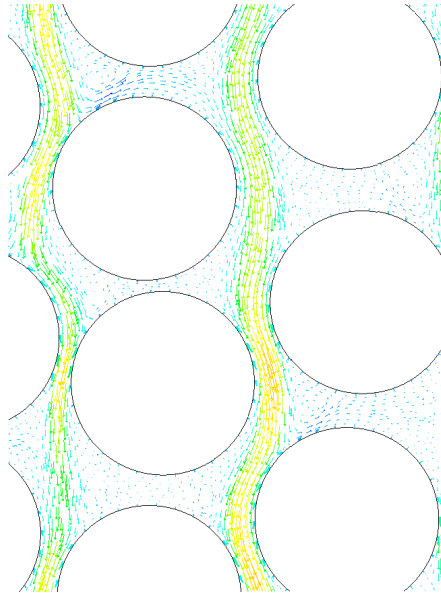


Figure 4.3: Axial velocity vectors inside the packed bed.

more detail. For a random particle distribution high velocities are observed in the region between the particles where the local porosity is high. On the contrary, local velocities are small if the local void fraction is low (Figure 4.4).

Figure 4.5 shows the axial average velocity profile in a cross section in the middle of the reactor (120 mm from the inlet) for three different superficial velocities of

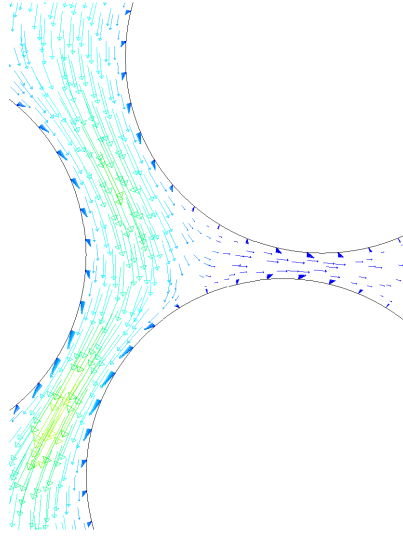


Figure 4.4: Axial velocity vectors between the particles inside the packed bed.

0.01083, 0.00627 and 0.000567 m/s with Reynolds number of 120.1, 70.7 and 6.4, respectively.

The average axial velocity is calculated by dividing the cross section in 25 intervals of equal size, for each interval the local velocity profile is averaged. The results for the average axial velocity inside the packed bed show that the average axial velocity increases from zero on the wall and small velocities near the wall towards higher velocities in the central region. The first maximum velocity is reached at approximately two particles diameter (about 5 mm) distance from the wall. The second peak appears at a distance of about four particles diameter from the wall. This result was found for the configuration that we investigated in this chapter. In general, large velocity variations can be observed within small distances (less than two particles sizes) from the wall due to the variable porosity. The local velocities fluctuate all over the packed bed depending on the arrangement of the particles and the local porosity. This indicates deviation from a flat profile i.e., plug flow on a particle size level. In addition, our study shows that the axial velocity is not constant along the packed bed reactor, and in some cases, the average velocity is substantially lower than the real local velocities.

4. CFD-based analysis of fluid flow in a 2-D packed bed reactor with random particle distribution

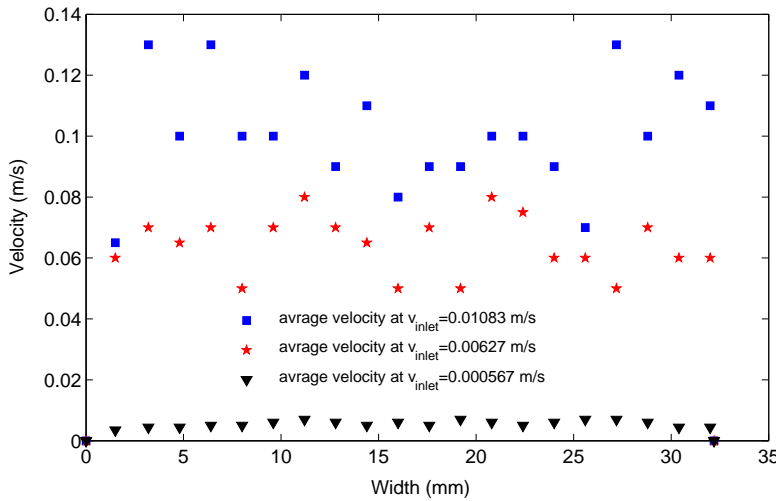


Figure 4.5: Average axial velocity inside the packed bed with three different superficial fluid velocities.

4.5.3 Channeling in packed beds

High local velocities near the wall or in the bulk of the packed bed observed in the experimental and theoretical investigations are known as wall effects or channeling. Channels of high velocity fluid are formed in packed beds in the direction of the flow. These channels reflect the original square grid used to give each particle a location. In Figure 4.6 and 4.7 the path lines (or stream lines) were shown inside the packed bed reactor near the wall or in the bulk for two different configurations of particles. These path lines show that the radial mixing or radial convection in the second configuration is larger than the first one.

For these two configurations we performed simulations with mass transfer (species transfer) to compare the radial convection. The feed of the reactor includes two species: Oxygen and Ethylene. Oxygen flows from the top right part into the reactor from a small part of the inlet (less than 10% of the whole inlet) and Ethylene flows from rest of the inlet. The mole fraction of Oxygen is shown in Figure 4.6 and 4.7 for the whole reactor for the two configurations. In the second configuration we reach to a constant mole fraction of Oxygen (in the radial direction) in a shorter distance from the inlet than the first one. So, the radial mixing in the second configuration is more than the first configuration.

For an almost regular geometry (Figure 4.6) channeling is observed more than for an irregular geometry (Figure 4.7). For a regular geometry channeling is structured near the wall or between the particles (Figure 4.6). For an irregular geometry, channeling is not structured but exists inside the packed bed reactor (Figure 4.7). The length of the channels in an irregular configuration of particles is smaller than in a regular or less random configuration of particles. Channeling depends on the arrangement of the particles. If the particles are arranged linear the probability of channeling is obviously higher than for a more random arrangement of the particles.

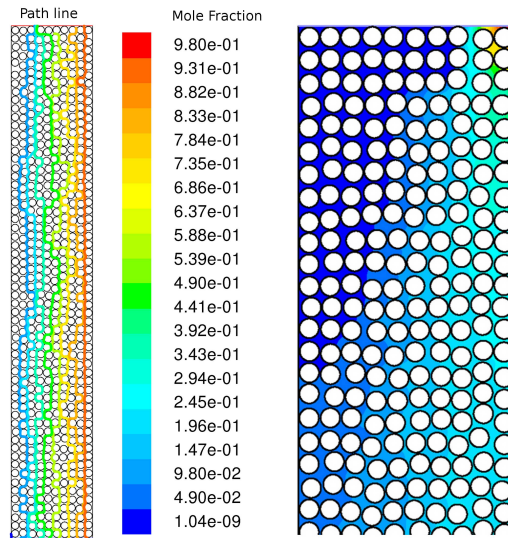


Figure 4.6: Path lines and distribution of Oxygen inside the packed bed with almost regular configuration.

In the regions with channeling inside the packed bed, the residence time of the fluid is smaller than the regions without channeling. A small residence time can affect the production rate of desired or undesired products from a reaction. With a shorter residence time it will not be possible to reach to the desired amount of product. This is the main disadvantage of the channeling in the packed bed. The other parameter which channeling can have effect on, is the radial dispersion. If a packed bed reactor suffers from channeling, it means that fluid mainly flows

4. CFD-based analysis of fluid flow in a 2-D packed bed reactor with random particle distribution

between the particles (Figure 4.6) along the reactor without propagation in the radial direction. So, the packed bed reactor has a weak radial dispersion. This is the other disadvantage of channeling. The radial dispersion can be very important in reactive flows in packed beds. The comparison of Figure 4.6 and 4.7 shows that in a packed bed with more random configuration the radial convection will be higher. In other words the dead zones in a packed bed with random distribution of particles will be less due to more radial convection.

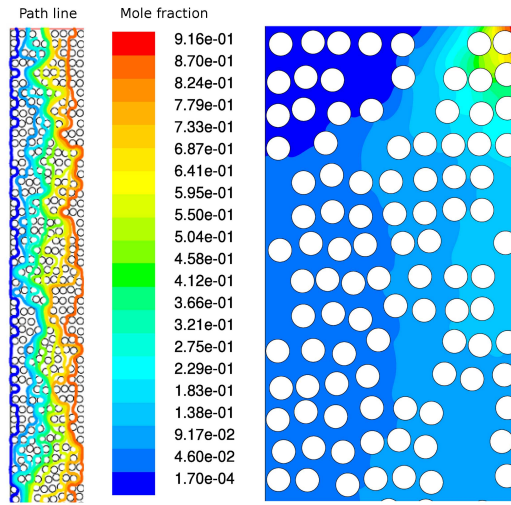


Figure 4.7: Path lines and distribution of Oxygen inside the packed bed with irregular configuration.

4.6 Grid independency

We tested the grid dependency of our CFD simulations by using three different meshes. The mesh sizes were 8×10^5 , 1.8×10^6 and 2.7×10^6 (1/2 : 1 : 3/2) grid cells respectively. Figure 4.8 shows the pressure drop of the bed at three mesh resolutions. The difference of calculated pressure drop from these three meshes are rather small. For our simulations we selected the mesh size of 1.8×10^6 and we used this grid size for the research presented in this chapter [16].

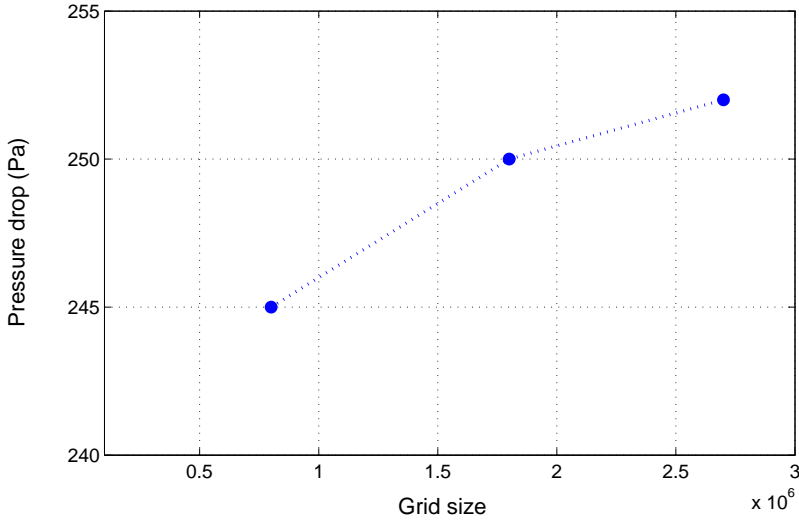


Figure 4.8: Pressure drop of packed beds for various meshes resolution.

4.7 CONCLUSIONS

In this work the flow field and pressure drop inside packed beds with random configuration of particles is studied using CFD. The axial velocity profile inside the packed bed shows that the velocity distribution is a function of voidage and arrangement of particles. In regions where the porosity is higher, the local velocity is also higher in comparison to the regions with lower porosity. Inside the packed bed average axial velocity profiles were calculated using the local velocities. The average axial velocity is low near the wall and getting high in regions far from the wall. But high local velocities near the wall or low local velocities in the bulk of the packed bed were observed. This indicates deviation from plug flow on a particle size level.

Channeling was observed inside the packed bed near the wall or in the bulk depending on the void fraction and arrangement of particles. In the channels between the particles the fluid velocity can be much higher than the superficial velocity.

4. CFD-based analysis of fluid flow in a 2-D packed bed reactor with random particle distribution

Channeling inside the packed bed mostly happens when the particles are distributed in a line along the reactor.

For validation of the simulations the Ergun pressure drop correlation is used. In applying the Ergun equation to calculate the pressure drop in packed beds with wall effects the Ergun constants should be modified. So, we used different Ergun constants ($A_E=210$ and $B_E=2.5$) than the original ones ($A_E=150$ and $B_E=1.75$). Comparing the CFD simulation results with the Ergun equation shows that the CFD simulations predict the pressure drop well. In addition, the wall of packed beds has a significant effect on the pressure drop and its effect cannot be neglected.

The developed CFD-based approach provides knowledge that is often difficult to obtain experimentally and can contribute to improve the design of packed beds. Furthermore, CFD simulations can be easily extended to account for the mass and heat transfer phenomena. With taking heat and mass transfer into account we are able to analyse packed beds with the effects of radial convection on heat and mass transfer.

Acknowledgement

The authors would like to thank Shell Global Solutions International B.V, Amsterdam for the financial support.

NOMENCLATURE

t	time	s
P	pressure	Pa
v	velocity	m/s
g	gravitational acceleration	m/s^2
F	force	N
d_p	particle diameter	m
L	length	m
I	unit tensor	—
A_E	Ergun constant	—
B_E	Ergun constant	—
h_p	particle height	m
ρ	density	kg/m^3
μ	molecular viscosity	$Pa.s$
τ	stress tensor	N/m^2
ε	porosity	—
x	x direction	—
y	y direction	—

4.8 Bibliography

- [1] H.P.A. Calis, J. Nijenhuis, B.C. Paikert, F.M. Dautzenberg, and C.M van den Bleek. CFD modelling and experimental validation of pressure drop and flow profile in a novel structured catalytic reactor packing. *Chemical Engineering Science*, 56:1713–1720, 2001.
- [2] J.N. Papageorgiou and G.F. Froment. Simulation models accounting for radial voidage profiles in fixed-bed reactors. *Chemical Engineering Science*, 56:3043–3056, 1995.
- [3] O. Bey and G. Eigenberger. Fluid flow through catalyst filled tubes. *Chemical Engineering Science*, 52:1365–1376, 1997.
- [4] M.K. Rottschfer and D. Vortmeyer. Measured and modeled superficial flow profiles in packed beds with liquid flow. *AIChE Journal*, 44:484–490, 1998.
- [5] M. Winterberg and E. Tsotsas. Impact of tube to particle diameter ratio on pressure drop in packed beds. *AIChE Journal*, 46:1084–1088, 2000.
- [6] G.E. Muller. Prediction of radial porosity distributions in randomly packed fixed beds of uniformly sized spheres in cylindrical containers. *Chemical Engineering Science*, 46:706–708, 1991.
- [7] A. de Klerk. Voidage variation in packed beds at small column to particle diameter ratios. *AIChE Journal*, 49:2022–2029, 2003.
- [8] M. Rhodes. *Introduction to particle technology*. 2008.
- [9] FLUENT Incorporate, Natick, MA. *Fluent 12.06.016 Theory Guide*, 2009.
- [10] S. Ergun. Fluid flow through packed columns. *Chem. Eng. Prog*, 48:89–94, 1952.
- [11] N. Damjan and J. Levec. Flow through packed bed reactors: 1. single-phase flow. *Chemical Engineering Science*, 60:6947–6957, 2005.
- [12] M.H. Pahl. Über die kennzeichnung diskret disperser systeme und die systematische variation der einugren zur ermittlung eines allgemeingltigeren widerstands-gesetzes der porenstrmung. 1975.
- [13] W. Reichelt. Zur berechnung des druckverlustes einphasig durchstrmter kugel- und zylinder-schttungen. *Chemie Ingenieur Technik*, 44:1068–1071, 1972.

- [14] R. England and D.J. Gunn. Dispersion, pressure drop and chemical reaction in packed beds of cylindrical particles. *Transactions of the Institution of Chemical Engineers*, 48:265–275, 1970.
- [15] Nian-Sheng Cheng. Wall effects on pressure drop in packed beds. *Powder Technology*, 210:261–266, 2011.
- [16] F. Mousazadeh, H.E.A. van den Akker, and R.F. Mudde. Eulerian simulation of heat transfer in a trickle bed reactor with constant wall temperature. *Chemical Engineering Journal*, 207-208:675–682, 2012.

4. CFD-based analysis of fluid flow in a 2-D packed bed reactor with random particle distribution

DIRECT NUMERICAL SIMULATION OF AN EXOTHERMIC GAS-PHASE REACTION IN A PACKED BED WITH RANDOM PARTICLE DISTRIBUTION

Abstract

We performed Direct Numerical Simulation (DNS) of an exothermic gas-phase reaction under laminar flow condition in a 2-D packed bed reactor with random distribution of cylindrical particles of 2.9 *mm* diameter. The reaction used in this work is of Arrhenius type between Ethylene and Oxygen with Ethylene Oxide as product. The gas flows into the reactor as a mixture of Ethylene and Oxygen. The simulations show that there is a region in the reactor with high reaction rate where basically all heat is produced. There is a large temperature gradient in this region in the radial direction and in the other parts of the reactor there is no temperature gradient in the radial direction. There is not a big convection term in the radial direction in the modeled packed bed. This rather small convection in the radial direction is the result of the arrangement of the particles. CFD simulations provide useful data on the flow field and radial convective term inside the packed beds which can be used for the improvement and further optimization on the design and operation of the packed bed reactors.

5.1 Introduction

Packed bed reactors have been widely used in numerous industrial applications for more than 70 years. They are applied in different chemical processes such as gas absorption, stripping and catalytic conversion. Although new structured catalysts and reactors have been developed, packed bed reactors will most probably be still in use in the forthcoming decades, mainly because of their low costs. Radial dispersion of mass and heat are of crucial importance for the design and operation of the packed bed reactors. Heat and mass are transferred in the radial direction in packed beds in two ways: molecular diffusion and convection [1], [2],[3]. When the gas flows into a packed bed and encounters the particles it moves in the radial direction and transfers mass and heat in the radial direction. The heat transfers effectively in the radial direction if there is a high convective term in the radial direction [4].

Two different numerical approaches can be found in literature to describe hydrodynamics and transport properties of packed beds. In the first method, packed beds are treated as a pseudo-homogeneous media, where modified Navier-Stokes equations are applied in conjunction with the Ergun pressure drop calculation to account for the fluid-solid interaction [5],[6],[7], [8]. To govern local phenomena, overall averaged quantities are replaced by functions describing the radial change of these quantities. For example, to account for the radial porosity variation, the overall averaged porosity of the whole packed bed reactor is replaced with a function accounting for the porosity distribution in the radial direction. Different empirical correlations have been developed for the radial porosity profiles and their application may result in large differences in the radial porosity profiles, especially in the case of packed beds with moderate tube/particle diameter ratios, thus leading to substantially different radial velocity profiles [7],[9], [10].

In the second approach, packed beds are simulated based on the consideration of the actual packed bed geometry. This yields a detailed description of the fluid flow and species distribution between the particles. In this method, no additional empirical correlation is required for the porosity distribution. To solve the fluid flow between particles, two different methods are used. The first one is the Lattice Boltzman Method (LBM). Freund [11] calculated the local velocity and the pressure drop in irregular arrangements of spheres in cylindrical containers with the Lattice Boltzman Method and the simulation results were in good agreement with the experimental data. In the second method, the Navier-Stokes equations are applied to the void between the spheres. In the work of Calis [1], the local velocity field in

both a regular and irregular configuration of spheres was studied in rectangular containers for tube to particle diameter ratio up to four. Furthermore, Dixon [12] investigated the relationship between the local flow field and the local wall heat flux in a packed bed of spheres. Kloker [13] studied the mass transfer phenomena for the different flow rates in spherical geometries. In our investigation we use the actual packed bed geometry.

The objective of this work is to investigate the effects of the velocity field or radial convection on the heat transfer in the radial direction in packed beds with an exothermic reaction in the gas phase.

5.2 Geometry and meshing

In this work a two-dimensional packed bed of non-overlapping cylindrical particles arranged on a regular square lattice with random position perturbation was used. To provide reference for predicting the flow and heat transfer in a packed bed the geometry shown in figure 5.1 is modeled. The packed bed contains 60×10 cylindrical particles with a diameter of $d_p = 2.9 \text{ mm}$. The two-dimensional computational domain has been made based on the streamwise length $L_x = 60d_p$ and a transverse length $L_y = 10d_p$ plus the space between the particles for both directions. The average distance between the particles in streamwise and transverse directions are about 1.09 mm and 0.8 mm respectively [14], [15]. We make this mesh by arranging 10 particles on a square lattice spanning the width of the reactor. Next the position of each particle is randomly perturbed such that the particle stays within its square. We put 60 of these configurations next to each other in the axial direction to make the whole packed bed. The length of the reactor is 240.6 mm and the width of the reactor is 38.3 mm . The reactor consists of 600 cylindrical particles of 2.9 mm diameter. There are 70 grid nodes on the surface of each particle and the boundary layer around each particle is made by a layer of 15 cells (figure 5.1). We use a structured mesh on the surface of the particles and an unstructured mesh in the bulk of the reactor. The number of grid nodes along the wall of the reactor is 3000 and along the inlet and outlet it is 500. We have considered mesh refinement at the surface of the wall. In total the whole domain consists of 1.8×10^6 grid cells. In addition, we have made two other meshes with 8×10^5 and 2.7×10^6 grid cells. Figure 5.1 shows the geometry of the modeled packed bed.

5. Direct numerical simulation of an exothermic gas-phase reaction in a packed bed with random particle distribution

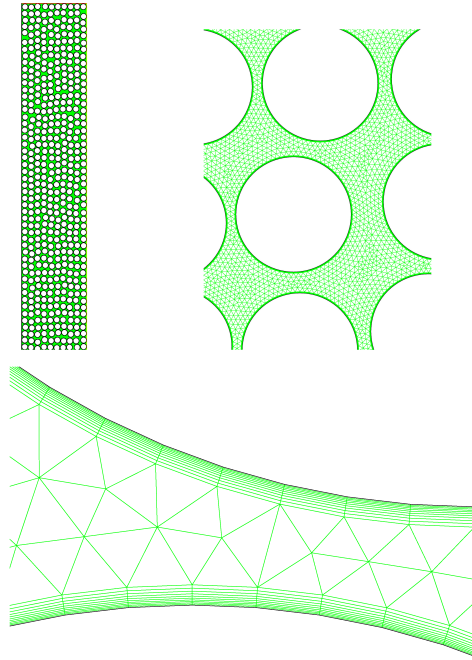


Figure 5.1: The geometry and meshing of the modeled packed bed.

5.3 Model description

5.3.1 CFD approach

In Computational fluid dynamics (CFD), numerical methods and algorithms are used to solve and analyse the problems that involve fluid flows. To describe the 2-D flow field between the particles inside the packed bed reactor the momentum and the continuity equations were solved. The flow through the packed bed was considered incompressible. The solid particles do not move and the void between them remains constant. The simulation was performed under laminar flow condition with a Reynolds number of 3.5 based on the particle diameter and interstitial velocity (v_{inlet}/ϵ). The equation of conservation of mass, momentum, energy and species can be written as follows.

Mass conservation equation:

$$\frac{\partial \rho}{\partial t} + \nabla \cdot (\rho \vec{v}) = 0 \quad (5.1)$$

Equation 5.1 is the general form of the mass conservation equation and is valid for incompressible as well as compressible flows. In the equation 5.1, ρ is the density of the fluid, \vec{v} is the velocity of the fluid and t is the time.

Momentum conservation equation:

$$\frac{\partial(\rho \vec{v})}{\partial t} + \nabla \cdot (\rho \vec{v} \vec{v}) = -\nabla P + \nabla \cdot \bar{\bar{\tau}} + \rho \vec{g} + \vec{F} \quad (5.2)$$

where P is the static pressure, $\bar{\bar{\tau}}$ is the stress tensor, \vec{g} is the gravity vector and \vec{F} includes all external body forces of the system. For our case there is no external body forces, so \vec{F} is zero.

The stress tensor $\bar{\bar{\tau}}$ is defined as:

$$\bar{\bar{\tau}} = -\mu[(\nabla \vec{v} + \nabla \vec{v}^T)] - \frac{2}{3}\mu \nabla \cdot \vec{v} I \quad (5.3)$$

where μ is the molecular viscosity and I is the unit tensor. The second term on the right hand side ($\frac{2}{3}\mu \nabla \cdot \vec{v} I$) is the effect of volume dilation which is zero in our system [16].

Energy conservation equation:

$$\frac{\partial(\rho h)}{\partial t} + \nabla \cdot (\rho \vec{v} h) = -\nabla \cdot (k \nabla T - \sum_{i=0}^N h_i \vec{J}_i) + S_h \quad (5.4)$$

where ρ is the density, t is the time, h is the enthalpy, \vec{v} is the velocity, k is the thermal conductivity of the fluid, c_p is the specific heat, h_i is the enthalpy of species i , \vec{J}_i is the diffusion flux of species i , T is the temperature and S_h is the heat source term due to the chemical reaction.

Conservation equation of species:

$$\frac{\partial(\rho Y_i)}{\partial t} + \nabla \cdot (\rho \vec{v} Y_i) = \nabla \cdot (\vec{J}_i) + R_i + S_i \quad (5.5)$$

5. Direct numerical simulation of an exothermic gas-phase reaction in a packed bed with random particle distribution

where ρ is the density, Y_i is the mass fraction of species i , \vec{v} is the velocity, t is the time, R_i is the net rate of production of species i by a chemical reaction and S_i is the rate of creation by any source. An equation of this form will be solved for $N-1$ species where N is the total number of chemical species present in the system. Since the mass fraction of the species should be 1, the N^{th} mass fraction is determined as one minus the sum of the $N-1$ solved mass fractions.

In Equation 5.5, \vec{J}_i is the diffusion flux of species i , which arises due to gradients of concentration and temperature. We used the Fick's law to model mass diffusion due to the concentration gradients, and the diffusion flux can be written as:

$$\vec{J}_i = -\rho D_{i,mix} \nabla Y_i - D_{T,i} \frac{\nabla T}{T} \quad (5.6)$$

where $D_{i,mix}$ is the mass diffusion coefficient for species i in the mixture, ρ is the density, Y_i is the mass fraction of species i , T is the temperature and $D_{T,i}$ is the thermal diffusion coefficient for species i in the mixture. For the calculation of $D_{i,mix}$ and $D_{T,i}$ we used the kinetic theory [17], [18]. In equation 5.6, $D_{i,mix}$ and $D_{T,i}$ are functions of temperature and concentration of species in the mixture. In addition, ρ is constant in equation 5.6.

The source of chemical species i due to the reaction is computed as of the Arrhenius type reaction:

$$R_i = M_{W,i} \hat{R}_i \quad (5.7)$$

where R_i is the Arrhenius mass rate of creation or destruction in the bulk of the fluid, $M_{W,i}$ is the molecular weight of species i and \hat{R}_i is the Arrhenius molar rate of creation or destruction of species i due to the reaction. In equation 5.7, $M_{W,i}$ is constant for each species and \hat{R}_i is a function of temperature and concentration of each species.

The equations 5.1, 5.2, 5.4 and 5.5 are subject to the following boundary conditions. At the inlet of the reactor we used the velocity inlet boundary condition with constant velocity. At the outlet of the reactor we used a pressure outlet boundary condition with zero gauge pressure. We have stationary walls with no slip boundary condition. The walls of the reactor are insulated and there is no heat transfer between the walls and the fluid. All particles are modeled as structured walls with no slip boundary condition. All particles are insulated and there is no heat transfer between particles and the fluid. Ethylene and Oxygen flow into the reactor as a mixture of gas with a mass fraction of 0.7 for Ethylene and 0.3 for Oxygen. The inlet velocity and temperature are 0.01 m/s and 450 K, respectively.

All simulations have been performed with the CFD code FLUENT version 12.0.16.

Meshing of the two-dimensional Cartesian computational domain was performed in Gambit version 2.4.6. The governing equations were discretised by the finite volume approach. The second-order UPWIND differencing method was used for discretization of the convection terms and the SIMPLE method was applied for simultaneous solution for the pressure velocity coupled equations. Mass and momentum equations were solved in two-dimensional transient formulations. Convergence limits of the sum of the absolute residuals for all the equations were set to 10^{-5} . Unsteady simulations with time step of 0.01 second were continued until steady state in the outlet velocity was reached. We are interested in final steady-state solution and this time step was used to reach to the final steady state solution. There is a fast reaction in the system and if transient calculations are points of interest, the simulations should have performed with much smaller time steps.

5.3.2 Reaction

The reaction which we used for our simulations is the reaction between Ethylene and Oxygen which produces Ethylene Oxide as the product. The reaction is a volumetric reaction of Arrhenius type with reaction order one. We assumed a reaction in the gas phase and not a catalytic reaction. For catalytic reaction deactivation of the catalyst in high temperature should be taken into account.



$$-\hat{R}_{C_2H_4} = 2.66 \times 10^{13} \exp\left(\frac{-15107}{T}\right) C_{C_2H_4} \quad (5.9)$$

where C_2H_4 is Ethylene, O_2 is Oxygen, C_2H_4O is Ethylene Oxide, \hat{R} is the molar rate of reaction, T is the temperature (in K) and C is the concentration.

The table 5.1 shows the physical and chemical properties of the fluid and species.

5. Direct numerical simulation of an exothermic gas-phase reaction in a packed bed with random particle distribution

Parameter	Unit	Ethylene	Oxygen	Gas mixture
Molecular weight	gr/mol	28	32	mixing law
Density	kg/m^3	1.137	1.29	incompressible ideal gas
Specific heat	$J/kg.k$	$-225 + 8.3T - 0.01T^2$	$834 + 0.29T$	mixing law
Thermal conductivity	$W/m.k$	0.0454	0.0454	0.0454
Mass diffusivity	m^2/s	2.8×10^{-5}	2.8×10^{-5}	kinetic theory

Table 5.1: Material properties of Ethylene, Oxygen and gas mixture.

5.4 Results and discussion

5.4.1 Velocity profile in the packed bed

When the gas flows into the reactor and the gas parcels encounter the particles they start moving in the radial direction and radial convection inside the packed bed

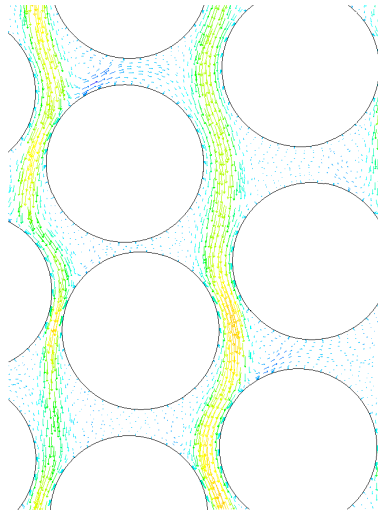


Figure 5.2: Axial velocity vectors inside the packed bed.

may develop increasing the radial mixing. The velocity profile is influenced by the walls and porosity profile. The velocity on the surface of the particles is zero and there is a velocity profile around the particles. Local velocities between the particles are approximately 2-8 times higher than the superficial or inlet velocity. It is clear that the gas tends to flow predominantly in the channels between the

particles. Figure 5.2 shows the axial velocity vectors inside the packed bed reactor. Channels of high velocity are formed in the direction of the flow. These channels reflect the original square grid used to give each particle a location.

Figure 5.3 shows the axial velocity vectors around and between the particles in more detail. For a random particle distribution high velocities are observed in the region between the particles where the local porosity is high. On the contrary, local velocities are small if the local void fraction is low (Figure 5.3).

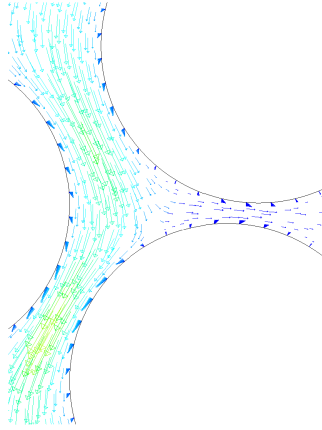


Figure 5.3: Axial velocity vectors between the particles inside the packed bed.

5.4.2 Species distribution in the packed bed

As mentioned before the feed flows into the reactor as a mixture of Ethylene and Oxygen and then they start reacting while moving through the reactor. Figure 5.4 shows the concentration of C_2H_4 as a reactant along the reactor (the dots). The reactants (C_2H_4 and O_2) start reacting just after the inlet of the reactor and the concentrations are decreasing along the reactor and at a distance of about 68 mm from the inlet the reaction is finished and the concentrations of reactants reach to zero.

At this point, it is worth mentioning that it is desirable to compare simulations with experimental data. However, we could not find detailed experimental data comparable to our case. For validation of the CFD simulation results, a one di-

5. Direct numerical simulation of an exothermic gas-phase reaction in a packed bed with random particle distribution

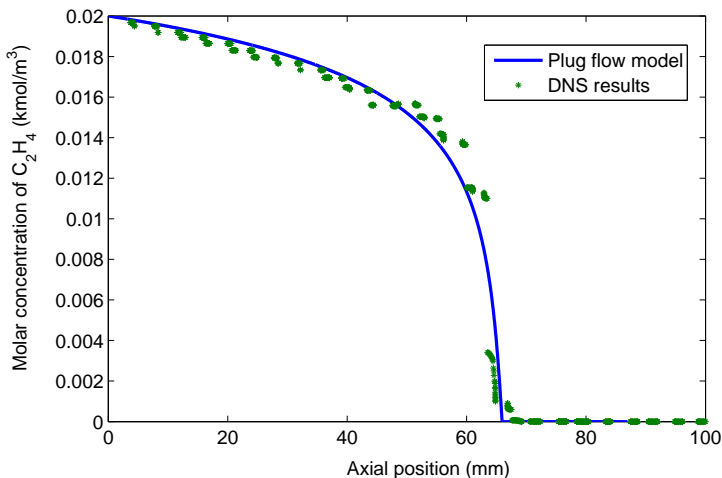


Figure 5.4: Molar concentration of Ethylene along the reactor for both the plug flow model and DNS.

mensional (1-D) model for the same Arrhenius type reaction in a plug flow reactor was constructed and solved numerically (solid line of figure 5.4). For the plug flow calculations we used a mass average velocity obtained from the CFD simulations. We computed the average velocity from three axial strips of the reactor, at a distance of 10, 20 and 30 *mm* from the right hand side wall. They more or less coincide with the location of the channels between the particles. Therefore, this computed velocity is substantially higher than the mean velocity based on the superficial velocity and the porosity (v_{inlet}/ϵ). The later is about 0.0175 *m/s*. It is obvious from figure 5.4 that such a low velocity would result in a depletion of the reactants at an axial position of about 40 *mm* from the inlet. This is also an indication that the reactants form in channels and that there are significant “dead zones” in between the particles that do hardly contribute to the reaction. From this it follows that the “dead zones” form about half of the space available for gas. This is in agreement with the velocity distribution shown in figure 5.2.

In figure 5.4 the results deviate slightly from plug flow condition. In general, the flow regime in packed beds is plug flow. This deviation is related to the velocity which we used in the plug flow model. We used the mass-weighted average velocity of entire reactor from the simulations in the calculation of the plug flow. With other methods of averaging (facet average, area-weighted average, etc) or averaging only over a line along the reactor instead of the whole reactor the results of the plug flow

model can coincide or differ from the results of the simulation shown in figure 5.4. The purpose of this 1-D model was to check the results of CFD simulations and to compare the two approaches. In this case the comparison is with a relatively simple one dimensional model of the plug flow reactor, where a simplified set of equations is solved. The high velocity required for the plug flow model indicates that the flow indeed does not mix radially. In the case of the 1-D model, it is necessary to include equations to describe the molar concentration of the reactants and temperature. The concentration of Ethylene and Oxygen reaches zero for both cases but not at the same position inside the packed bed. For the 1-D plug flow case it reaches to zero at about 65 mm from the inlet and for the CFD case about 68 mm from the inlet.

Figure 5.5 shows the concentration of Ethylene Oxide as the product along the reactor. The concentration of the product is increasing along the reactor and it obviously reaches a constant concentration exactly at the point where reactants are finished (about 68 mm from the inlet of the reactor). Then it remains constant along the reactor due to a lack of the reactants. The number of moles of consumed reactant is the same as the produced product due to the reaction. According to the figure 5.5 the results of the CFD simulation and plug flow model are in agreement.

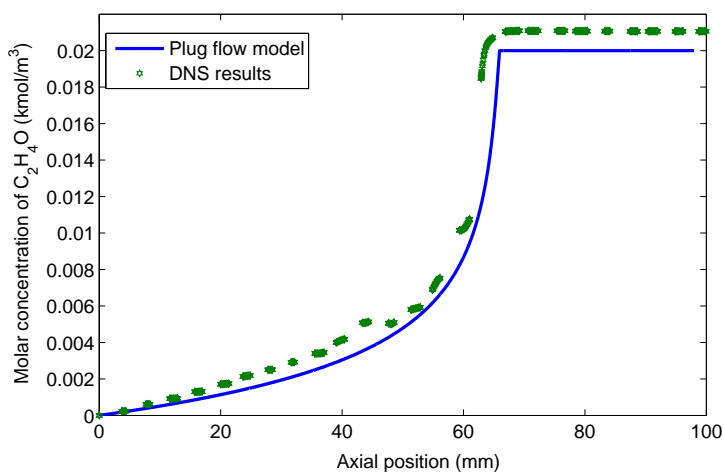


Figure 5.5: Molar concentration of Ethylene Oxide along the reactor in the middle of the reactor.

5.4.3 Temperature distribution in the packed bed

Figure 5.6 shows the temperature profile along the reactor at a distance of 10, 20 and 30 mm from the right hand side wall. Inside the reactor at the region between a distance of 55 to 60 mm from the inlet of the reactor there is a high temperature gradient in the radial direction. For example, at a distance of about 60 mm from the inlet there is a large difference between the temperature of these three lines. This temperature gradient is because of the wall effects and low convective term in the radial direction. The fluid flowing near the wall flows slower (on average) than the fluid far from the wall. So, the residence time of the fluid flowing near the wall is larger than the residence time of the fluid flowing in the bulk of the reactor and therefore the reaction and consequently the heat production should occur closer to the inlet in the wall region than in the central part of the reactor. Also, the temperature difference in the lateral direction is rather big over small distances. This shows that there is not a big radial convection in our system. This rather weak radial convection is due to the (almost) linear arrangement of the particles. Note that in the figures 5.5 and 5.6 the lines are not full lines because the particles occupy some parts of the reactor.

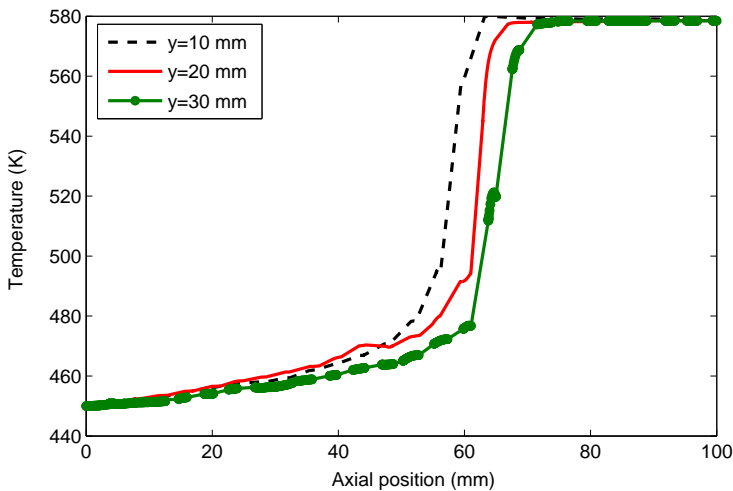


Figure 5.6: Temperature distribution along the reactor in three lines of 10, 20 and 30 mm distance from the right hand side wall.

Figure 5.7 shows the temperature contours inside the packed bed reactor. In this graph we also observe a high temperature gradient in the radial direction inside the packed bed after around 60 mm from the inlet.

In this research, the Peclet numbers for mass and heat transport, defined as vd_p/D and vd_p/α respectively, (with $D = 2.88 \times 10^{-5} m^2/s$ and $\alpha = 3.3 \times 10^{-5} - 4.9 \times 10^{-5} m^2/s$) are in the range of 1.73-22.8 and 1.96-16. So, there is not a very large axial dispersion in the system. Thus the heat produced at the distance of 60 mm from the inlet cannot transfer in the radial direction fast and we do not observe flat temperature profile in this region.

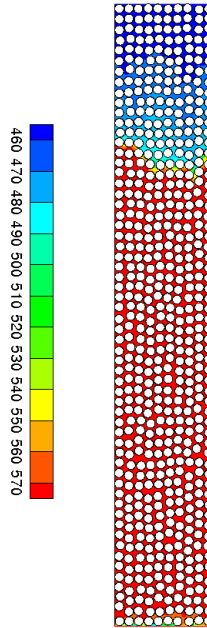


Figure 5.7: Temperature contours inside the packed bed reactor.

For validation of the temperature profile resulted from the CFD simulations, we used the plug flow model to solve the energy equation to see the temperature profile along the reactor. Figure 5.8 shows the temperature profile along the reactor for both the simple 1-D plug flow model and the CFD simulation. The temperature

5. Direct numerical simulation of an exothermic gas-phase reaction in a packed bed with random particle distribution

reaches to the maximum of 580K for both cases at around 68 mm from the inlet and the temperature distribution has the same trend for both cases.

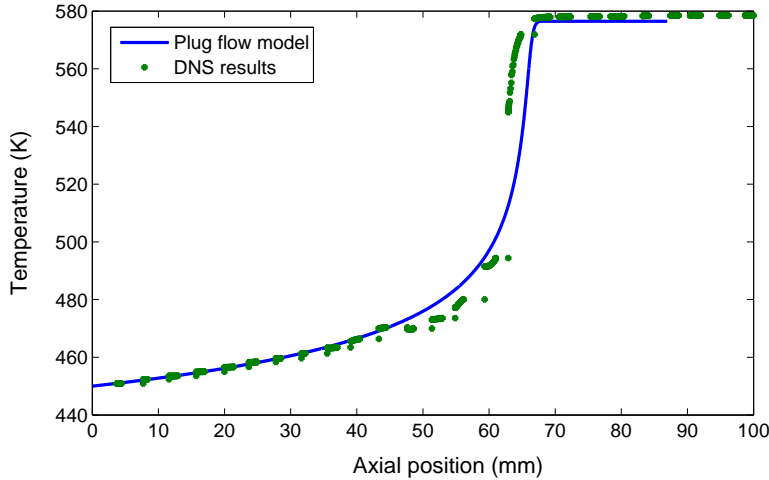


Figure 5.8: Temperature distribution along the reactor according to the CFD simulation and the simple plug flow model.

5.4.4 Grid independency

We tested the grid dependency of our CFD simulations by using three different meshes. The mesh sizes were 8×10^5 , 1.8×10^6 and 2.7×10^6 ($1/2 : 1 : 3/2$) grid cells respectively. Figure 5.9 shows the pressure drop of the bed at three mesh resolutions. For testing the grid dependency one more mesh is required with about 4×10^6 grid nodes. We tried to run the simulations with this mesh but it is computationally very expensive and we have not reached a converged solution after several months. Therefore, we performed grid independency with above mentioned three meshes. It can be seen that the difference of calculated pressure drops from these three meshes are rather small. For our simulation we selected the mesh size of 1.8×10^6 and we used this grid size for the research presented in this chapter [19].

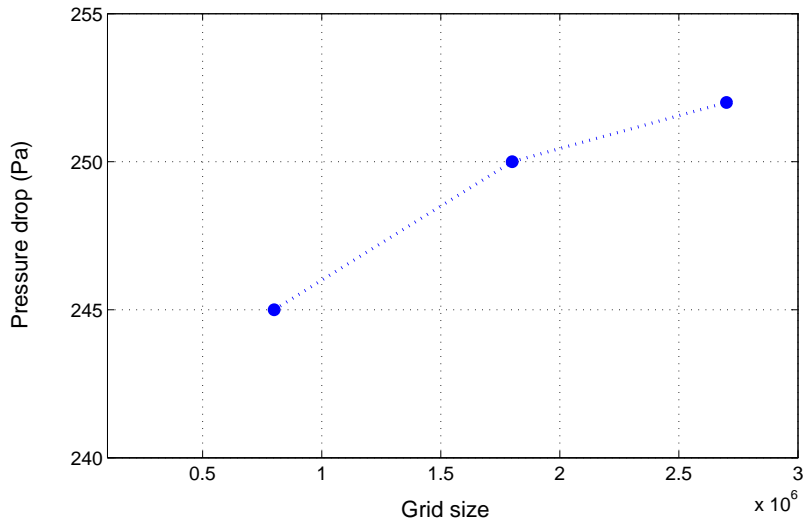


Figure 5.9: Pressure drop for various mesh resolutions.

5.5 CONCLUSIONS

In this work the flow field, based on a square lattice stacking with random perturbations, and an exothermic gas phase reaction inside a 2-D packed bed with random configuration of particles is studied using Computational Fluid Dynamics (CFD). The axial velocity profile inside the packed bed shows that the velocity distribution is a function of voidage and arrangement of the particles. In the regions where the porosity is higher, the local velocity is also higher in comparison to the regions with lower porosity. Inside the packed bed average axial velocity profiles were calculated using the local velocities. The average axial velocity is low near the wall and getting high in the regions far from the wall.

There is a region in the reactor with high reaction rate where basically all heat is produced. In this region there is a large gradient of temperature in the radial and axial direction. In the other parts of the reactor there is no temperature gradient in the radial direction. This high temperature gradient in the radial direction shows that convection in the radial direction is small in the modeled packed bed. This rather small convection in the radial direction is the result of the arrangement of the particles. The particles are distributed less randomly than in real packed bed. Future investigation can be rearrangement of the particles in a different random configuration to have higher convective term and mixing in the radial direction. The developed CFD-based approach provides knowledge that is often difficult to obtain with experiments and can contribute to improve the design of the packed beds with reacting flow. These CFD simulations provide useful data on the flow field and radial convective term inside the packed beds which can be used for the improvement and further optimization on the design and operation of the packed bed reactors.

Acknowledgement

The authors would like to thank Shell Global Solutions International B.V, Amsterdam for the financial support.

NOMENCLATURE

ρ	density	kg/m^3
t	time	s
\vec{v}	velocity vector	m/s
P	pressure	Pa
τ	stress tensor	N/m^2
\vec{g}	gravity acceleration	m/s^2
\vec{F}	force	N
μ	molecular viscosity	kg/ms
L	length	m
I	unit tensor	-
h	enthalpy	J/kg
k	conductivity	W/mK
c_p	specific heat	J/kgK
S_h	heat source	J/s
Y_i	mass fraction of species i	-
\vec{J}_i	diffusion flux of species i	kg/m^2s
R_i	reaction rate of production	kg/m^3s
S_i	rate of creation by other sources	kg/m^3s
$D_{i,mix}$	mass diffusion coefficient of species i	m^2/s
$D_{T,i}$	thermal diffusion coefficient of species i	m^2/s
\hat{R}_i	molar rate of reaction	mol/m^3s
C_2H_4	Ethylene	-
O_2	Oxygen	-
C_2H_4O	Ethylene Oxide	-
C	concentration	mol/m^3
M_w	molecular weight	gr/mol
T	temperature	K
d_p	particle diameter	m
D	mass diffusion coefficient	m^2/s
α	thermal diffusivity	m^2/s
ε	porosity	-

INDICES

<i>h</i>	heat source
<i>i</i>	species
<i>mix</i>	mixture
<i>r</i>	reaction
<i>exp</i>	exponential factor
<i>inlet</i>	inlet
<i>W</i>	weight
<i>x</i>	<i>x</i> direction
<i>y</i>	<i>y</i> direction

5.6 Bibliography

- [1] H.P. A. Calis, J. Nijenhuis, B.C. Paikert, F.M. Dautzenberg, and C.M. van den Bleek. CFD modeling and experimental validation of pressure drop and flow profile in a novel structured catalytic reactor packing. *Chemical Engineering Science*, 56:1713–1720, 2001.
- [2] T. Atmakidis and E.Y. Kenig. CFD-based analysis of the wall effect on the pressure drop in packed beds with moderate tube/particle diameter ratios in the laminar flow regime. *Chemical Engineering Journal*, 155:404–410, 2009.
- [3] Gao. Xi, Zhu Ya-Ping, and Luo Zheng-hong. CFD modeling of gas flow in porous medium and catalytic coupling reaction from carbon monoxide to diethyl oxalate in fixed-bed reactors. *Chemical Engineering Science*, 66:6028–6038, 2011.
- [4] S.T. Kolaczowski, R. Chao, S. Awdry, and A. Smith. Application of a CFD code (fluent) to formulate models of catalytic gas phase reactions in porous catalyst pellets. *Chemical Engineering Research and Design*, 85:1539–1552, 2007.
- [5] J.N. Papageorgiou and G.F. Froment. Simulation models accounting for radial voidage profiles in fixed-bed reactors. *Chemical Engineering Science*, 56:3043–3056, 1995.
- [6] O. Bey and G. Eigenberger. Fluid flow through catalyst filled tubes. *Chemical Engineering Science*, 52:1365–1376, 1997.
- [7] M.K. Rottschäfer and D. Vortmeyer. Measured and modeled superficial flow profiles in packed beds with liquid flow. *AIChE*, 44:484–490, 1998.
- [8] M. Winterberg and E. Tsotsas. Impact of tube-to-particle-diameter ratio on pressure drop in packed beds. *AIChE*, 46:1084–1088, 2000.
- [9] G.E. Muller. Prediction of radial porosity distributions in randomly packed fixed beds of uniformly sized spheres in cylindrical containers. *Chemical Engineering Science*, 46:706–708, 1991.
- [10] A. de Klerk. Voidage variation in packed beds at small column to particle diameter ratios. *AIChE*, 49:2022–2029, 2003.

5. *Direct numerical simulation of an exothermic gas-phase reaction in a packed bed with random particle distribution*

- [11] H. Freund, T. Zeiser, F. Huber, E. Klemm, G. Brenner, F. Durst, and G. Emig. Numerical simulations of single phase reacting flows in randomly packed fixed-bed reactors and experimental validation. *Chemical Engineering Science*, 58:903–910, 2003.
- [12] A.G. Dixon and M. Nijemeisland. CFD as a design tool for fixed-bed reactors. *Ind. Eng. Chem. Res*, 40:5246–5254, 2001.
- [13] M. Kloker, E.Y. Kenig, R. Piechota, S. Burghoff, and Y. Egorov. CFD-based study on hydrodynamics and mass transfer in fixed catalyst beds. *Chem. Eng. Technol*, 28:31–36, 2005.
- [14] D. Ambesi and C.R. Kleijn. Laminar forced convection heat transfer to ordered and disordered single rows of cylinders. *International Journal of Heat and Mass Transfer*, 55:6170–6180, 2012.
- [15] T. Jin, K. Luo, J. Fan, and J. Yang. Immersed boundary method for simulations of erosion on staggered tube bank by coal ash particles. *Powder Technology*, 225:196–205, 2012.
- [16] MA Natick. *Fluent 12.06.016 Theory Guide*. Ansys Inc, USA, 2009.
- [17] H.A. McGee. *Molecular Engineering*. McGraw Hill Press, New York, 1991.
- [18] K.K. Kuo. *Principles of Combustion*. John Wiley and Sons, New Jersey, 1986.
- [19] F. Mousazadeh, H.E.A. van den Akker, and R.F. Mudde. Eulerian simulation of heat transfer in a trickle bed reactor with constant wall temperature. *Chemical Engineering Journal*, 207-208:675–682, 2012.

EULERIAN SIMULATION OF HEAT TRANSFER IN A TRICKLE BED REACTOR WITH CONSTANT WALL TEMPERATURE

Abstract

This chapter reports a study of steady-state heat transfer of gas and liquid flowing through a packed bed with spherical particles of 2.06 mm and constant wall temperature with Computational Fluid Dynamics (CFD). The effect of gas and liquid flow rates on heat transfer in packed beds are discussed. The effective radial bed conductivity (λ_{er}) is calculated based on the steady-state two dimensional model. The results of the CFD simulations have been validated with experiments and they are in a good agreement. For most of the cases the results of the CFD simulations deviate from the experimental results not more than 10%. The results show that the effective radial bed conductivity increases with increase of the velocity of gas and liquid. In trickle flow regime the effective radial bed conductivity is much bigger than in a dry gas flow regime.

6.1 Introduction

Trickle bed reactors (TBRs) are multi-phase reactors consisting of a packed bed of catalyst with co-current down-flow of gas and liquid. They are used extensively for hydro-treating and hydro-desulfurization applications in the refining industry and for hydrogenation and oxidation applications in chemical industry [1]. Relatively few studies have been done on the heat transfer in TBRs in comparison to hydrodynamics and mass transfer [2]. Heat transfer characteristics and spatial temperature distributions in trickle beds are important in design and analysis of the trickle bed catalytic reactors. The principal modes of heat transfer in trickle beds are conduction, convection and radiation, which is important at high temperatures. The mechanisms of heat transfer inside trickle beds are: conduction through the particles, conduction through contact surfaces of two particles, conduction through the fluid film near the contact surface of two particles, convection in fluids and radial mixing of fluids. All these mechanisms play a role in radial heat transfer in trickle beds. The contribution of each of these methods to the overall heat transfer are linearly additive but the interaction of different heat transfer modes need to be taken into account [3], [4].

Two different numerical approaches can be found in literature to describe hydrodynamics and transport properties of trickle beds. In the first method, packed beds are treated as a pseudo-homogeneous media, where modified Navier-Stokes equations are applied in conjunction with the Ergun pressure drop calculation to account for the fluid-solid interaction [5], [6], [7], [8]. In the second approach, packed beds are simulated based on the consideration of the actual packed bed geometry. This yields a detailed description of the fluid flow and temperature between the particles [9], [10], [11].

In this chapter heat transfer in two-phase dry gas flow and three-phase flow (trickle flow) in a packed bed have been investigated by using a heterogeneous model which takes into account each phase separately: i.e. by considering that there is heat transfer between the phases. In our investigation we used the first approach. We carried out CFD simulations to investigate radial heat transfer in packed beds with dry gas flow and trickle flow (gas and liquid) condition. Then we calculated the effective radial bed conductivity from the results of the CFD simulations and evaluated our model results against experiments.

6.2 Modeling

6.2.1 Mathematical models and correlations

The effective radial bed conductivity (λ_{er}) can be expressed in terms of a static contribution (stationary gas and/or liquid), dynamic contribution (flowing gas and liquid) and other parameters such as interaction between the phases (i.e, the drag force influences the flow and thereby the heat transfer, etc). The static contribution comprises both the fluid and solid molecular contributions to heat transfer in the absence of the fluid flow. The dynamic contributions are determined by the hydrodynamics and the effects of the gas and liquid hold-up. They depend on the density and viscosity of the fluids and on the particle size. Moreover, the flow regime (laminar or turbulent) is important. We can write the effective radial bed conductivity in a three phase trickle bed reactor as [12]:

$$\lambda_{er} = \lambda_{st} + \lambda_{eg} + \lambda_{el} \quad (6.1)$$

in which λ_{er} is the effective radial conductivity of the bed, λ_{st} is the static contribution (without any flowing gas or liquid) of the radial conductivity, λ_{eg} and λ_{el} are the dynamic contributions of the radial conductivity due to the gas and liquid flow. Equation 6.1 shows that the effective radial conductivity of the bed is a function of material conductivity (solid, gas and/or liquid), hydrodynamic properties of the bed (for instance, flow regime) and shape of the catalyst.

The effective radial thermal conductivity is usually determined by evaluating a steady-state heat flux between two parallel plates separated by a packed bed. Many theoretical and experimental studies have been carried out on estimation of the effective thermal conductivity [13]. Using one-directional heat flow, Kunii and Smith [14] evaluated radial thermal conductivity of packed beds by an analytical solution. This model assumes that the heat flow paths are parallel at both microscopic and macroscopic levels.

The two-dimensional heat flow model is more realistic than the one-directional heat flow model. By assuming that a packed bed consists of a bundle of long cylinders, Krupiczka [15] found a numerical solution which gives the effective thermal conductivity of a quiescent cylindrical bed. By extending the concept to a packed bed with spherical particles, Krupiczka expressed the effective thermal conductivity of a quiescent bed of spherical particles. Blumberg and Schlunder investigated the thermal conductivity of a quiescent packed bed wetted with a binary mixture both theoretically and experimentally [16]. The model of Zehner and Bauer combines

6. Eulerian simulation of heat transfer in a trickle bed reactor with constant wall temperature

the conductivities of the wetted pores and the solid matrix to provide effective thermal conductivity for the particles as well as to predict the effective conductivity of the quiescent packed bed [17]. Zehner and Schlunder considered the effective thermal conductivity through a cylindrical unit cell containing both the solid and fluid phases. The critical part of the correlation is that Zehner and Schlunder have drawn an analogy between mass transfer experiment and thermal conduction to obtain an empirical curve to describe the effective thermal conductivity [18]. C.T. HSU and K.W. Wong [19] modified Zehner-Schlunder model for calculations of the stagnant thermal conductivity of two types of porous media with spatially periodic structures. The area contact model is developed to take into consideration finite area contacts between spheres in a packed bed. It is shown that the results based on the area contact model are in a better agreement with experimental data than those based on the original Zehner-Schlunder model specially at high ratio of solid to fluid thermal conductivity.

If the fluid flows, then the convective contribution augments the heat transfer [20],[21]. Even in the direction normal to the mean flow the convective heat transfer dominates the heat transfer. Lamine investigated hydrodynamics and radial heat transfer in packed bed reactor with co-current down-flow of gas and liquid. The effect of flow regimes, of gas and liquid flow rates and of liquid properties are discussed. Effective thermal conductivity always increases with liquid heat capacity. They proposed some correlations for different flow regimes and operating condition [22]. Other researchers have also performed experiments to develop correlations or simple models for calculation of the effective radial bed conductivity. All these models are based on radial and axial temperature distribution inside packed beds. Some investigations have been done on heat transfer in trickle bed reactors. Recently N. Habtu and F. Stuber [1] worked on heat transfer in trickle bed reactors. They analyzed the effect of operating conditions on overall and wall-to-bed heat transfer coefficient using a dynamic pseudo-homogeneous one parameter model. Their results show that the gas flow rate only marginally affects the heat transfer whereas increasing the liquid flow rate enhances the heat transfer from wall to bed. Babu and Sastry [12] used the orthogonal collocation method combined with an optimization technique, differential evolution to estimate the heat transfer parameters using radial temperature profile measurements in a gas-liquid co-current down-flow trickle bed reactor. E. Tsotsas and E.U. Schlunder [23] described heat transfer in adiabatic packed tubes using wall-to-bed heat transfer coefficient. They used a quasi-homogeneous two dimensional model which they called the standard model. Though the concept of the standard model seems to be simple, the behavior of the heat transfer coefficient at the wall from the model

compared to measurements is quite discouraging [23]. Hatta and Maeda [24],[25] correlated their data of the effective radial thermal conductivity into the form of $\lambda_{er}/k_f = aRe^b$ and obtained a and b as a function of Reynolds number. Coberly and Marshall [26], however, found that their data were best fitted using a linear function of the Reynolds number as follows:

$$\lambda_{er}/k_f = a + bRe \quad (6.2)$$

where a and b are constant, k_f is thermal conductivity of the fluid and Re is the Reynolds number based on the particle size. Smirnov and Zolotarskii performed some experiments on the effective radial thermal conductivities of cylindrical beds formed of spheres, cylinders and Rashig rings. They compared heat transfer parameters with literature data.

They proposed a model with a linear variation of λ_{er} in the vicinity of the wall

Authors	Effective radial conductivity of the bed	Experimental conditions
Bunnell et al. (1977) [27]	$\lambda_{er}/k_f = 5 + 0.06Re_p$	Glass Spheres
Bey and Eigenberger (2001) [28]	$\lambda_{er}/k_f = \lambda_{st}/k_f + 0.1Re_pPr$	Glass spheres $3.3 < D_T/d_p < 11$
Demirel et al. (2000) [29]	$\lambda_{er}/k_f = 2.894 + 0.068Re_p$	Raschig rings $5.6 < D_T/d_p < 6.6$
Demirel et al. (2000) [29]	$\lambda_{er}/k_f = 10.433 + 0.0481Re_p$	Polystyrene spheres $4.5 < D_T/d_p < 7.5$

Table 6.1: Experimental correlations for the effective radial conductivity of packed beds.

to describe the radial heat transfer in the packed bed [30]. J.T. Freire described the application of a pseudo-homogeneous mathematical model for describing heat transfer in packed beds with the oscillatory profiles of velocity and porosity using a radius-dependent model for the effective thermal conductivity [31]. In all models λ_{er} is a function of the Reynolds number. It is not possible to discuss all correlations and experiments which exist in this area in this chapter. So, we show some of them which are close to our experimental and numerical set-up in terms of operating condition, size of particles, etc in the table 6.1.

6.2.2 CFD approach

In Computational Fluid Dynamics, numerical methods and algorithms are used to solve and analyse the problems that involve fluid flows. In this work the Euler-Euler multi-phase approach has been used to solve the average mass, flow and energy equations for each phase separately as well as the volume fraction equation. In the Euler-Euler approach, the different phases are treated mathematically as interpenetrating continua. Since the volume of one phase cannot be occupied by the other phases, the concept of phasic volume fraction is introduced. The volume fractions are assumed to be continuous function of space and time and their summation is equal to one. Coupling is achieved through the pressure and interaction between the phases such as drag force and heat transfer. The transport equations of the Euler-Euler model are [32]:

Mass conservation equation:

$$\partial(\alpha_q \rho_q)/\partial t + \nabla \cdot (\alpha_q \rho_q \vec{v}_q) = \sum_{p=1}^n (\dot{m}_{pq} - \dot{m}_{qp}) + S_{mq} \quad (6.3)$$

where α_q is the volume fraction of phase q , ρ_q is the density of phase q , \vec{v}_q is the velocity of phase q , t is the time, \dot{m}_{pq} characterizes the mass transfer from the p^{th} to the q^{th} phase, \dot{m}_{qp} characterizes the mass transfer from the q^{th} to the p^{th} phase and S_{mq} is the mass source of phase q .

In the mass conservation equation all terms on the right hand side are zero because there are no mass transfer and source terms in our system.

Momentum conservation equation:

$$\partial(\alpha_q \rho_q \vec{v}_q)/\partial t + \nabla \cdot (\alpha_q \rho_q \vec{v}_q \vec{v}_q) = -\alpha_q \nabla P + \nabla \cdot \vec{\tau}_q + \alpha_q \rho_q \vec{g} + \sum_{p=1}^n (\vec{R}_{pq} + \dot{m}_{pq} \vec{v}_{pq} - \dot{m}_{qp} \vec{v}_{qp}) + \vec{F}_q + \vec{F}_{lift,q} + \vec{F}_{vm,q} \quad (6.4)$$

where P is the pressure, $\vec{\tau}_q$ is the stress strain tensor of phase q , \vec{g} is the gravity vector, \vec{R}_{pq} is the interaction force between the phases, \vec{v}_{pq} is the interphase velocity defined as follows: if $\dot{m}_{pq} > 0$ (mass transfer from the p^{th} to the q^{th} phase) then $\vec{v}_{pq} = \vec{v}_p$, if $\dot{m}_{pq} < 0$ (mass transfer from the q^{th} to the p^{th} phase) then $\vec{v}_{pq} = \vec{v}_q$, likewise if $\dot{m}_{qp} > 0$ then $\vec{v}_{qp} = \vec{v}_q$, if $\dot{m}_{qp} < 0$ then $\vec{v}_{qp} = \vec{v}_p$, \vec{F}_q includes all external

body forces, $\vec{F}_{lift,q}$ is the lift force and $\vec{F}_{vm,q}$ is the virtual mass force. $\bar{\tau}_q$ is defined as:

$$\bar{\tau}_q = \alpha_q \mu_q [(\nabla \vec{v}_q + \nabla \vec{v}_q^T)] - \frac{2}{3} \alpha_q \mu_q \nabla \cdot \vec{v}_q I \quad (6.5)$$

where μ_q is the viscosity of phase q and I is the unit tensor. The gravity force was taken into account in all simulations. The lift force and virtual mass force were neglected because they are much smaller than the drag force between the phases. There is no external body force in the system, therefore \vec{F}_q is zero. As mentioned above \vec{R}_{pq} is the interaction force between the phases and is calculated by:

$$\sum_{p=1}^n \vec{R}_{pq} = \sum_{p=1}^n K_{pq} (\vec{v}_p - \vec{v}_q) \quad (6.6)$$

where K_{pq} is the interphase momentum exchange coefficient. For gas-liquid flows, the liquid phase is assumed to form droplets. The exchange coefficient for these types of gas-liquid flows can be written in a general form:

$$K_{pq} = \alpha_q \alpha_p \rho_p f_{dr} / \tau_{par} \quad (6.7)$$

where f_{dr} , the drag function, is defined differently for different exchange coefficient models and τ_{par} is the particulate relaxation time and defined as:

$$\tau_{par} = \rho_p d_{pq}^2 / 18 \mu_q \quad (6.8)$$

where d_{pq} is the diameter of the droplets of phase q . All definitions of f_{dr} include a drag coefficient (C_D) which is based on the relative Reynolds number (Re_s). The relative Reynolds number (between gas-liquid) is defined as:

$$Re_s = \rho_l d_p |\vec{v}_s - \vec{v}_l| / \mu_l \quad (6.9)$$

For the fluid-solid exchange coefficient we used the model of Wen and Yu [33]:

$$K_{sl} = \frac{3}{4} C_D \alpha_s \alpha_l \rho_l |\vec{v}_s - \vec{v}_l| \alpha_l^{-2.65} / d_{ps} \quad (6.10)$$

where

$$C_D = \frac{24}{\alpha_l Re_s} [1 + 0.15(\alpha_l Re_s)^{0.687}] \quad (6.11)$$

6. Eulerian simulation of heat transfer in a trickle bed reactor with constant wall temperature

For the drag coefficient between gas and liquid we used the model of Schiller and Naumann [34] which is in the following form:

$$f_{dr} = C_D Re_{pq}/24 \quad (6.12)$$

where

$$C_D = 24(1 + 0.15 Re_{pq}^{0.687})/Re_{pq} \quad (6.13)$$

where Re_{pq} is the relative Reynolds number between the p^{th} and q^{th} phases. The relative Reynolds number for the primary phase p and secondary phase q is obtained from:

$$Re_{pq} = \rho_q |\vec{v}_p - \vec{v}_q| d_p / \mu_q \quad (6.14)$$

Energy conservation equation:

$$\begin{aligned} \partial(\alpha_q \rho_q H_q) / \partial t + \nabla \cdot (\alpha_q \rho_q \vec{v}_q H_q) = & -\alpha_q (\partial P_q / \partial t) + \\ \bar{\tau}_q : \nabla \vec{v}_q - \nabla \cdot \alpha_q \vec{q}_q + S_q + \sum_{p=1}^n (Q_{pq} + \dot{m}_{pq} H_{pq} - \dot{m}_{qp} H_{qp}) \end{aligned} \quad (6.15)$$

where H_q is the enthalpy of phase q , \vec{q}_q is the heat flux, S_q is the heat source, Q_{pq} is the heat exchange between the p^{th} and q^{th} phases, \dot{m}_{pq} characterizes the mass transfer from p^{th} to the q^{th} phase, \dot{m}_{qp} characterizes the mass transfer from q^{th} to the p^{th} phase and H_{pq} and H_{qp} are the interphase enthalpies (e.g., the enthalpy of the vapor in case of evaporation and enthalpy of the liquid in case of condensation). The heat flux, \vec{q}_q is defined as:

$$\vec{q}_q = -k_q \partial T / \partial \vec{r} \quad (6.16)$$

where k_q is the conductivity of each phase.

The rate of energy transfer between the phases (Q_{pq}) is assumed to be a function of the temperature difference between the phases:

$$Q_{pq} = h_{pq}(T_p - T_q) \quad (6.17)$$

where h_{pq} is the heat transfer coefficient between the p^{th} and q^{th} phase. The heat transfer coefficient is related to the p^{th} phase Nusselt number, Nu_p , by

$$h_{pq} = 6k_q \alpha_p \alpha_q Nu_p / d_p \quad (6.18)$$

Here k_q is the thermal conductivity of the q^{th} phase. The Nusselt number can be determined from many correlations in the literature. For the heat transfer between liquid and gas we used Ranz-Marshall equation [35] which for sphere is:

$$Nu_p = 2 + 0.6Re_p^{1/2}Pr_q^{1/3} \quad (6.19)$$

Re_p is the Reynolds number based on diameter of the p^{th} phase bubbles or particles and the relative velocity and Pr_q is the Prandtl number of the q^{th} phase. For the heat transfer between fluid and solid we used Gunn equation [36] which is applicable to a porosity range of 0.35 – 1 and the Reynolds number up to 10^5 [32].

$$Nu_s = (7 - 10\alpha_f + \alpha_f^2)(1 + 0.7Re_s^{0.2}Pr_f^{1/3}) + (1.33 - 2.4\alpha_f + 1.2\alpha_f^2)Re_s^{0.7}Pr_f^{1/3} \quad (6.20)$$

where α_f is the volume fraction of each fluid and Pr_f is the Prandtl number of each fluid. We used the above equation for the calculation of both the gas-solid and liquid-solid heat transfer coefficients.

Volume fraction equation:

$$\sum_{q=1}^n \alpha_q = 1 \quad (6.21)$$

The equations 6.3, 6.4, 6.15 and 6.21 are subject to the following boundary condition.

At the inlet of the reactor we used a velocity inlet boundary condition with constant velocity and temperature. At the outlet of the reactor we used a pressure outlet boundary condition with zero gauge pressure. We have stationary walls and no slip condition with constant temperature.

All simulations have been performed with the CFD code FLUENT version 12.0.16. Meshing of the two-dimensional axi-symmetric computational domain was performed in Gambit version 2.4.6. The mesh consisted of 40000 grid cells. The governing equations were discretised by the finite volume approach. The second-order UPWIND differencing method was used for discretization of the convection terms and the SIMPLE method was applied for simultaneous solution for the pressure velocity coupled equations. The flow was assumed laminar and incompressible. All mass, momentum, energy and volume fraction equations were solved in two-dimensional and cylindrical transient formulations. The solid particles are assumed to be stagnant ($v = 0$) with constant volume fraction. Convergence limits of the sum of the absolute residuals for all the equations were set to 10^{-6} . Unsteady

6. Eulerian simulation of heat transfer in a trickle bed reactor with constant wall temperature

simulations with time step of 0.001 second were continued until steady state in the outlet velocity and temperature profile was reached.

6.2.3 Packed bed reactor

The packed bed reactor system consists of the solid catalysts, with gas and liquid flowing in between them. A simple and actual schematic of the annular trickle bed reactor is illustrated in the figure 6.1.

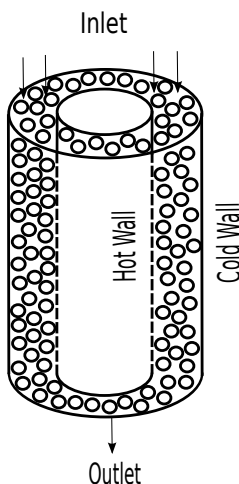


Figure 6.1: Schematic of an annular trickle bed reactor.

We did not use the actual geometry of a trickle bed reactor but an effective medium approach. So, we do not have an actual geometry of the particles and their distribution in the bed and the void fraction is the same everywhere inside the trickle bed. The gas and liquid flow from the top of the reactor co-currently. We considered glass spheres as the solid phase. The hot wall temperature is 323.15K and the cold wall temperature is 275.15-277.15K depending on the case. The temperature of the inlet gas and liquid is 298.15K. The fluid properties such as density ρ , viscosity μ and specific heat c_p are assumed to be constant. The total length of the computational domain is 100 mm and the width of the annulus is 20 mm. We have

considered two situations: a two phase (solid and gas) and a three phase (solid, gas and liquid) flow. Typical process data and liquid and gas phase properties are listed in the Table 6.2 and 6.3.

To account for the heat transfer in the radial direction we considered the conductivity of the flowing fluids as a linear function of the Reynolds and Prandtl number according to the following equation:

$$k_{fluid} = k_f + 0.1k_f Re_p Pr_f \quad (6.22)$$

where k_{fluid} is the enhanced conductivity of the fluid, k_f is the fluid conductivity, Re_p is the Reynolds number based on particle size and Pr_f is the Prandtl number of the fluid. So, we implemented a dynamic contribution as an enhanced fluid conductivity which is a function of the Reynolds and Prandtl numbers.

Parameter	Unit	Quantity
Operating pressure	<i>bar</i>	6
Operating temperature	<i>K</i>	298.15
Inlet temperature	<i>K</i>	298.15
Hot wall temperature	<i>K</i>	323.15
Cold wall temperature	<i>K</i>	275.15-277.15
Gravity	<i>N/kg</i>	9.81
Porosity	—	0.347
Particle diameter	<i>mm</i>	2.06

Table 6.2: Process data.

Parameter	Gas	Liquid	Unit
Density	1.138	742	<i>kg/m³</i>
Viscosity	1.66×10^{-5}	0.00129	<i>kg/m.s</i>
Specific heat	1040	2220	<i>J/kg.K</i>
Thermal conductivity	0.0242	0.137	<i>W/m.K</i>

Table 6.3: Property of the liquid and gas phases.

6.3 Experimental set-up

The annular heat transfer cell (AHTC) is an apparatus designed to measure heat transfer parameters of trickle flow beds under realistic operating condition. The AHTC consists of two cylindrical tubes which form an annular cylinder between them. The inner cylinder, which is heated electrically, has an outside diameter of 60 mm and the outer cylinder which is cooled with water has an inside diameter of 100 mm. The 20 mm annulus is a packed bed with catalyst or carrier particles with the gas and/or liquid flowing down co-currently. This annulus simulates a narrow tube of hydraulic diameter of 40 mm. The inlet and outlet of the AHTC measurement section is thermally isolated by separator rings to minimise axial heat losses. Furthermore at the inlet and outlet of the catalyst beds four sets of five thermocouples are used to measure the temperature. Each set of thermocouples is positioned radially 90 degrees relative to each other, while each of the five individual thermocouples of each set is positioned equidistantly from the inner wall to the outer wall and are bent upwards to face the flow direction.

The temperature of the walls were maintained constant. The gas (N_2) and liquid (n-dodecane) are supplied to the top of the bed. A special liquid distributor plate at the inlet is used to ensure uniform liquid distribution. The experiments were carried out with the glass spheres with a mean diameter of 2.06 mm and a porosity of 0.375. The operating pressure in the AHTC system in all experiments is 6 bar. The experiments were done for gas flow over dry packing and trickle flow at superficial liquid velocities of 1.49 mm/s and 4.78 mm/s.

6.4 Results and discussion

To calculate the effective radial conductivity of the bed we write Fourier's law for a packed bed in the radial direction considering λ_{er} as the effective radial bed conductivity which includes all heat transfer phenomena (conduction in all phases, heat transfer between the phases, heat transfer due to dynamic contribution, etc) between hot and cold wall:

$$\varphi = -\lambda_{er}(2\pi rL)(\partial T/\partial r) \quad (6.23)$$

where φ is the heat flow from hot wall to cold wall, λ_{er} is the effective radial conductivity of the bed, T is the temperature, r is the radius and L is the length of the

reactor.

For calculation of λ_{er} from the experimental results the average temperature at five radial positions were determined. The temperature in the bed at each of five radial positions is the average of eight thermocouples (four in the upper part of the bed and four in the lower part of the bed). If the above equation is integrated, then we have:

$$T(r) = (-1/\lambda_{er})(\varphi \ln r / 2\pi L) + \text{const} \quad (6.24)$$

For calculation of λ_{er} , $\varphi \ln r / 2\pi L$ should be evaluated for radial positions. We have φ from the heat load of the heating apparatus which is in the centre of the annular heat transfer cell, so we determine the slope of the curve from the equation 6.24.

For calculation of λ_{er} from the simulation results we used the same technique. We used the average φ of the hot and cold wall resulting from the simulations to calculate λ_{er} .

The result section is split in two parts: dry gas flow (two-phase flow) and trickle flow (three-phase flow).

6.4.1 Two-phase dry gas flow (solid and gas)

The first part of the results includes the results for the two-phase flow (dry gas flowing through the packed bed reactor). The experiments and CFD simulations were done for various gas fluxes which were in the range of $0.3080 \text{ kg}/\text{m}^2\text{s}$ to $3.62 \text{ kg}/\text{m}^2\text{s}$.

Figure 6.2 illustrates the axial velocity profile inside the reactor for minimum mass flux of gas for steady-state conditions from simulations. The flow regime inside the reactor is close to plug flow. The Reynolds number based on particle size and interstitial velocity is in the range of 60 to 700. This means that there is not a fully laminar flow condition in the packed bed [37]. So, the packed bed is in transient condition (not fully laminar and not fully turbulent) but closer to the laminar flow than the turbulent flow. Therefore, there is not a very high heat transfer rate in the radial direction due to the average convective term. As mentioned before we enhanced the conductivity of the fluid to describe the increased heat transfer in the radial direction. With increasing the conductivity of the fluid we also enhanced the heat transfer in the axial direction which is small in comparison with the convective term in the axial direction.

Figure 6.3 illustrates the radial temperature distribution inside the reactor for the

6. Eulerian simulation of heat transfer in a trickle bed reactor with constant wall temperature

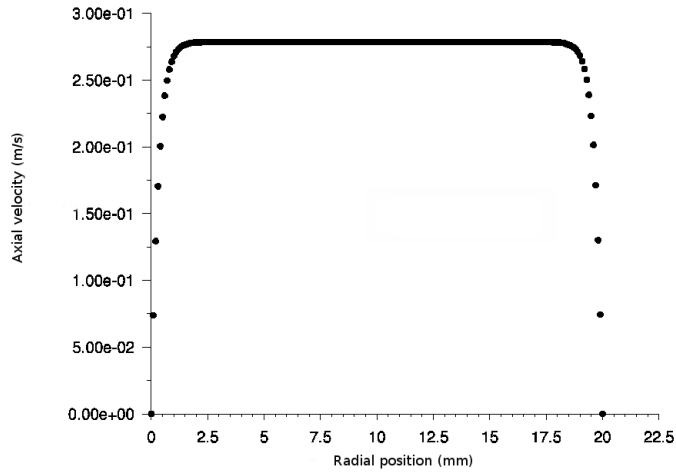


Figure 6.2: Axial velocity (m/s) profile of the gas phase inside the packed bed for mass flux of $0.308 \text{ kg}/m^2s$.

dry gas flow system with maximum mass flux which is $3.62 \text{ kg}/m^2s$ from simulations.

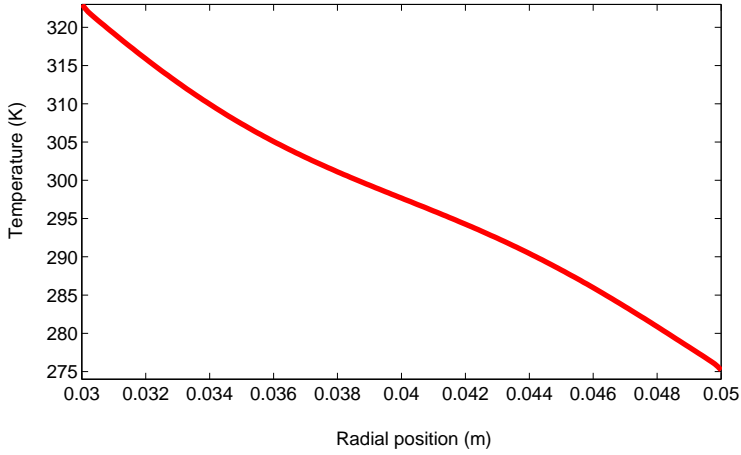


Figure 6.3: Radial temperature profile of the two-phase dry gas flow for mass flux of $3.62 \text{ kg/m}^2\text{s}$.

To validate the CFD simulations, the effective radial bed conductivity is calculated according to the temperature profile. Figure 6.4 illustrates the effective radial bed conductivity for both the experiments and CFD simulations for different mass fluxes of gas. Figure 6.4 shows that the results for the calculated effective radial bed conductivity from the experiments and CFD simulations are in a good agreement. The line with dots shows the effective radial bed conductivity based on only diffusion in the radial direction. This graph shows that at low Reynolds number heat transfers in the radial direction due to both convection and diffusion but the convection term is rather small. The sudden jump in line with triangle of figure 6.4 shows that at higher velocity, the effect of velocity on the radial bed conductivity is much more than the lower velocity.

6. Eulerian simulation of heat transfer in a trickle bed reactor with constant wall temperature

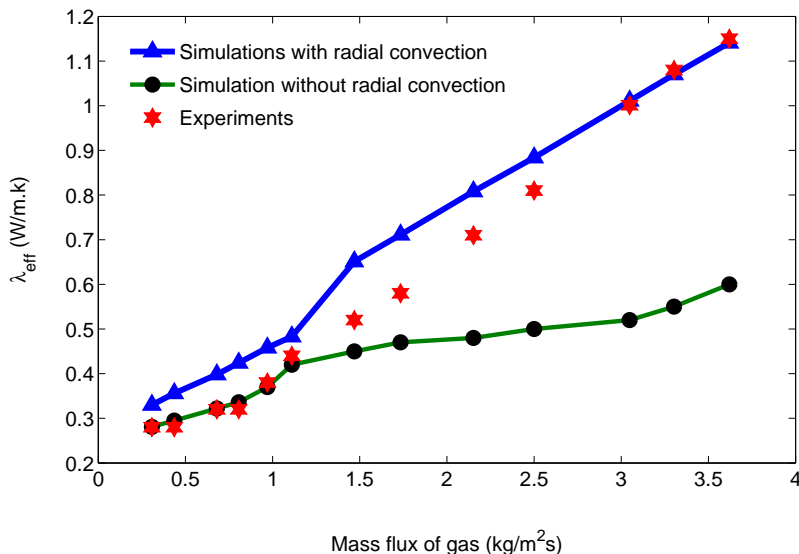


Figure 6.4: The effective radial bed conductivity of the dry gas system.

6.4.2 Three-phase trickle flow (solid, liquid and gas)

The second part of the results are for the trickle flow reactor. The experimental and simulation conditions are similar to the dry gas flow case. The experiments and simulations have been done for different gas mass fluxes in the range of $0.3080 \text{ kg/m}^2\text{s}$ to $3.3 \text{ kg/m}^2\text{s}$ for two different liquid superficial velocities of 1.49 m m/s and 4.78 m m/s . From the simulations we find that the velocity profile inside the reactor is plug flow for both the gas and liquid phase.

Figure 6.5 illustrates the radial temperature distribution for the case of trickle flow of 1.49 m m/s liquid superficial velocity with $3.303 \text{ kg/m}^2\text{s}$ mass flux of gas.

To validate the CFD simulations, the effective radial bed conductivity is calculated according to the temperature profile. Figures 6.6 and 6.7 show the results for the effective radial bed conductivity for the trickle flow of 1.49 m m/s and 4.78 m m/s liquid superficial velocity.

The results of the experiments and simulations for the effective radial bed conductivity for both cases of the trickle flow (liquid superficial velocity of 1.49 m m/s and 4.78 m m/s) have the same trend (figures 6.6 and 6.7).

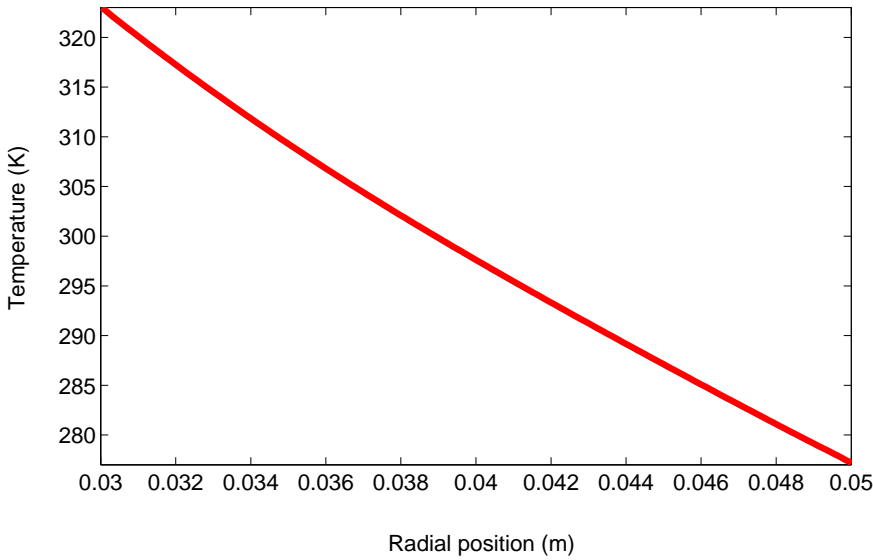


Figure 6.5: Radial temperature profile in the trickle flow (1.49 m m/s liquid superficial velocity) reactor with $3.303 \text{ kg/m}^2\text{s}$ mass flux of gas.

For some cases (for example, gas mass flux of 0.96 and $1.34 \text{ kg/m}^2\text{s}$, see figure 6.7) the effective radial bed conductivity obtained from the simulations deviates from the experimental results by around 15%. We think that this deviation or underprediction for the effective radial bed conductivity of trickle flow with the liquid velocity of 4.78 m m/s is due to high Reynolds number and more deviation from laminar flow and getting closer to turbulent flow. In the case of high Reynolds number turbulence can have effect on the heat transfer in the radial direction and consequently on the radial heat conductivity of the bed. In addition, these deviations can be because of measurement errors in experiments. It is worth mentioning that we tried to have the same conditions for both the experiments and simulations but they cannot be exactly the same due to the possible errors (such as temperature and pressure measurements) and this also can be another reason for these deviations.

Trickling liquid strongly affects heat transfer in packed beds. It improves heat transfer in the radial direction. For example, at a gas mass flux of $2.5 \text{ kg/m}^2\text{s}$ the effective radial bed conductivity is about 0.9 W/m K for dry gas flow, 2.5 W/m K for trickle flow of 1.49 m m/s liquid superficial velocity and 3.6 W/m K for trickle

6. Eulerian simulation of heat transfer in a trickle bed reactor with constant wall temperature

flow of 4.78 $m\,m/s$ liquid superficial velocity. It shows that in the trickle flow regime, heat transfer in the radial direction is larger than the dry gas flow regime. In addition, in trickle flow regime when the velocity of the liquid is higher, heat transfer in the radial direction is higher than for lower liquid velocities. When a liquid parcel encounters a particle it moves in the radial direction and this movement transfers also heat in the radial direction (convective term). So, the effective radial conductivity of the bed (λ_{er}) with high liquid velocity is larger than the low liquid velocity.

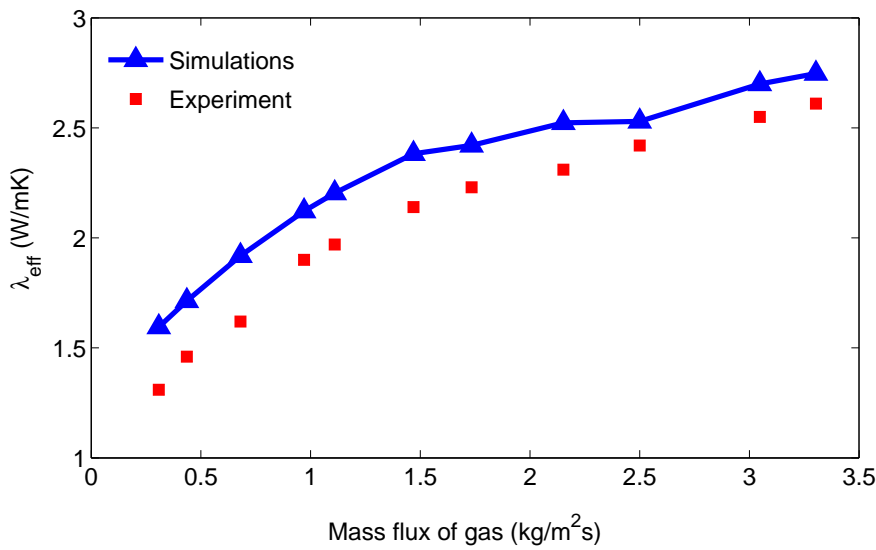


Figure 6.6: The effective radial bed conductivity of the trickle flow reactor with 1.49 $m\,m/s$ liquid superficial velocity.

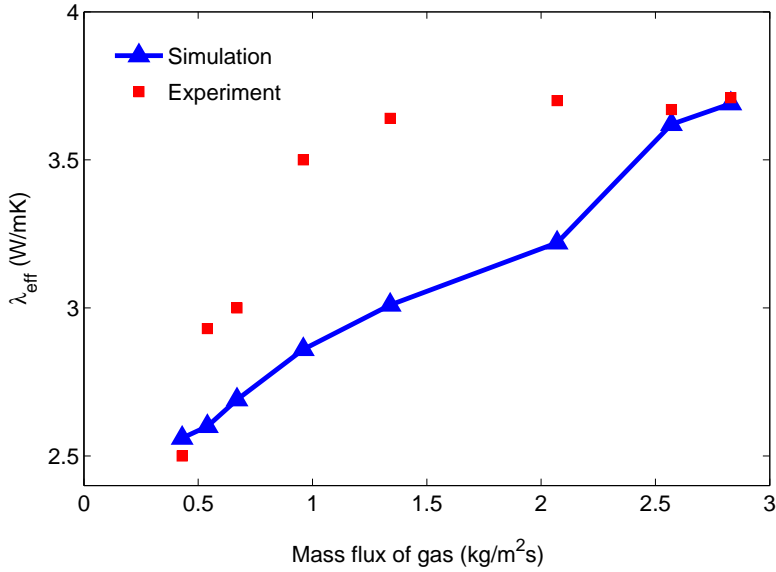


Figure 6.7: The effective radial bed conductivity of the trickle flow reactor with 4.78 m/s liquid superficial velocity.

6.4.3 Grid independency

Numerical simulation is not complete without a study of grid-size independence. To confirm that the CFD results are independent from the mesh size, the simulation of the system with 25×25 , 50×50 , 100×100 , 200×200 , 400×400 and 800×800 grids (radial \times axial) are performed. Figure 6.8 shows the effective radial conductivity of the bed for dry gas flow at six mesh resolutions. It can be seen that the last three simulations predict almost the same effective radial conductivity of the bed. For our simulation we selected the mesh size of 200×200 and we used this grid size for all simulations of this research.

6. Eulerian simulation of heat transfer in a trickle bed reactor with constant wall temperature

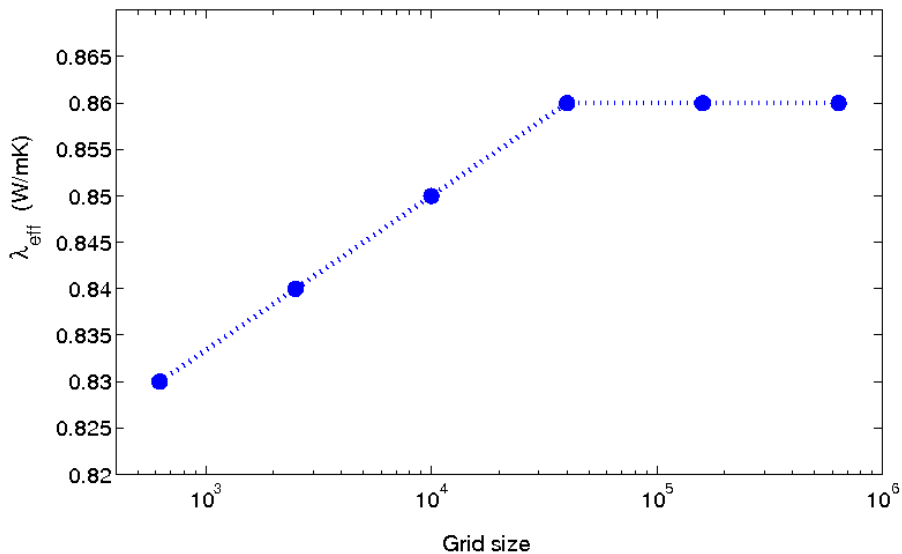


Figure 6.8: The effective radial bed conductivity of the dry gas flow reactor for various mesh resolutions.

6.4.4 Accuracy of the model

As mentioned the Euler-Euler multi-phase approach was used for the modeling of heat transfer in the packed bed. The model was examined for two-phase and three-phase (trickle flow) reactors. The model predicts the temperature profile inside the packed beds (two and three phase). The model was validated with the calculation of the effective radial bed conductivity. For the two-phase dry gas packed bed, the results of the modeling show that for most of the cases the calculated effective radial bed conductivity deviate from the experimental results not more than 10%. For the trickle flow reactor with the superficial liquid velocity of 1.49 m m/s the results of the modeling deviate from the experimental results for most of the cases not more than 10%. But, when the liquid superficial velocity is higher then the deviation of the modeling results from the experimental results are higher. For the trickle flow with the superficial liquid velocity of 4.78 m m/s the model does not work as good as the dry gas flow and the trickle flow of 1.49 m m/s superficial liquid velocity and the deviation of the modeling results from the experimental results are more than 10% for half of the cases. So, the proposed model is more

accurate at low Reynolds numbers than high Reynolds numbers. For high Reynolds number the proposed model underestimates the effective radial bed conductivity. The high Reynolds number flow regime is getting closer to the turbulent regime. Therefore, to have proper results for three phase trickle flow systems with high Reynolds number the effects of turbulence of the system should be implemented in the model.

6.5 CONCLUSIONS

Heat transfer in trickle beds can be conventionally expressed by the concept of an effective radial bed conductivity which is based on the assumption that on a macroscale, the bed can be described by a continuum. The effective radial bed conductivity has been derived based on a steady state two-dimensional model. The results show that heat transfer in the radial direction (the effective radial bed conductivity) increases if we increase the mass flux of the gas. In case of trickle flow, the effective radial bed conductivity is a function of both gas and liquid mass fluxes but the effect of the liquid flow is much more significant than the gas flow because of higher conductivity of the liquid. In addition, in trickle flow regime the effective radial conductivity of the bed is 2-5 times higher than the dry gas flow system and if the superficial velocity of the liquid is higher the effective radial bed conductivity is larger. In the trickle flow regime an increase of the liquid flow rate is an effective way to increase the heat transfer rate in the radial direction.

Acknowledgement

The authors would like to thank Shell Global Solutions International B.V, Amsterdam for the technical and financial support.

NOMENCLATURE

α	volume fraction	—
ρ	density	kg/m^3
t	time	s
\vec{v}	velocity vector	m/s
P	pressure	Pa
τ	stress strain tensor	N/m^2
\vec{g}	gravity	N/kg
\vec{F}	force	N
H	enthalpy	J/kg
\vec{q}	heat flux	W/m^2
Q_{pq}	intensity of heat exchange between the phases	W/m^2
λ	radial bed conductivity	W/mK
Re	Reynolds number	—
Pr	Prandtl number	—
k	conductivity of material	W/mK
Nu	Nusselt number	—
T	temperature	K
d_s, d_{pq}	particle or droplet diameter	m
μ	molecular viscosity	kg/ms
φ	heat flow	W
L	length	m
r	radius	m
$\nabla \cdot \vec{v}_q$	effect of volume dilation	—
Re_p	Reynolds number based on particle diameter	—
\dot{m}_{pq}	mass transfer from p^{th} to the q^{th} phase	$\text{kg/m}^3\text{s}$
\dot{m}_{qp}	mass transfer from q^{th} to the p^{th} phase	$\text{kg/m}^3\text{s}$
S_q	heat source	W
S_{mq}	mass source	kg
\vec{F}_q	body force	N
\vec{F}_{vm}	virtual mass force	N
\vec{F}_{lift}	lift force	N
\vec{v}_{pq}	interphase velocity	m/s
\vec{R}_{pq}	interaction force between the phases	—
μ_q	viscosity of phase q	kg/ms
τ_{par}	particulate relaxation time	s

C_D	drag coefficient	—
f_{dr}	drag function	—
Re_l	Reynolds number of the liquid	—
Pr_l	Prandtl number of the liquid	—
Re_s	relative Reynolds of solid and fluid	—
Re_{pq}	relative Reynolds of fluid and fluid	—
D_T	column diameter	m
a	constant	—
b	constant	—
k_{fluid}	conductivity of fluid	W/mK
$\bar{\tau}_q$	stress strain tensor	kg/m^2s^2
K_{pq}	interphase momentum exchange coefficient	—
d_p	particle diameter	m
K_{sl}	fluid-solid exchange coefficient	—
H_{pq}	interphase enthalpy	J/kg
h_{pq}	heat transfer coefficient between the phases	W/m^2K
I	unit tensor	—
k_f	the conductivity of each phase	W/mK
n	number of phases	—

INDICES

p	phase p
q	phase q
pq	interaction between phase p and q
er	effective radial conductivity
st	static radial coefficient
eg	dynamic contribution for gas phase
el	dynamic contribution for liquid phase
l	liquid
g	gas
s	solid
f	fluid
$const$	constant
$fluid$	fluid
vm	virtual mass force
$lift$	lift force

6.6 Bibliography

- [1] N. Habtu, J. Font, A. Fortuny, C. Bengoa, A. Fabregat, P. Haure, A. Ayude, and F. Stuber. Heat transfer in trickle bed column with constant and modulated feed temperature: experiments and modeling. *Chemical Engineering Science*, 66:3358–3368, 2011.
- [2] Dudukovic M.P., Larachi F., and Mills P.L. Multi-phase catalytic reactors: a perspective on current knowledge and future trends. *Catalysis Reviews: Science and Engineering*, 44:123–246, 2002.
- [3] G. Flamant, J.D. Lu, and B. Variot. Towards a generalized model for vertical walls to gas-liquid fluidized beds heat transfer, radiative heat transfer and temperature effect. *Chemical Engineering Science*, 48:2493, 1993.
- [4] J.D. Lu, G. Flamant, and B. Variot. Theoretical study of combined conductive, convective and radiative heat transfer between plates and packed beds. *Chemical Engineering Science*, 37:727, 1994.
- [5] J.N. Papageorgiou and G.F. Froment. Simulation models accounting for radial voidage profiles in fixed-bed reactors. *Chemical Engineering Science*, 56:3043–3056, 1995.
- [6] O. Bey and G. Eigenberger. Fluid flow through catalyst filled tubes. *Chemical Engineering Science*, 52:1365–1376, 1997.
- [7] M.K. Rottschäfer and D. Vortmeyer. Measured and modeled superficial flow profiles in packed beds with liquid flow. *AIChE*, 44:484–490, 1998.
- [8] M. Winterberg and E. Tsotsas. Impact of tube-to-particle-diameter ratio on pressure drop in packed beds. *AIChE*, 46:1084–1088, 2000.
- [9] Rodrigo J.G. Lopes, M.L.N. Perdigato, Teresa S.A. Almeida, Rosa M. Quinta-Ferreira, and F. Larachi. Multiphase CFD simulations of catalytic wet oxidation of phenol-like compounds in high-pressure trickle-bed reactors: Reactive flow and temperature behaviour. *Chemical Engineering Research and Design*, Article in press, 2012.
- [10] Rodrigo J.G. Lopes and Rosa M. Quinta-Ferreira. Three-dimensional numerical simulation of pressure drop and liquid hold-up for high-pressure trickle-bed reactor. *Chemical Engineering Journal*, 145:112–120, 2008.

-
- [11] Rodrigo J.G. Lopes and Rosa M. Quinta-Ferreira. Evaluation of multiphase CFD models in gas-liquid packed-bed reactors for water pollution abatement. *Chemical Engineering Science*, 65:291–297, 2010.
- [12] B.V. Babu, K.J. Shah, and V. Govardhana Rao. Lateral mixing in trickle bed reactors. *Chemical engineering science*, 62:7053–7059, 2007.
- [13] A.B. Duncan, G.P. Peterson, and L.S. Fletcher. Effective thermal conductivity with packed beds of spherical particles. *Journal of Heat Transfer*, 111:830, 1989.
- [14] D. Kunii and J.M. Smith. Heat transfer characteristics of porous rocks. *AHChE J*, 6:71, 1971.
- [15] R. Krupiczka. Analysis of thermal conductivity in granular materials. *Int. Chem. Eng*, 7:122, 1967.
- [16] W. Blumberg and E.U. Schlunder. Thermal conductivity of packed beds consisting of porous particles wetted with binary mixtures. *Chemical Engineering and Processing*, 34:339–346, 1995.
- [17] R. Bauer and E.U. Schlunder. Effective radial thermal conductivity of packing in gas flow. *Int Chem Eng*, 18:189–204, 1978.
- [18] W. van Antwerpen, C.G. du Toit, and P.G. Rousseau. A review of correlations to model the packing structure and effective thermal conductivity in packed beds of mono-sized spherical particles. *Nuclear Engineering and Design*, 240:1803–1818, 2010.
- [19] C.T. HSU, P. Cheng, and K.W. Wong. Modified zehner-schlunder models for stagnant thermal conductivity of porous media. *International Journal of Heat Mass Transfer*, 17:2751–2759, 1994.
- [20] Luiz Mario de Matos Jorge, Regina Maria Matos Jorge, and Reinaldo Giudici. Experimental and numerical investigation of dynamic heat transfer parameters in packed bed. *Heat mass transfer*, 46:1355–1365, 2010.
- [21] R.A. Dekhtyar, D.Ph. Sikovsky, A.V. Gorine, and V.A. Mukhin. Heat transfer in a packed bed in moderate values of the Reynolds number. *Teplofizika Vysokikh Temperature*, 40:748–755, 2002.

6. Eulerian simulation of heat transfer in a trickle bed reactor with constant wall temperature

- [22] A.S. Lamine, L. Gerth, H. LE Gall, and G. Wild. Heat transfer in a packed bed reactor with co-current down flow of a gas and liquid. *Chemical Engineering Science*, 51:3813–3827, 1996.
- [23] E. Tsotsas and E.U. Schlunder. Heat transfer in packed beds with fluid flow: Remarks on the meaning and the calculation of a heat transfer coefficient at the wall. *Chemical Engineering Science*, 45:819–837, 1990.
- [24] S. Hatta and Maeda. Heat transfer in beds of granular catalyst i. *Chem Engng Japan*, 12:56, 1948.
- [25] S. Hatta and Maeda. Heat transfer in beds of granular catalyst ii. *Chem Engng Japan*, 13:79, 1949.
- [26] C.A. Coberly and W.R. Marshall. Temperature gradients in gas streams flowing through fixed granular beds. *Chem Engng Progr*, 47:141, 1951.
- [27] D.G. Bunnell, H.B. Irvin, R.W. Olson, and J.M. Smith. Effective thermal conductivities in gas-solid systems. *Industrial and Engineering Chemistry Research and Development*, 41:1977–1998, 1977.
- [28] O. Bey and G. Eigenberger. Gas flow and heat transfer through catalyst filled tubes. *International journal of Thermal Science*, 40:152–164, 2001.
- [29] Y. Demirel, R.N. Sharma, and H.H. Al-Ali. On the effective heat transfer parameters in a packed bed. *International journal of Heat and Mass Transfer*, 43:327–332, 2000.
- [30] E.I. Smirnov, A.V. Muzykantov, V.A. Kuzmin, A.E. Kronberg, and I.A. Zolotarskii. Radial heat transfer in packed beds of spheres, cylinders and rachig rings verification of model with a linear variation of λ_{er} in the vicinity of the wall. *Chemical Engineering Journal*, 91:243–248, 2003.
- [31] Rodrigo Bettega, Marcos Flavio Pinto Moreira, Ronaldo Guimaraes Correa, and Jose Teixeira Freire. Mathematical simulation of radial heat transfer in packed beds by pseudohomogeneous modeling. *Particuology*, 9:107–113, 2011.
- [32] FLUENT Incorporate, Natick, MA. *Fluent 12.06.016 Theory Guide*, 2009.
- [33] C.Y. Wen and Y.H. Yu. Mechanics of fluidization. *Chemical engineering Progress Symposium Series*, 62:100–111, 1966.

- [34] L. Schiller and Z. Naumann. A drag coefficient correlation. *Verein Deutscher Ingenieure*, 77:318, 1935.
- [35] W.E. Ranz and W.R.E. Marshall. Evaporation from drops, part 1. *Chemical engineering Progress*, 48:141–146, 1952.
- [36] D.J Gunn. Transfer of heat or mass to particles in fixed and fluidized beds. *Journal of heat and mass transfer*, 21:467–476, 1978.
- [37] Martin Rhodes. *Introduction to Particle Technology*. John Wiley and Sons.

6. Eulerian simulation of heat transfer in a trickle bed reactor with constant wall temperature

NORMAL OPERATION AND HOT SPOTS FORMATION IN A TRICKLE BED REACTOR

Abstract

This chapter reports a Computational Fluid Dynamics (CFD) study on the thermal performance of a three-phase trickle bed reactor. In the reactor we have mass transfer from gas to liquid, an exothermic reaction in the liquid phase and heat transfer between the phases. We study the temperature distribution in a trickle bed reactor under both normal flow conditions and in the case of local mal-distribution. The results of the 2-D CFD simulations under normal flow condition have been validated with a simple 1-D plug flow model. They are in a good agreement. We observe hot spots in the case of local blockage inside the trickle bed reactor. The results show that the local blockage against flow can cause hot spots due to a weak convection of heat in the blocked region.

7.1 Introduction

In multi-phase reactors more than one phase is present at the same time. Most catalytic reactors are multi-phase reactors. Trickle bed reactors have a fixed-bed of solid catalysts through which liquid and gas flow in co-current or counter current. Reactions take place at the surface of the catalyst [1]. A uniform distribution of the two phase flow is important in these reactors because flow non-uniformities in the bed may lead to the formation of hot spots [2]. Trickle bed reactors have two main categories of flow condition: low interaction regime (LIR) and high interaction regime (HIR). LIR occurs when there are relatively low flows of gas and liquid. At higher flow rates of the liquid and gas phases there is intense gas-liquid shear. Various HIR flow patterns can result, depending on the ratio of the flows of the two phases. According to literature hot spots are observed in the low interaction regime (mostly under the trickle flow condition) [3]. Trickle bed reactors operate continuously and are used in petroleum, petrochemical and chemical industries in applications like [2]:

- Hydrogenation of Hydrocarbons
- Hydrodesulphurization
- Hydro-finishing of lubricating oils

The presence of the particles causes a plug flow of the gas and liquid inside trickle bed reactors. This makes them preferred over other three-phase reactors in which the catalyst is not stationary. The high catalyst loading per unit volume of the liquid in trickle bed reactors makes them an attractive alternative to slurry reactors. However, the disadvantages of trickle bed reactors are their impracticality for reactions with fast deactivating catalysts such as in heavy oil hydro-treating processes and the possibility of liquid mal-distribution, which may cause hot spots and reactor runaways [4].

A lot of industrial processes involve exothermic reaction between liquid and gas. In trickle bed reactors, mal-distribution and incomplete external wetting can occur due to trickle flow condition. In large scale trickle bed reactors with an exothermic reaction high radial temperature gradients can exist when there is mal-distribution in the reactor. Due to the high temperature as the result of exothermic reaction a partial or total phase change can happen. This complicates both reaction and transport phenomena in trickle beds. The formation of hot spot can increase locally the reaction rate. As a consequence, locally even more heat can be produced, leading to a growth of the hot spot and potentially a runaway of the reactor [5],[6],[7],[8]. When these hot spots exceed some critical value it may lead to a reactor runaway

caused by an increase in the rate of the desired or undesired reaction, which has a negligible rate under normal operating conditions. Some literature exists on this subject, reviewed recently by Varma, Morbidelli and Wu [9]. The formation of hot zones may have a harmful impact on the yield of the desired product (or products) and it may deactivate the catalyst. When a hot zone exists next to the wall of a reactor, it may decrease the mechanical strength of the wall. Thus, a hot zone may lead to severe safety problems. Therefore, it is of great practical importance to understand the nature and origin of these hot spots and predict formation of hot spots [5]. The reaction kinetics and the initial condition of the feed of the reactor are very important issues in the investigation of hot spots. The inlet gas temperature can have a significant effect on the hot spot temperature and size [10].

In this research we use the Euler-Euler multi-phase approach for modeling of the transport phenomena and reaction inside a trickle bed. In this approach, all phases are treated as continua. All phases share the domain and may interpenetrate as they move within it. In this method, it is required to represent coupling between different phases by suitable interphase transport models (closure relations).

In the Euler-Euler method, trickle beds are treated as pseudo-homogeneous media. Modified Navier-Stokes equations are applied in conjunction with closure equations to account for the fluid-solid and fluid-fluid interactions [11], [12], [13], [14]. To account for radial porosity variations, the overall averaged porosity of the whole trickle bed reactor is replaced by a function accounting for the porosity distribution in the radial direction [13],[15].

The objective of this work is to investigate the effect of mal-distribution on the performance of a trickle bed reactor. We focus on the effect of the chemical reaction and on that of the mal-distribution on the thermal performance of the trickle bed reactor rather than the hydrodynamics. A two-dimensional trickle bed reactor with an Eulerian structured mesh is used. The computations are slow. To avoid excessive computation times and to avoid further complication we have excluded the possibility of evaporation and condensation in the present work.

7.2 Geometry and setup

The trickle bed in our study is a two-dimensional, Cartesian rectangle, see figure 7.1. The length of the reactor is $L_x=1.6\text{ m}$ and the width of the reactor is $L_y=0.30\text{ m}$.

7. Normal operation and hot spots formation in a trickle bed reactor

For the simulations we use three different configurations. In the first one (A), we use a normal flow (plug flow regime) reactor, in the second one (B), we trap the fluid near the wall with a closed obstacle and in the third one (C) we locally change the direction of the flow with three diagonal barriers.

The reactor operates at 60 *bar* and we take the gravitational acceleration (9.8 m/s^2)

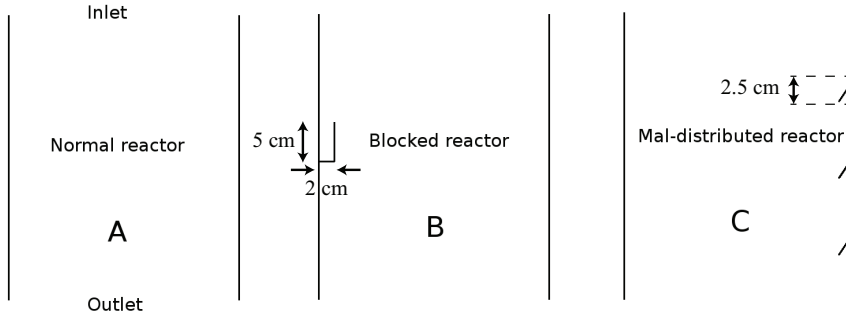


Figure 7.1: Geometry of the modeled trickle bed reactors with (A) normal flow (plug flow regime), (B) blocked flow condition and (C) mal-distributed flow (diagonal barrier).

into account. The gas and liquid flow from top to bottom. The hydraulic diameter of the particles is 2.9 mm and the porosity of the bed is 40%. The liquid and gas flow into the reactor as a mixture. The gas phase contains the species Hydrogen (H_2 , 98%) and inert material (Ar 2%). For these species, enthalpy of formation, density, specific heat, thermal conductivity and viscosity are assumed to be constant. For the properties of the gas mixture, we use the ideal gas law with the assumption that the density is a function of temperature and not pressure (we use a constant operating pressure of the reactor for the calculation of the density, $\rho = \frac{P_{op} M_W}{RT}$, $P_{op} = cte = 60 \text{ bar}$), constant specific heat, thermal conductivity and viscosity. The mass diffusivity is $2.88 \times 10^{-5} \text{ m}^2/\text{s}$. The liquid phase contains the species n-Hexene (C_6H_{12} , 22%), n-Hexane (C_6H_{14} , 0%), inert material (Cyclohexane, C_6H_{12} , 72%) and Hydrogen (H_2 , 6%). For all these species, enthalpy of formation, density, specific heat, thermal conductivity and viscosity are constant. For the properties of the liquid mixture, we use constant density, specific heat, thermal conductivity and viscosity. The mass diffusivity of Hydrogen (H_2) is $2.88 \times 10^{-6} \text{ m}^2/\text{s}$.

All properties of the solid phase i.e density, specific heat and thermal conductivity are assumed to be constant. Properties of the gas mixture, liquid mixture and solid phase are listed in the table 7.1.

Parameter	Gas Mixture	Liquid Mixture	Solid
Density	$\rho = P_{op} M_W / \mathbf{R} T, P_{op} = 60 \text{ bar}$	763 kg/m^3	2500 kg/m^3
Specific heat	6560 J/kg K	2030 J/kg K	670 J/kg K
Thermal conductivity	0.0454 W/m K	0.454 W/m K	1 W/m K
Viscosity	$1.04 \times 10^{-5} \text{ kg/ms}$	$3.27 \times 10^{-4} \text{ kg/ms}$	—
Mass diffusivity	$2.88 \times 10^{-5} \text{ m}^2/\text{s}$	$2.88 \times 10^{-6} \text{ m}^2/\text{s}$	—

Table 7.1: Properties of the liquid mixture, gas mixture and solid phase [16], [17].

7.3 Model description

7.3.1 Euler-Euler approach

In this work the Euler-Euler multi-phase approach is used to solve the average mass, momentum, species and energy equations for each phase separately. In the Euler-Euler approach, the different phases are treated mathematically as interpenetrating continua. Since the volume of one phase cannot be occupied by the other phases, the concept of phase volume fraction is introduced. The volume fractions are continuous functions of space and time and their summation is equal to one. Coupling of the pressure and velocity is achieved through the interaction between the phases such as the drag force [18]. The transport equations of the Euler-Euler model are as follows [19].

Mass conservation equation:

$$\frac{\partial(\alpha_q \rho_q)}{\partial t} + \nabla \cdot (\alpha_q \rho_q \vec{v}_q) = \sum_{p=1}^n (\dot{m}_{pq} - \dot{m}_{qp}) + S_{mq} \quad (7.1)$$

where α_q is the volume fraction of phase q , ρ_q is the density of phase q , \vec{v}_q is the velocity of phase q , t is the time, \dot{m}_{pq} is the mass transfer from the p^{th} to the q^{th} phase, \dot{m}_{qp} is the mass transfer from the q^{th} to the p^{th} phase and S_{mq} is the mass source of phase q .

Momentum conservation equation:

$$\frac{\partial(\alpha_q \rho_q \vec{v}_q)}{\partial t} + \nabla \cdot (\alpha_q \rho_q \vec{v}_q \vec{v}_q) = -\alpha_q \nabla P + \nabla \cdot \bar{\bar{\tau}}_q + \alpha_q \rho_q \vec{g} + \sum_{p=1}^n (\dot{m}_{pq} \vec{v}_{pq} - \dot{m}_{qp} \vec{v}_{qp}) + \vec{F}_q + \vec{F}_{lift,q} + \vec{F}_{vm,q} + \sum_{p=1}^n K_{pq} (\vec{v}_p - \vec{v}_q) \quad (7.2)$$

where P is the pressure, $\bar{\bar{\tau}}_q$ is the stress tensor of phase q , \vec{g} is the gravity vector, \vec{v}_{pq} is the interphase velocity defined as follows: if $\dot{m}_{pq} > 0$ (mass transfer from the p^{th} to the q^{th} phase) then $\vec{v}_{pq} = \vec{v}_p$, if $\dot{m}_{pq} < 0$ (mass transfer from the q^{th} to the p^{th} phase) then $\vec{v}_{pq} = \vec{v}_q$, likewise if $\dot{m}_{qp} > 0$ then $\vec{v}_{qp} = \vec{v}_q$, if $\dot{m}_{qp} < 0$ then $\vec{v}_{qp} = \vec{v}_p$, \vec{F}_q includes all external body forces except gravity, $\vec{F}_{lift,q}$ is the lift force, $\vec{F}_{vm,q}$ is the virtual mass force, $K_{pq}(\vec{v}_p - \vec{v}_q)$ is the drag force between the phases and K_{pq} is the interphase momentum exchange coefficient.

$\bar{\bar{\tau}}_q$ is defined as:

$$\bar{\bar{\tau}}_q = \alpha_q \mu_q [(\nabla \vec{v}_q + \nabla \vec{v}_q^T)] - \frac{2}{3} \alpha_q \mu_q \nabla \cdot \vec{v}_q I \quad (7.3)$$

where μ_q is the viscosity of phase q and I is the unit tensor. The gravity force is taken into account in all simulations and the lift force and virtual mass force are neglected because they are much smaller than the drag force between the phases. There is no other external body force (except gravity) in the system, therefore \vec{F}_q is zero.

For gas-liquid flows, the liquid phase is assumed to form droplets. The exchange coefficient for these types of gas-liquid flows can be written in the form:

$$K_{gl} = \frac{\alpha_g \alpha_l \rho_g f_{dr}}{\tau_{par}} \quad (7.4)$$

where f_{dr} , the drag function, is defined differently for different exchange coefficient models and τ_{par} is the particulate relaxation time and is defined as:

$$\tau_{par} = \frac{\rho_g d_{gl}^2}{18\mu_l} \quad (7.5)$$

where d_{gl} is the diameter of the droplets of phase l . All definitions of f_{dr} include a drag coefficient (C_D) which is based on the relative Reynolds number.

For the drag coefficient between gas and liquid we use the model of Schiller and Naumann [20] in the following form:

$$f_{dr} = 1 + 0.15 Re_{gl}^{0.687} \quad (7.6)$$

where Re_{gl} is the relative Reynolds number between the gas and liquid phases. The relative Reynolds number for the primary gas phase and secondary liquid phase is obtained from:

$$Re_{gl} = \frac{\rho_g |\vec{v}_g - \vec{v}_l| d_g}{\mu_g} \quad (7.7)$$

In our simulations for the solid-gas and solid-liquid interaction we use the model of Gidaspow [21] which is a combination of the Wen and Yu model [22] and the Ergun equation [23]. According to Gidaspow model [21] when $\alpha_f > 0.8$, the fluid-solid exchange coefficient K_{sf} is of the following form:

$$K_{sf} = \frac{3}{4} C_D \frac{\alpha_s \alpha_f \rho_f |\vec{v}_s - \vec{v}_f|}{d_s} \alpha_f^{-2.65} \quad (7.8)$$

where

$$C_D = \frac{24}{\alpha_f Re_{sf}} (1 + 0.15(\alpha_f Re_{sf})^{0.687}) \quad (7.9)$$

Re_{sf} is the relative Reynolds number between fluid and solid. When $\alpha_f \leq 0.8$, the fluid-solid exchange coefficient K_{sf} is of the following form.

$$K_{sf} = 150 \frac{\alpha_s (1 - \alpha_f) \mu_f}{\alpha_f d_s^2} + 1.75 \frac{\rho_f \alpha_s |\vec{v}_s - \vec{v}_f|}{d_s} \quad (7.10)$$

Energy conservation equation:

$$\begin{aligned} \frac{\partial(\alpha_q \rho_q H_q)}{\partial t} + \nabla \cdot (\alpha_q \rho_q \vec{v}_q H_q) = & -\alpha_q \frac{\partial P}{\partial t} + \vec{\tau}_q : \nabla \vec{v}_q - \nabla \cdot \alpha_q \vec{q}_q + S_q + \\ & \sum_{p=1}^n (Q_{pq} + \dot{m}_{pq} H_{pq} - \dot{m}_{qp} H_{qp}) \end{aligned} \quad (7.11)$$

where H_q is the enthalpy of phase q per unit mass, \vec{q}_q is the heat flux, S_q is the heat source, Q_{pq} is the heat exchange between the p^{th} and q^{th} phases, \dot{m}_{pq} is the mass transfer from p^{th} to the q^{th} phase, \dot{m}_{qp} is the mass transfer from q^{th} to the p^{th} phase and H_{pq} and H_{qp} are the interphase enthalpies (e.g., the enthalpy of the vapor in case of evaporation (formation enthalpy of species which evaporate) and enthalpy of the liquid in case of condensation (formation enthalpy of species which condensate)).

The heat flux, \vec{q}_q is defined as:

$$\vec{q}_q = -k_q \frac{\partial T}{\partial \vec{r}} \quad (7.12)$$

where k_q is the conductivity of phase q .

The rate of energy transfer between the phases (Q_{pq}) is assumed to be a function of the temperature difference between the phases:

$$Q_{pq} = h_{c,pq}(T_p - T_q) \quad (7.13)$$

where $h_{c,pq}$ is the heat transfer coefficient between the p^{th} and q^{th} phase.

Volume fraction equation:

The description of multi-phase flow as interpenetrating continua incorporates the concept of phase volume fractions, denoted here by α_q . Volume fractions represent the space occupied by each phase and the laws of conservation of mass and momentum are satisfied by each phase individually. The derivation of the conservation equations can be done by ensemble averaging the local instantaneous balance for each of the phases [24] or by using the mixture theory approach [25].

The volume fractions satisfy the following equation.

$$\sum_{q=1}^n \alpha_q = 1 \quad (7.14)$$

Species transport can also be applied to multi-phase flows. We solve the conservation equations for chemical species in multi-phase flows for each phase q . The local mass fraction of each species Y_i can be predicted by the solution of a convection-diffusion equation for the i^{th} species.

Conservation equation of species:

$$\frac{\partial(\rho_q \alpha_q Y_{iq})}{\partial t} + \nabla \cdot (\rho_q \alpha_q \vec{v}_q Y_{iq}) = -\nabla \cdot (\alpha_q \vec{J}_{iq}) + \alpha_q R_{iq} + \sum_{p=1}^n (\dot{m}_{p^i q^j} - \dot{m}_{q^j p^i}) + \mathbb{R} \quad (7.15)$$

where R_{iq} is the net rate of production of homogeneous species i by a chemical reaction for phase q , $\dot{m}_{q^j p^i}$ is the mass transfer source between species i and j from phase q to p and \mathbb{R} is the heterogeneous reaction rate. In addition, α_q is the volume

fraction for phase q , Y_{iq} is the mass fraction of species i and \vec{J}_{iq} is the diffusion flux of species i , which arises due to gradients of concentration and temperature. We used the Ficks' law to model the mass diffusion due to the concentration gradients:

$$\vec{J}_{iq} = -\rho_q D_{i,mix} \nabla Y_{iq} - D_{T,i} \frac{\nabla T}{T} \quad (7.16)$$

where $D_{i,mix}$ is the mass diffusion coefficient for species i in the mixture and $D_{T,i}$ is the thermal diffusion coefficient for species i in the mixture.

The source of chemical species i due to the reaction is computed as of the Arrhenius reaction source that the species participate in:

$$R_{iq} = M_{W,i} \hat{R}_{iq} \quad (7.17)$$

where R_{iq} is the Arrhenius mass rate of creation or destruction, $M_{W,i}$ is the molecular weight of species i and \hat{R}_{iq} is the Arrhenius molar rate of creation or destruction of species i due to the reaction.

7.3.2 Heat transfer

Heat transfer characteristics and spatial temperature distributions in trickle beds are important in design and analysis of the trickle bed catalytic reactors. The principal modes of heat transfer in trickle beds are conduction, convection and radiation, which is important at high temperatures. The mechanisms of heat transfer inside trickle beds are: conduction through the particles, conduction through contact surfaces of two particles, conduction through the fluid film near the contact surface of two particles and radial mixing of fluids.

The rate of energy transfer between the phases is assumed to be a function of the temperature difference between the phases:

$$Q_{pq} = h_{c,pq} (T_p - T_q) \quad (7.18)$$

where $h_{c,pq}(= h_{c,qp})$ is the heat transfer coefficient between the p^{th} phase and the q^{th} phase. The heat transfer coefficient is related to the p^{th} phase Nusselt number, Nu_{pl} by:

$$h_{c,pq} = \frac{6k_p \alpha_p \alpha_q Nu_{pl}}{d_p} \quad (7.19)$$

Here k_p is the thermal conductivity of the p^{th} phase. The Nusselt number is typically determined from one of the many correlations reported in the literature. For the heat transfer between liquid and gas we use the Ranz-Marshall equation [26] which for spheres is:

$$Nu_l = 2 + 0.6Re_l^{1/2}Pr_l^{1/3} \quad (7.20)$$

Re_l is the Reynolds number based on the diameter of the liquid phase droplets or particles and the relative velocity and Pr_l is the Prandtl number of the liquid phase. For the heat transfer between fluid and solid we use the Gunn equation [27] which is applicable to a porosity range of 0.35 – 1 and Reynolds number up to 10^5 [19].

$$Nu_s = (7 - 10\alpha_f + \alpha_f^2)(1 + 0.7Re_{sf}^{0.2}Pr_f^{1/3}) + (1.33 - 2.4\alpha_f + 1.2\alpha_f^2)Re_{sf}^{0.7}Pr_f^{1/3} \quad (7.21)$$

where α_f is the volume fraction of each fluid (gas or liquid) and Pr_f is the Prandtl number of each fluid.

7.3.3 Mass transfer

In the trickle bed reactor modeled, we assume constant mass transfer of species H_2 from gas to the liquid phase for simplicity. The unidirectional mass transfer model defines a positive mass flow rate per unit volume from the gas phase to the liquid phase:

$$\dot{m}_{gl} = \max[0, \lambda_{gl}] - \max[0, -\lambda_{gl}] \quad (7.22)$$

where

$$\lambda_{gl} = \dot{r}\alpha_g\rho_l \quad (7.23)$$

and \dot{r} is a constant mass transfer rate.

If the gas phase is a mixture and a mass transfer mechanism is defined for species i of gas phase then:

$$\lambda_{gl} = \dot{r}\alpha_g Y_{g,i}\rho_l \quad (7.24)$$

where $Y_{g,i}$ is the mass fraction of species i in the gas phase.

7.3.4 Reaction

For the reaction we use a volumetric Arrhenius type of reaction in the liquid phase. The reaction occurs in the liquid phase between H_2 and C_6H_{12} and produces C_6H_{14} as product. The reaction is:



where H_2 is Hydrogen, C_6H_{12} is n-Hexene and C_6H_{14} is n-Hexane. The reaction is an exothermic reaction with the heat of reaction equal to $144 \text{ kJ/mol } H_2$ and the rate of reaction is:

$$-\hat{R}_{C_6H_{12}} = 6.17 \exp\left(\frac{-20700}{RT}\right) C_{C_6H_{12}} \quad (7.26)$$

where $\hat{R}_{C_6H_{12}}$ is the reaction rate, T is the temperature, R is the gas universal constant and $C_{C_6H_{12}}$ is the concentration of C_6H_{12} in the liquid phase.

7.3.5 Mesh

For our modeling we use a structured mesh. The number of grid nodes in the axial direction is 640 and in the spanwise direction 120 resulting in a total number of cells of 76800. In addition, we have three other meshes with 4800, 19200 and 307200 grid cells. We use finer grid cells in the mal-distributed and blocked area in comparison with the other parts of the reactor. In the area with mal-distribution the size of each grid cell is about 1 mm . In the area with normal flow condition the size of each grid cell is about 3 mm . The fine mesh in mal-distributed regions helps to have precise results.

7.3.6 Boundary conditions and solver details

The equations 7.1, 7.2, 7.11, 7.14 and 7.15 are subject to the following boundary condition.

At the inlet of the reactor we use a velocity inlet boundary condition with constant velocity and temperature. The velocity of liquid and gas at the inlet are 0.0016 m/s and 0.007 m/s respectively and the inlet temperature of both phases is 354 K . The

volume fraction of the liquid and gas at the inlet are 0.1 and 0.3. Both gas and liquid are considered as mixtures. In the liquid phase we have C_6H_{12} (22%), C_6H_{14} (0%), H_2 (6%) and inert material (72%) and in the gas phase we have H_2 (98%) and inert material (2%). At the outlet of the reactor we use a pressure outlet boundary condition. We have stationary walls and no slip condition. There is no heat transfer between the walls and the fluids.

All simulations are performed with the CFD code Fluent version 13.0.0. Meshing of the two-dimensional computational domains are performed in Gambit version 2.4.6. The governing equations are discretised by the finite volume approach. The Second-order Upwind differencing method is used for discretization of the convection terms and the Simple method is applied for simultaneous solution for the pressure velocity coupled equations. The flow is assumed laminar and incompressible. All mass, momentum, energy, species transport and volume fraction equations are solved in two-dimensional transient formulation. The solid particles are assumed to be stagnant ($v_s = 0$) with a constant volume fraction of 0.6. Convergence limits of the sum of the absolute residuals for all the equations are set to 10^{-6} . Unsteady simulations with time step of 10^{-2} second are continued until steady state in the outlet velocity and temperature profile is reached.

7.4 Results and discussion

7.4.1 Volume fraction distribution

Figure 7.2 shows the volume fraction of the liquid and gas phases along the trickle bed reactor under normal flow (plug flow regime) condition. The volume fraction of the liquid is decreasing along the reactor from the inlet of the reactor to about 0.5 m downstream the inlet. The liquid and gas flow into the reactor and the reaction between Hydrogen (H_2) and Hexene (C_6H_{12}) immediately starts in the liquid phase. The rate of reaction is very high, so, the volume of the liquid phase is decreasing due to the consumption of Hydrogen in the liquid phase. In addition, a lot of heat is generated due to the exothermic reaction and the gas phase expands and shows an increase in the volume fraction. After about 0.5 m downstream the inlet the reaction is finished and the temperature remains constant. In this part the volume fraction of the liquid increases very little due to mass transfer from the gas phase to the liquid phase.

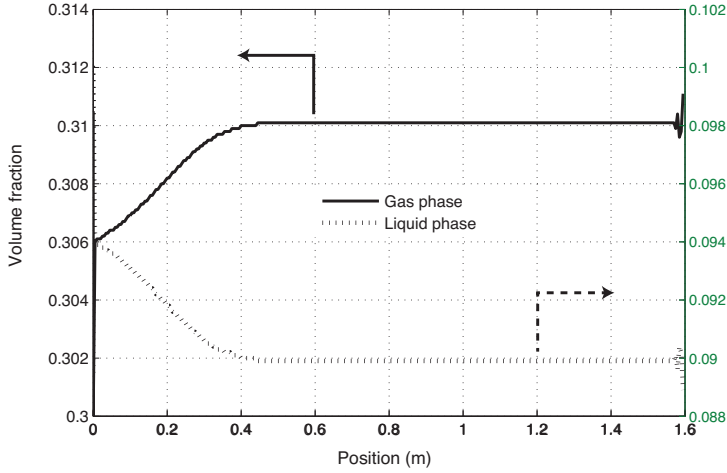


Figure 7.2: Volume fraction of the liquid and gas phases along the trickle bed reactor.

At the outlet of the reactor the volume fraction fluctuates. These fluctuations are observed because of a reverse flow at the outlet of the reactor.

The Damkohler numbers (Da) are dimensionless numbers used to relate chemical reaction time scales to the time scale of other phenomena occurring in a system, for example mass transfer. There are several Damkohler numbers and their definition varies according to the system under consideration.

In continuous chemical processes with a chemical reaction $A \rightarrow B$ of n^{th} order, the general definition of the Damkohler number is:

$$Da = \frac{\text{Reaction rate}}{\text{Convective mass transfer rate}} = \frac{kC_0^{n-1}}{k_g a} \quad (7.27)$$

where $k_g a$ is the mass transfer coefficient which is $1.2 \times 10^{-3}/s$ [28], [29], [30].

Figure 7.3 shows the Damkohler number along the reactor. This figure shows that in the first 0.5 m of the reactor the Damkohler number is much larger than 1. This means that the reaction is much faster than the mass transfer rate. So, the Hydrogen content of the liquid phase and also the Hydrogen transferred from the gas phase to the liquid phase disappear very fast due to the high reaction rate. Consequently, the volume of the liquid phase decreases. Figure 7.3 confirms our explanation for

the volume fraction changes along the reactor. For the behavior of volume fractions of the phases, expansion of gas due to the temperature increase is more important than the decrease of gas in the liquid phase due to the consumption in the reaction.

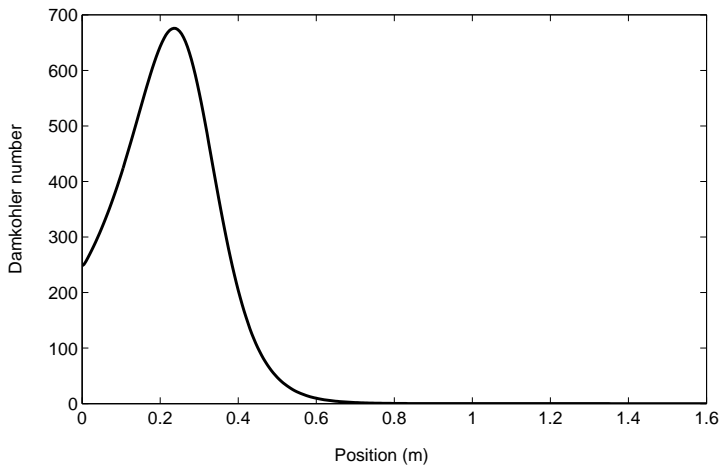


Figure 7.3: The Damkohler number along the trickle bed reactor.

7.4.2 Species distribution

7.4.2.1. Distribution of Hydrogen in the gas phase

Figure 7.4 shows the molar flow rate of Hydrogen in the gas phase along the reactor. The molar flow rate of Hydrogen is slightly decreasing along the reactor. It decreases from about 1.26 mol/s to 1.24 mol/s because of mass transfer from gas to the liquid phase.

There are fluctuations in the molar flow rate of Hydrogen near the outlet of the reactor. These fluctuations are observed because of the reverse flow at the outlet of the reactor.

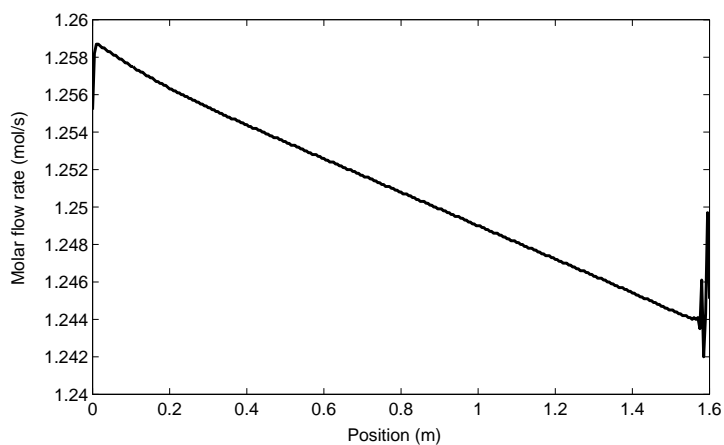


Figure 7.4: Molar flow rate of Hydrogen in the gas phase along the reactor.

7.4.2.2. Distribution of Hydrogen, Hexene and Hexane in the liquid phase

Figure 7.5 shows the molar flow rate of Hydrogen in the liquid phase. This graph shows that the molar flow rate of Hydrogen decreases fast along the reactor near the inlet of the reactor because of the high reaction rate in the liquid phase. Then it

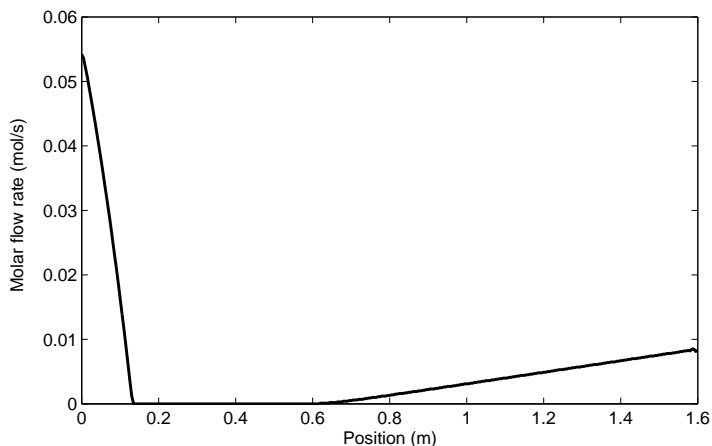


Figure 7.5: Molar flow rate of Hydrogen in the liquid phase along the reactor.

7. Normal operation and hot spots formation in a trickle bed reactor

is zero virtually from about 0.15 m to 0.6 m along the reactor because all Hydrogen which transfers from the gas phase to the liquid phase is immediately consumed in the reaction. After a distance of 0.6 m downstream the inlet of the reactor it increases because there is no reaction in the reactor due to a lack of C_6H_{12} .

Figure 7.6 shows the molar flow rate of C_6H_{12} and C_6H_{14} in the liquid phase along the reactor. The reaction starts from the beginning of the reactor and the molar flow rate of C_6H_{12} is decreasing from about 0.09 mol/s to 0 along the reactor because

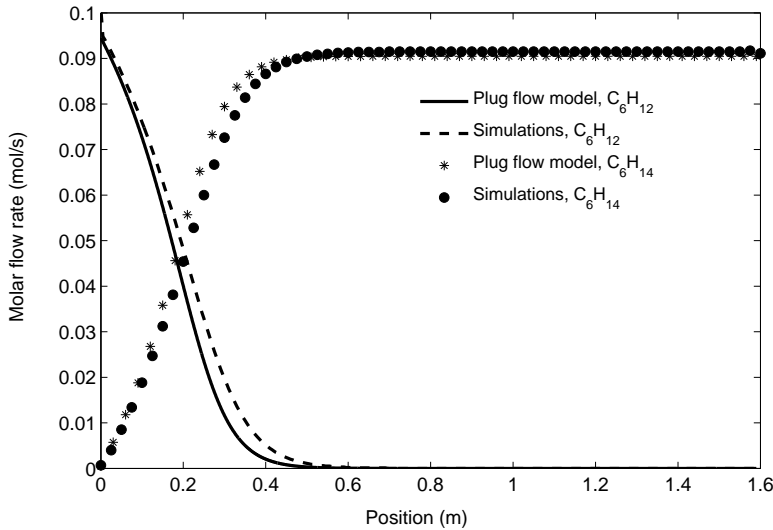


Figure 7.6: Molar flow rate of C_6H_{12} and C_6H_{14} in the liquid phase along the reactor.

of the consumption of reactants in the liquid phase. The molar flow rate of C_6H_{14} is increasing from 0 to 0.09 mol/s along the reactor because of the production due to the reaction in the liquid phase. After about 0.5 m from the inlet the molar flow rate of C_6H_{12} is zero and the reaction is finished. A simple 1-D plug flow model is used to validate the simulations. In the plug flow model we considered one phase flow with constant velocity. We assumed that there is enough Hydrogen and all C_6H_{12} will be consumed in the reaction. In addition, all properties of the fluid such as density and specific heat are constant. Figure 7.6 shows that the results of the CFD simulations and 1-D plug flow model are in good agreement.

As mentioned before there are inert species in both gas and liquid phases. There is no mass transfer or reaction in the reactor for the inert species. Therefore, the molar flow rate of the inert species is constant everywhere along the reactor.

7.4.3 Temperature distribution

7.4.3.1. Temperature distribution in the trickle bed reactor under the normal flow condition

Figure 7.7 shows the temperature profile along the reactor. The temperature is increasing from the inlet of the reactor due to the heat of reaction. Then it is constant after a distance of about 0.5 m downstream the inlet because there is no reaction in the reactor due to the lack of reactant (C_6H_{12}). The temperature distribution along the reactor is also validated with the simple 1-D plug flow model. Figure 7.7 shows that the results of the CFD simulations and 1-D plug flow model are in good agreement.

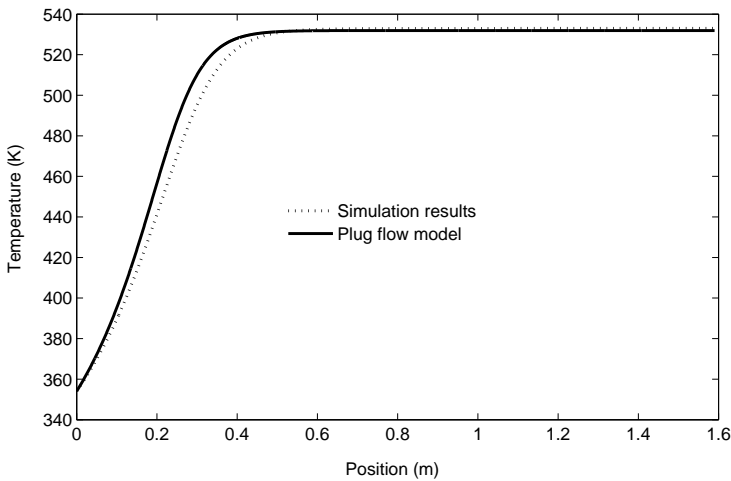


Figure 7.7: Temperature profile along the trickle bed reactor.

7.4.3.2. Temperature distribution under mal-distributed flow condition

Figure 7.8 shows contours of the temperature and volume fraction of the liquid phase in the trickle flow reactor with obstruction against flow in it. All walls of the reactor are insulated and there is no heat transfer between the walls and the fluids. The length of the obstruction is 5 cm and the width is 2 cm . In the regions without blockage the temperature distribution is the same as in the reactor under normal flow conditions. But the temperature distribution is different in the blocked area near the wall. There is a hot spot at the top of the blocked area. The fluid, mostly liquid (figure 7.8), is trapped in this area and cannot convect along the reactor. The reaction rate increases more and more due to the heat accumulation and we observe a hot spot in this area.

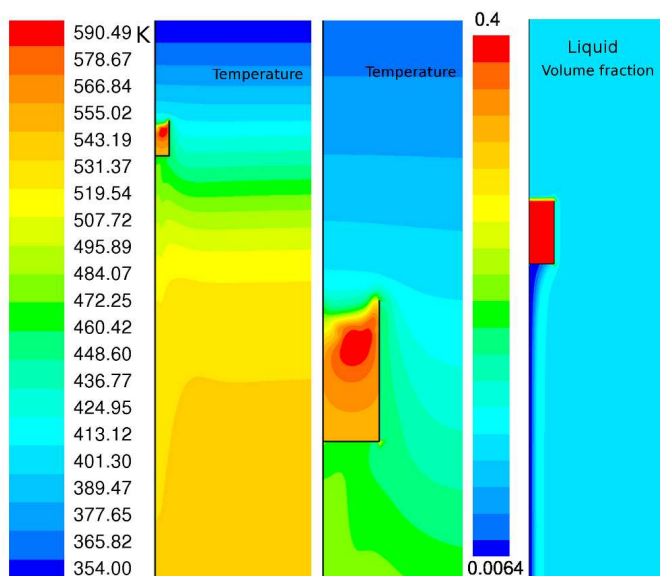


Figure 7.8: Temperature distribution, local hot spot and volume fraction distribution of liquid phase in the trickle bed reactor with blocked region.

As mentioned before the walls of the reactor and barriers are insulated. So, there is no heat conduction through the walls. The only way through which heat can transfer out of the blocked area is conduction in the liquid, solid and gas phases

through the open part of the blocked area. For estimating the temperature difference between the hot spot and surrounding area we assume that the heat transfers via conduction in the liquid and solid phases. The conductivity of the gas is much smaller than the conductivity of the liquid and solid. Moreover, as shown in figure 7.8 there is hardly any gas in the blocked area. So, we neglect the heat transfer due to conduction in the gas phase. Diffusion into the blocked area can be written according to equation 7.28.

$$\phi_m = -D_{l,diff}\alpha_l \frac{\partial C}{\partial x} A \quad (7.28)$$

We consider heat flow out of the blocked area via two possibilities of parallel channels and serial arrangement. According to figures 7.9 for parallel channels for heat flow we can write equation 7.29.

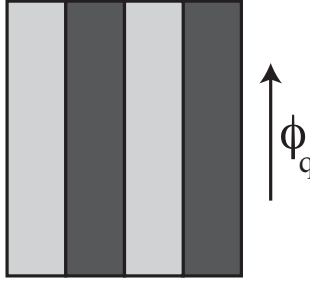


Figure 7.9: Parallel channels for heat flow.

$$\phi_q = -k_l \alpha_l \frac{\partial T}{\partial x} A - k_s \alpha_s \frac{\partial T}{\partial x} A \quad (7.29)$$

If we consider serial arrangement according to figure 7.10 heat flow through the blocked area can be written as equation 7.30.

$$\phi_q = -k_l \frac{\partial T_l}{\partial x} A = -k_s \frac{\partial T_s}{\partial x} A \quad (7.30)$$

We can write equation 7.30 in the form of equation 7.31.

$$\phi_q = k_l \frac{\Delta T_l}{\Delta x_l} A = k_s \frac{\Delta T_s}{\Delta x_s} A \quad (7.31)$$



Figure 7.10: Serial arrangement for heat flow.

We can rewrite the left side of equation 7.31 in the form of equation 7.32.

$$\phi_q = k_l \frac{\Delta T_l}{\Delta x_l} A = k_l \frac{\Delta T_l}{\alpha_l \Delta x} A \quad (7.32)$$

then we will have:

$$\frac{\Delta T_l}{\Delta x} = \frac{\alpha_l}{k_l} \cdot \frac{\phi_q}{A} \quad (7.33)$$

If we do the same for the solid phase, then we will have:

$$\frac{\Delta T_s}{\Delta x} = \frac{\alpha_s}{k_s} \cdot \frac{\phi_q}{A} \quad (7.34)$$

So, for heat flow in the blocked area if we add the above two equations and use $\Delta T = \Delta T_l + \Delta T_s$ then, we reach to equation 7.35.

$$\phi_q = -k_{eff} \frac{\partial T}{\partial x} A \quad (7.35)$$

with:

$$\frac{1}{k_{eff}} = \frac{\alpha_l}{k_l} + \frac{\alpha_s}{k_s} \quad (7.36)$$

If we couple heat and mass via the reaction we will have:

$$\phi_q = \Delta H_r \phi_m \quad (7.37)$$

The concentration of Hydrogen in the liquid phase is smaller than the concentration of n-Hexene. So, the reaction is controlled by the Hydrogen content of the

liquid phase. Therefore, we used the concentration of Hydrogen in the calculation based on equation 7.28. The concentration of Hydrogen at the inlet, the heat of reaction, the mass diffusion coefficient in the liquid phase and the conductivity of the liquid and solid are 564 mol/m^3 , -145800 J/mol , $2.88 \times 10^{-6} \text{ m}^2/\text{s}$, 0.45 W/m.K , 1 W/m.K , respectively. According to equation 7.29 and 7.30 if we consider heat transfer in the both liquid and solid phases based on the parallel and serial arrangements, the temperature difference between the hot spot and surrounding area is 117 K and 136 K for parallel and serial cases, respectively. From the simulation results the temperature difference between the hot spot and surrounding area is about 120 K .

In addition, for more investigation of the results of hot spot formation in the blocked area we performed a simple simulation, which is the steady state temperature dis-

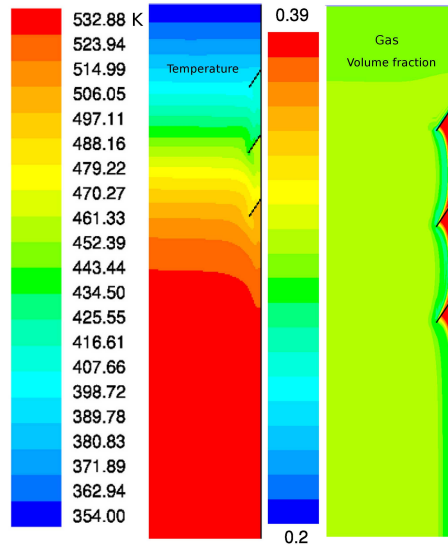


Figure 7.11: Temperature and volume fraction distribution of gas phase in the trickle bed reactor with diagonal barrier.

tribution for a rectangle with local heat production, three isolated walls and one wall fixed at a constant temperature. The result of this simple simulation pretty much has the features of our hot spot. The simulation keeps on changing towards a steady state, but the progress is very slow. So, the heat diffusion in the blocked area is very slow process and can take very long time to reach to the steady state

condition. In addition, this simple simulation shows that the temperature profile in the pocket will stay there even if we perform the simulation for a very long time to reach to the steady-state solution.

Figure 7.11 shows contours of the temperature and volume fraction of the gas phase in the trickle flow reactor with diagonal barriers against flow. This figure shows that the temperature distribution is the same as the reactor with normal flow condition. For this case, gas phase fills the back of the barriers (figure 7.11) because it is much lighter than liquid (density of gas is about 200 times less than the density of liquid and can move easily). So, there is no liquid in this area and therefore no reaction. Consequently, in this case there is no hot spot or hot zone in the area with mal-distribution. In addition, in this reactor, gas and liquid can flow downstream in the mal-distributed area and the heat of reaction can transfer due to the convection in the axial direction.

7.4.4 Grid independence

We tested the grid dependency of our CFD simulations by using four different meshes. The meshes contain 4800, 19200, 76800 and 307200 (1 : 4 : 16 : 64) grid

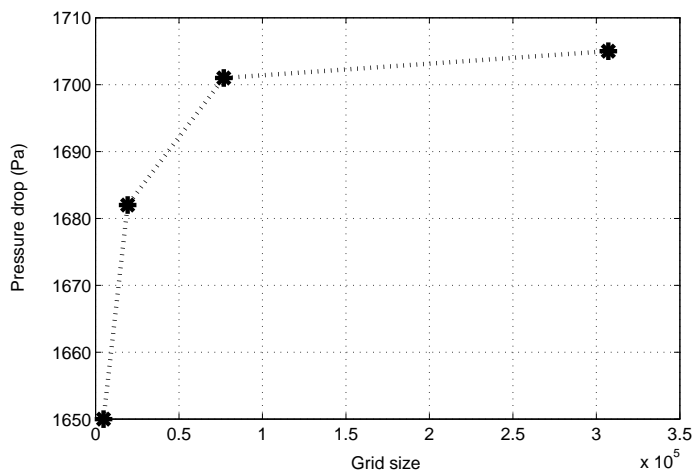


Figure 7.12: Pressure drop of the trickle bed reactor for various meshes.

cells, respectively. Figure 7.12 shows the pressure drop of the bed for four mesh

resolutions. It can be seen that the difference of the calculated pressure drops from the last two meshes is rather small. So, the results are (almost) independent from the grid size. For our simulation we selected the mesh size of 76800 and we used this grid size for the research presented in this paper [18].

7.5 CONCLUSIONS

In this work the operation of a trickle bed reactor with an exothermic reaction is studied using CFD. The results show that trickle bed reactors with an exothermic reaction have the potential of hot spot formation.

A hot spot is observed in the trickle flow reactor with a local blockage which prevents fluid from flowing downstream the reactor. The size of the hot spot is not more than the size of several particles. It is possible to estimate the hot spot temperature with a simple energy balance. For the case that we have here, the temperature difference of hot spot with surroundings resulted from simulations (120 K) is not very much different than the temperature calculated (117 K or 136 K) with simple energy balance. This difference is because of neglecting some parameters in the simple energy balance. This simple estimation can help us to forecast the formation of hot spots and prevent reactors from possible damages. In addition, we conclude that if the reactor is blocked for any reason (physical obstruction, non-uniform distribution of particles, etc) hot spots may form in the reactor.

In the other case with diagonal barriers against flow, hot spots are not observed. This is because of the convection in the radial as well as axial direction in this case. For this case, liquid and gas are not trapped and can flow down stream the reactor. This helps the produced heat in the reactor to convect away and hot spots cannot be formed.

The developed CFD-based model provides knowledge that is often difficult to obtain with experiments and can contribute to improve the design of trickle bed reactors with reacting flow. These CFD simulations provide useful data on the temperature profile, thermal performance and formation of hot spots in trickle bed reactors which can be used for the improvement and further optimization on the design and operation of the trickle bed reactors.

Acknowledgement

The authors would like to thank Shell Global Solutions International B.V, Amsterdam for the scientific and financial support.

NOMENCLATURE

ρ	density	kg/m^3
t	time	s
\vec{v}	velocity vector	m/s
P	pressure	Pa
τ	stress tensor	N/m^2
\vec{g}	gravitational acceleration vector	m/s^2
\vec{F}	force	N
μ	molecular viscosity	kg/ms
$\nabla \cdot \vec{v}_q$	effect of volume dilation	$1/s$
S_m	mass source	kg/m^3s
I	unit tensor	—
k	conductivity	W/mK
S_q	heat source	J/m^3s
Y_i	mass fraction of species i	—
\vec{J}_i	diffusion flux of species i	kg/m^2s
R_i	reaction rate of production of species i	kg/m^3s
$D_{i,mix}$	mass diffusion coefficient of species i	m^2/s
$D_{T,i}$	thermal diffusion coefficient of species i	m^2/s
$\hat{R}_{i,r}$	molar rate of reaction	mol/m^3s
$M_{W,i}$	molecular weight	gr/mol
\dot{m}	mass transfer rate	kg/m^3s
K	interphase momentum exchange coefficient	Ns/m
α	volume fraction	—
R	universal gas constant	$J/molK$
Q_{pq}	energy transfer between the phases	J/m^3s
\vec{v}_{pq}	interphase velocity	m/s
λ_{gl}	mass transfer rate	kg/m^3s
\dot{r}	mass transfer rate	kg/m^3s
$Y_{g,i}$	mass fraction of species i in the gas phase	—
C	concentration	mol/m^3
Da	Damkohler number	—
f	drag function	—
τ_{par}	particulate relaxation time	s
L	length	m

7. Normal operation and hot spots formation in a trickle bed reactor

r	rate of reaction	kg/m^3s
d_p	particle diameter	m
C_D	drag coefficient	—
H	enthalpy	J/mol
\vec{q}_q	heat flux	W/m^2s
\mathbb{R}	heterogeneous reaction rate	mol/m^3s
T	temperature	K
k	reaction rate constant	—
n	reaction order	—
k_g	mass transfer coefficient	m/s
a	interfacial area	m^2
$h_{c,pq}$	heat transfer coefficient between the phases	W/m^2K
d_s	solid phase diameter	m
τ_s	particulate relaxation time	s
Re	Reynolds number	—
Nu	Nusselt number	—
Pr	Prandtl number	—
Re_{sf}	Relative Reynolds of solid and fluid (gas or liquid)	—
Re_{gl}	Relative Reynolds of gas and liquid	—
x	distance	m
ΔH_r	heat of reaction	J/mol
D_{diff}	diffusion coefficient	m^2/s
ϕ_m	liquid flow due to diffusion	mol/s
ϕ_q	heat flow	W
A	area	m^2

INDICES

p	phase p
q	phase q
pq	interaction between phase p and q
l	liquid phase
g	gas phase
s	solid phase
f	fluid
vm	virtual mass force
$lift$	lift force
m	mass source
h	heat source
i	species i
j	species j
mix	mixture
W	weight
H_2	Hydrogen
C_6H_{12}	Hexene
C_6H_{14}	Hexane
max	maximum
T	transpose
n	number of phases
exp	exponential factor
par	particulate relaxation time
dr	drag force
x	x direction
y	y direction
0	initial condition
$diff$	diffusion coefficient
op	operating condition
r	reaction
eff	effective

7.6 Bibliography

- [1] Muthanna, H.Al-Dahhan, Faical Larachi, Milorad P. Dudukovic, and Andre Laurent. High pressure trickle bed reactors : A review. *Ind. Eng. Chem. Res.*, 36:3292–3314, 1997.
- [2] M. Martinez, J. Pallares, J. Lopez, A. Lopez, F. Albertos, M.A. Garcia, I. Cuesta, and F.X. Grau. numerical simulation of the liquid distribution in a trickle bed reactor. *Chemical Engineering Science*, 76:49–57, 2012.
- [3] Wayne Strasser. Cfd study of an evaporative trickle bed reactor: mal-distribution and thermal runaway induced by feed disturbances. *Chemical Engineering Journal*, 161:257–268, 2010.
- [4] Mc Manus, R.K. Funk, G.A. Harold M.P, and Ng K.M. Experimental study of reaction in trickle bed reactors with liquid maldistribution. *Ind. Eng. Chem. Res.*, 32:570, 1993.
- [5] Chaudhari R.V, Jaganathan R, Mathew S.P, Julcour C, and Delmas H. Hydrogenation of 1,5,9-cyclododecatriene in fixed bed reactors: down vs upflow modes. *AIChE Journal*, 48:110, 2002.
- [6] Jing Guo, Yi Jiang, and Muthanna H. Al-Dahhan. Modeling of trickle bed reactors with exothermic reactions using cell network approach. *Chemical Engineering Science*, 63:751–764, 2008.
- [7] Anna A. Lysova, Agnes von Garnier, Edme H. Hardy, Rainer Reimert, and Igor V. Koptug. The influence of an exothermic reaction on the spatial distribution of the liquid phase in a trickle bed reactor: Direct evidence provided by nmr imaging. *Chemical Engineering Journal*, 173:552–563, 2011.
- [8] Giuseppe Biardi and Giancarlo Baldi. Three-phase catalytic reactors. *Catalysis Today*, 52:223–234, 1999.
- [9] Varma, Morbidelli, and Wu. Parametric sensitivity in fixed-bed catalytic reactors with reverse flow operation. *Chem. Eng. Sci.*, 54:4579–4588, 1999.
- [10] Chen X et al. CFD modeling using heterogeneous reaction kinetics for catalytic dehydrogenation syngas reactions in a fixed-bed reactor. *Particuology*, 2013.
- [11] J.N. Papageorgiou and G.F. Froment. Simulation models accounting for radial voidage profiles in fixed-bed reactors. *Chem. Eng. Sci.*, 56:3043–3056, 1995.

-
- [12] O. Bey and G. Eigenberger. Fluid flow through catalyst filled tubes. *Chem. Eng. Sci*, 52:1365–1376, 1997.
- [13] M.K. Rottschäfer and D. Vortmeyer. Measured and modeled superficial flow profiles in packed beds with liquid flow. *AIChE J*, 44:484–490, 1998.
- [14] M. Winterberg and E. Tsotsas. Impact of tube-to-particle-diameter ratio on pressure drop in packed beds. *AIChE J*, 46:1084–1088, 2000.
- [15] A. de Klerk. Voidage variation in packed beds at small column to particle diameter ratios. *AIChE J*, 49:2022–2029, 2003.
- [16] D. Lide. *CRC handbook of chemistry and physics*. CRC Press, 1994.
- [17] Robert H. Perry, James O. Maloney, and Don W. Green. *Perry's Chemical Engineers' Handbook*. McGraw Hill, 1984.
- [18] F Mousazadeh, H.E.A. van den Akker, and R.F. Mudde. Eulerian simulation of heat transfer in trickle bed reactor with constant wall temperature. *Chemical Engineering Journal*, 207-208:675–682, 2012.
- [19] FLUENT Incorporate, Natick, MA. *Fluent 12.06.016 Theory Guide*, 2009.
- [20] L. Schiller and Z. Naumann. A drag coefficient correlation. *Verein Deutscher Ingenieure*, 77:318, 1935.
- [21] D. Gidaspow, R. Bezburuah, and J. Ding. Hydrodynamics of circulating fluidized beds, kinetic theory approach. In *fluidization VII, Proceeding 7th Engineering foundation conference on fluidization*, 7:75–82, 1992.
- [22] C.Y. Wen and Y.H. Yu. Mechanics of fluidization. *Chemical engineering Progress Symposium Series*, 62:100–111, 1966.
- [23] S. Ergun. Fluid flow through packed columns. *Chem. Eng. Prog*, 42:89–94, 1952.
- [24] T.B. Anderson and R. Jackson. A fluid mechanical description of fluidized beds. *I and EC Fundam*, 6:527–534, 1967.
- [25] R.M. Bowen. *Theory of mixtures*. Academic Press, 1976.
- [26] W.E. Ranz and W.R.E. Marshall. Evaporation from drops, part 1. *Chemical Engineering Progress*, 48:141–146, 1952.

- [27] D.J. Gunn. Transfer of heat or mass to particles in fixed and fluidized beds. *Journal of Heat and Mass Transfer*, 21:467–476, 1978.
- [28] Gianetto A and Silveston P.L. *Multiphase chemical reactors: Theory, design, scale-up*. 1986.
- [29] Saroha A.K and Nigam K.D.P. Trickle bed reactors, *Reviews in Chemical Engineering*. 12(3-4):207–347, 1996.
- [30] Korsten H. and Hoffmann U. Three phase reactor model for hydrotreating in pilot trickle bed reactors. *AIChE Journal*, 42 (5):1350–1360, 1996.

CHAPTER 8

NORMAL OPERATION AND EVAPORATION IN A TRICKLE BED

Abstract

This chapter reports a Computational Fluid Dynamics (CFD) study on the performance of a three phase trickle bed reactor. We study the performance of a trickle bed reactor under normal operating condition and with evaporation but we focus more on the reactor with evaporation. In the reactor there is an exothermic reaction in the liquid phase, heat transfer between the phases and evaporation in the liquid phase. Evaporation is an endothermic phenomenon and decreases the temperature along the reactor. In addition, it can affect the production rate of desired and undesired species due to the effects on the temperature and volume fraction of the phases. Evaporation plays an important role in the investigation of hot spots because of its significant effect on the thermal performance of the reactor. The results of the 2-D CFD simulations under normal flow condition have been validated with a simple 1-D plug flow model. They are in good agreement.

8.1 Introduction

In multi-phase reactors more than one phase is present at the same time. Trickle bed reactors have a fixed-bed of solid catalysts through which liquid and gas flow co-current or counter current [1]. These reactors operate continuously and are used in petroleum, petrochemical and chemical industries such as:

- Hydrogenation of Hydrocarbons
- Hydrodesulphurization
- Hydro-finishing of lubricating oils

A review on hydrodynamics of trickle bed reactors is given by Al-Dahhan et al. [1]. Trickle bed reactors typically have two main flow condition: a low interaction regime (LIR) and a high interaction regime (HIR). When there are relatively low flow rates of gas and liquid we have the low interaction regime. At higher flow rates of gas and liquid there is intense gas-liquid shear and this flow regime is called high interaction regime. Different high interaction regimes exist depending on the flow rate of gas and liquid. These regimes are liquid-continuous at low gas flow rates or gas-continuous at high gas flow rates.

The Eulerian-Eulerian multi-phase approaches have been used to study trickle bed reactors. Examples can be found in the work of Dudokovic et al. [2], [3], R. Quita-Ferreira et al. [4], [5], [6], P.R. Gunjan [7] and V. Alopaeus [8]. With this method, the individual catalyst particles are not modeled. Few researchers have modeled individual catalyst particles using a porous medium approach. They showed that it is a useful strategy and requiring much less computational effort. An informative comparison of volume of fluid (VOF) and Eulerian-Eulerian CFD methodologies involving individual modeled catalyst particles is given by Lopez and Quinta-Ferreira [4]. It was shown that due to the formulation of the Eulerian-Eulerian interaction term, the VOF method (no interaction terms between the phases) was a worse predictor of hydrodynamics responses. Gunjal and Ranade [7] investigated hydrodynamic effects that are influenced by kinetics. They have done a mass transfer related study in which gas phase solubility in the liquid phase is incorporated but they have not taken evaporation into account. Mal-distribution in trickle bed reactors was studied by Jiang et al. [2] and Farzad et al. [9]. There have been no CFD studies we are aware of involving evaporation in trickle flow reactors.

The objective of this work is to investigate the effect of evaporation on the performance of a trickle bed reactor. In this work, we focus on the effect of evaporation on the temperature profile and volume fraction in the reactor. We compare the opera-

tion of a trickle bed reactor under normal flow condition to a case with evaporation.

8.2 Geometry and setup

The trickle bed in our study is two-dimensional and axi-symmetric, see figure 8.1. The length of the reactor is $L_x=1.6\text{ m}$ and the radius of the reactor is $L_y=0.15\text{ m}$.

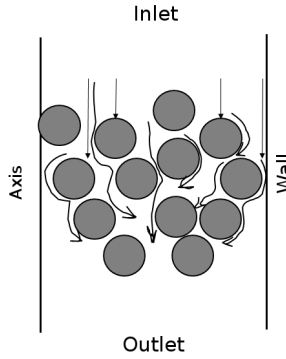


Figure 8.1: Geometry of the modeled trickle bed reactor.

The reactor operates at 60 bar pressure and we take the gravitational acceleration (9.8 m/s^2) into account. The gas and liquid flow from top to bottom. The hydraulic diameter of the particles is 2.9 mm and the porosity of the bed is 40%. The liquid and gas flow into the reactor as a mixture. The gas phase contains the species Hydrogen (H_2 , 98%), inert material (Ar 2%) and Benzene ($C_6H_6(v)$ 0%). For these species, enthalpy of formation, density, specific heat, thermal conductivity and viscosity are assumed to be constant. For the properties of the gas mixture, we use the ideal gas law with the assumption that the density is a function of temperature and not pressure (we use a constant operating pressure of the reactor for the calculation of the density, $\rho = \frac{P_{op}M_W}{RT}$, $P_{op} = cte = 60\text{ bar}$), constant specific heat, thermal conductivity and viscosity. The mass diffusivity of each species in the gas mixture is $2.88 \times 10^{-5}\text{ m}^2/\text{s}$. The liquid phase contains the species n-Hexene (C_6H_{12} , 22%), n-Hexane (C_6H_{14} , 0%), inert material (Cyclohexane, C_6H_{12} , 60%),

Benzene ($C_6H_6(l)$, 12%) and Hydrogen (H_2 , 6%). For all these species, enthalpy of formation, density, specific heat, thermal conductivity and viscosity are constant. For the properties of the liquid mixture, we use constant density, specific heat, thermal conductivity and viscosity. The mass diffusivity of each species in the liquid mixture is $2.88 \times 10^{-6} \text{ m}^2/\text{s}$.

All properties of the solid phase i.e. density, specific heat and thermal conductivity are assumed to be constant. Properties of the gas mixture, liquid mixture and solid phase are listed in the table 8.1.

Parameter	Gas Mixture	Liquid Mixture	Solid
Density	$\rho = P_{op} M_W / RT, P_{op} = cte$	763 kg/m^3	2500 kg/m^3
Specific heat	6560 J/kg K	2030 J/kg K	670 J/kg K
Thermal conductivity	0.0454 W/m K	0.454 W/m K	1 W/m K
Viscosity	$1.04 \times 10^{-5} \text{ kg/ms}$	$3.27 \times 10^{-4} \text{ kg/ms}$	–
Mass diffusivity	$2.88 \times 10^{-5} \text{ m}^2/\text{s}$	$2.88 \times 10^{-6} \text{ m}^2/\text{s}$	–

Table 8.1: Properties of the liquid mixture, gas mixture and solid phase.

8.3 Model description

8.3.1 Euler-Euler approach

In this work the Euler-Euler multi-phase approach is used to solve the average mass, momentum, species and energy equations for each phase separately. In the Euler-Euler approach, the different phases are treated mathematically as interpenetrating continua. Since the volume of one phase cannot be occupied by the other phases, the concept of phase volume fraction is introduced. The volume fractions are continuous functions of space and time and their summation is equal to one. Coupling of the pressure and velocity is achieved through the interaction between the phases such as the drag force [10]. The transport equations of the Euler-Euler model are as follows [11].

Mass conservation equation:

$$\frac{\partial(\alpha_q \rho_q)}{\partial t} + \nabla \cdot (\alpha_q \rho_q \vec{v}_q) = \sum_{p=1}^n (\dot{m}_{pq} - \dot{m}_{qp}) + S_{mq} \quad (8.1)$$

where α_q is the volume fraction of phase q , ρ_q is the density of phase q , \vec{v}_q is the velocity of phase q , t is the time, \dot{m}_{pq} is the mass transfer from the p^{th} to the q^{th} phase, \dot{m}_{qp} is the mass transfer from the q^{th} to the p^{th} phase and S_{mq} is the mass source of phase q .

Momentum conservation equation:

$$\frac{\partial(\alpha_q \rho_q \vec{v}_q)}{\partial t} + \nabla \cdot (\alpha_q \rho_q \vec{v}_q \vec{v}_q) = -\alpha_q \nabla P + \nabla \cdot \bar{\bar{\tau}}_q + \alpha_q \rho_q \vec{g} + \sum_{p=1}^n (\dot{m}_{pq} \vec{v}_{pq} - \dot{m}_{qp} \vec{v}_{qp}) + \vec{F}_q + \vec{F}_{lift,q} + \vec{F}_{vm,q} + \sum_{p=1}^n K_{pq}(\vec{v}_p - \vec{v}_q) \quad (8.2)$$

where P is the pressure, $\bar{\bar{\tau}}_q$ is the stress tensor of phase q , \vec{g} is the gravity vector, \vec{v}_{pq} is the interphase velocity defined as follows: if $\dot{m}_{pq} > 0$ (mass transfer from the p^{th} to the q^{th} phase) then $\vec{v}_{pq} = \vec{v}_p$, if $\dot{m}_{pq} < 0$ (mass transfer from the q^{th} to the p^{th} phase) then $\vec{v}_{pq} = \vec{v}_q$, likewise if $\dot{m}_{qp} > 0$ then $\vec{v}_{qp} = \vec{v}_q$, if $\dot{m}_{qp} < 0$ then $\vec{v}_{qp} = \vec{v}_p$, \vec{F}_q includes all external body forces except gravity, $\vec{F}_{lift,q}$ is the lift force, $\vec{F}_{vm,q}$ is the virtual mass force, $K_{pq}(\vec{v}_p - \vec{v}_q)$ is the drag force between the phases and K_{pq} is the interphase momentum exchange coefficient. $\bar{\bar{\tau}}_q$ is defined as:

$$\bar{\bar{\tau}}_q = \alpha_q \mu_q [(\nabla \vec{v}_q + \nabla \vec{v}_q^T)] - \frac{2}{3} \alpha_q \mu_q \nabla \cdot \vec{v}_q I \quad (8.3)$$

where μ_q is the viscosity of phase q and I is the unit tensor. The gravity force is taken into account in all simulations and the lift force and virtual mass force are neglected because they are much smaller than the drag force between the phases. There is no other external force (except gravity) in the system, therefore, \vec{F}_q is zero. For gas-liquid flows, the liquid phase is assumed to form droplets. The exchange coefficient for these types of gas-liquid flows can be written in the form:

$$K_{gl} = \frac{\alpha_g \alpha_l \rho_g f_{dr}}{\tau_{par}} \quad (8.4)$$

where f_{dr} , the drag function, is defined differently for different exchange coefficient models and τ_{par} is the particulate relaxation time and is defined as:

$$\tau_{par} = \frac{\rho_g d_{gl}^2}{18 \mu_l} \quad (8.5)$$

where d_{gl} is the diameter of the droplets of phase l . All definitions of f_{dr} include a drag coefficient (C_D) which is based on the relative Reynolds number.

For the drag coefficient between gas and liquid, we use the model of Schiller and Naumann [12] in the following form:

$$f_{dr} = 1 + 0.15 Re_{gl}^{0.687} \quad (8.6)$$

where Re_{gl} is the relative Reynolds number between the gas and liquid phases. The relative Reynolds number for the primary gas phase and secondary liquid phase is obtained from:

$$Re_{gl} = \frac{\rho_g |\vec{v}_g - \vec{v}_l| d_g}{\mu_g} \quad (8.7)$$

In our simulations for the solid-gas and solid-liquid interaction we use the model of Gidaspow [13] which is a combination of the Wen and Yu model [14] and the Ergun equation [15]. According to Gidaspow model [13] when $\alpha_f > 0.8$, the fluid-solid exchange coefficient K_{sf} is of the following form:

$$K_{sf} = \frac{3}{4} C_D \frac{\alpha_s \alpha_f \rho_f |\vec{v}_s - \vec{v}_f|}{d_s} \alpha_f^{-2.65} \quad (8.8)$$

where

$$C_D = \frac{24}{\alpha_f Re_{sf}} (1 + 0.15 (\alpha_f Re_{sf})^{0.687}) \quad (8.9)$$

Re_{sf} is the relative Reynolds number between fluid and solid. When $\alpha_f \leq 0.8$, the fluid-solid exchange coefficient K_{sf} is of the following form.

$$K_{sf} = 150 \frac{\alpha_s (1 - \alpha_f) \mu_f}{\alpha_f d_s^2} + 1.75 \frac{\rho_f \alpha_s |\vec{v}_s - \vec{v}_f|}{d_s} \quad (8.10)$$

Energy conservation equation:

$$\begin{aligned} \frac{\partial (\alpha_q \rho_q H_q)}{\partial t} + \nabla \cdot (\alpha_q \rho_q \vec{v}_q H_q) = -\alpha_q \frac{\partial P}{\partial t} + \bar{\epsilon}_q : \nabla \vec{v}_q - \nabla \cdot \vec{q}_q + S_q + \\ \sum_{p=1}^n (Q_{pq} + \dot{m}_{pq} H_{pq} - \dot{m}_{qp} H_{qp}) \end{aligned} \quad (8.11)$$

where H_q is the enthalpy of phase q per unit mass, \vec{q}_q is the heat flux, S_q is the heat source, Q_{pq} is the heat exchange between the p^{th} and q^{th} phases, \dot{m}_{pq} is the

mass transfer from p^{th} to the q^{th} phase, \dot{m}_{qp} is the mass transfer from q^{th} to the p^{th} phase and H_{pq} and H_{qp} are the interphase enthalpies (e.g., the enthalpy of the vapor in case of evaporation and enthalpy of the liquid in case of condensation).

The heat flux, \vec{q}_q is defined as:

$$\vec{q}_q = -k_q \frac{\partial T}{\partial \vec{r}} \quad (8.12)$$

where k_q is the conductivity of phase q .

The rate of energy transfer between the phases (Q_{pq}) is assumed to be a function of the temperature difference between the phases:

$$Q_{pq} = h_{c,pq}(T_p - T_q) \quad (8.13)$$

where $h_{c,pq}$ is the heat transfer coefficient between the p^{th} and q^{th} phase.

Volume fraction equation:

The description of multi-phase flow as interpenetrating continua incorporates the concept of phase volume fractions, denoted here by α_q . Volume fractions represent the space occupied by each phase and the laws of conservation of mass and momentum are satisfied by each phase individually. The derivation of the conservation equations can be done by ensemble averaging the local instantaneous balance for each of the phases [16] or by using the mixture theory approach [17].

The volume fractions satisfy the following equation.

$$\sum_{q=1}^n \alpha_q = 1 \quad (8.14)$$

Species transport can also be applied to multi-phase flows. We solve the conservation equations for chemical species in multi-phase flows for each phase q . The local mass fraction of each species Y_i can be predicted by the solution of a convection-diffusion equation for the i^{th} species.

Conservation equation of species:

$$\frac{\partial(\rho^q \alpha^q Y_i^q)}{\partial t} + \nabla \cdot (\rho^q \alpha^q \vec{v}^q Y_i^q) = -\nabla \cdot (\alpha^q \vec{J}_i^q) + \alpha^q R_i^q + \sum_{p=1}^n (\dot{m}_{p^i q^j} - \dot{m}_{q^j p^i}) + \mathbb{R} \quad (8.15)$$

where R_i^q is the net rate of production of homogeneous species i by chemical reaction for phase q , \dot{m}_{qjpi} is the mass transfer source between species i and j from phase q to p and \mathbb{R} is the heterogeneous reaction rate. In addition, α^q is the volume fraction for phase q , Y_i^q is the mass fraction of species i and \vec{J}_i^q is the diffusion flux of species i , which arises due to gradients of concentration and temperature. We used Ficks' law to model the mass diffusion due to the concentration and temperature gradients:

$$\vec{J}_i^q = -\rho^q D_{i,mix} \nabla Y_i^q - D_{T,i} \frac{\nabla T}{T} \quad (8.16)$$

where $D_{i,mix}$ is the mass diffusion coefficient for species i in the mixture and $D_{T,i}$ is the thermal diffusion coefficient for species i in the mixture.

The source of chemical species i due to the reaction is computed as an Arrhenius reaction source that the species participate in:

$$R_i^q = M_{W,i} \hat{R}_i^q \quad (8.17)$$

where R_i^q is the Arrhenius mass rate of creation or destruction, $M_{W,i}$ is the molecular weight of species i and \hat{R}_i^q is the Arrhenius molar rate of creation or destruction of species i due to the reaction.

8.3.2 Evaporation

The evaporation model which is used for the simulations in this work is a mechanistic model with a physical basis [18]. Based on the following temperature regimes, the evaporation (mass transfer from liquid to gas phase) can be described:

If $T > T_{sat}$, then

$$\dot{m}_{e \rightarrow v} = coeff * \alpha_l \rho_l \frac{(T - T_{sat})}{T_{sat}} \quad (8.18)$$

If $T < T_{sat}$, then

$$\dot{m}_{e \rightarrow v} = coeff * \alpha_v \rho_v \frac{(T - T_{sat})}{T_{sat}} \quad (8.19)$$

$\dot{m}_{e \rightarrow v}$ represents the rate of mass transfer from the liquid phase to the gas (vapor) phase with unit of $kg/s/m^3$. α , ρ and T_{sat} are the phase volume fraction, density and saturation temperature, respectively. The source term for the energy equation

can be obtained by multiplying the rate of mass transfer by the latent heat. In the above equation, $coeff$ is the inverse of the relaxation time (1/s) and is defined as:

$$coeff = \frac{6}{d} \beta L \sqrt{\frac{M_W}{2\pi \mathbf{R} T_{sat}}} \cdot \frac{\rho_l}{\rho_l - \rho_g} \quad (8.20)$$

where β is the accommodation coefficient, M_W is the molecular weight, L is the latent heat, d is the diameter of bubbles and \mathbf{R} is the universal gas constant.

In our system, Benzene (C_6H_6) molecules evaporate (due to the heat of reaction) and they transfer from the liquid phase to the gas phase. For the calculations of this research we assumed $coeff=10/s$ and $T_{sat}=400\text{ K}$.

8.3.3 Reaction

For the reaction we use a volumetric Arrhenius type of reaction in the liquid phase. The reaction occurs in the liquid phase between H_2 and C_6H_{12} and produces C_6H_{14} as product. The reaction is:



where H_2 is Hydrogen, C_6H_{12} is n-Hexene and C_6H_{14} is n-Hexane. The reaction is an exothermic reaction with the heat of reaction equal to $144\text{ kJ/mol } H_2$ and the rate of reaction is:

$$-\hat{R}_{C_6H_{12}} = 6.17 \exp\left(\frac{-20700}{\mathbf{R}T}\right) C_{C_6H_{12}} \quad (8.22)$$

where $\hat{R}_{C_6H_{12}}$ is the reaction rate, T is the temperature, \mathbf{R} is the gas universal constant and $C_{C_6H_{12}}$ is the concentration of C_6H_{12} in the liquid phase.

8.3.4 Mesh

For our modeling we use a structured mesh. The geometry is axi-symmetric and the number of grid nodes in the axial direction is 320 and in the radial direction 30, resulting in a total number of cells of 9600. The size of each grid cell is about 5 mm . In addition, we have three other meshes with 2400, 38400 and 153600

grid cells. The computation time for these simulations are very high and we have chosen the smallest number of grid cells that we could perform the simulations with independent results from the grid size. We have discussed mesh size in detail in section 8.4.4.

8.3.5 Boundary conditions and solver details

The equations 8.1, 8.2, 8.11 and 8.15 are subject to the following boundary condition.

At the inlet of the reactor we use a velocity inlet boundary condition with constant velocity and temperature. The velocity of liquid and gas at the inlet are 0.0016 m/s and 0.007 m/s respectively and the inlet temperature of both phases is 354 K . The volume fraction of the liquid and gas at the inlet are 0.1 and 0.3. Both gas and liquid are mixtures. In the liquid phase we have C_6H_{12} (22%), C_6H_{14} (0%), H_2 (6%), inert material (60%) and $C_6H_6(l)$ (12%) and in the gas phase we have H_2 (98%), inert material (2%) and $C_6H_6(v)$ (0%). At the outlet of the reactor we use a pressure outlet boundary condition. We have stationary walls and no slip condition. There is no heat transfer between the walls and the fluids. The saturation temperature (boiling point) for evaporative species ($C_6H_6(l)$) is assumed 400 K .

All simulations are performed with the CFD code Fluent version 13.0.0. Meshing of the two-dimensional computational domains is performed in Gambit version 2.4.6. The governing equations are discretised by the finite volume approach. The Second-order Upwind differencing method is used for discretization of the convection terms and the Simple method is applied for simultaneous solution for the pressure velocity coupled equations. The flow is assumed laminar and incompressible. All mass, momentum, energy, species transport and volume fraction equations are solved in a two-dimensional axi-symmetric transient formulation. The solid particles are assumed to be stagnant ($v_s = 0$) with a constant volume fraction of 0.6. Convergence limits of the sum of the absolute residuals for all the equations are set to 10^{-6} . Unsteady simulations with time step of 10^{-2} second are continued until steady state in the outlet velocity and temperature profile is reached.

8.4 Results and discussion

8.4.1 Volume fraction distribution in the trickle bed reactor

Figure 8.2 shows the volume fraction of the liquid and gas phases along the trickle bed reactor under normal flow condition and with evaporation. The volume fraction of the liquid in the reactor without evaporation is decreasing along the reactor from the inlet of the reactor to about 0.5 m downstream the inlet. The liquid and gas flow into the reactor and the reaction between Hydrogen (H_2) and Hexene (C_6H_{12}) immediately starts in the liquid phase. The rate of reaction is very high, so, the volume of the liquid phase is decreasing due to the consumption of Hydrogen in the liquid phase. In addition, a lot of heat is generated due to the exothermic reaction and the gas phase expands and shows an increase in the volume fraction. After about 0.5 m downstream the inlet the reaction is finished and the temperature remains constant. At the outlet of the reactor the volume fraction fluctuates. These fluctuations are observed because of a reverse flow at the outlet of the reactor.

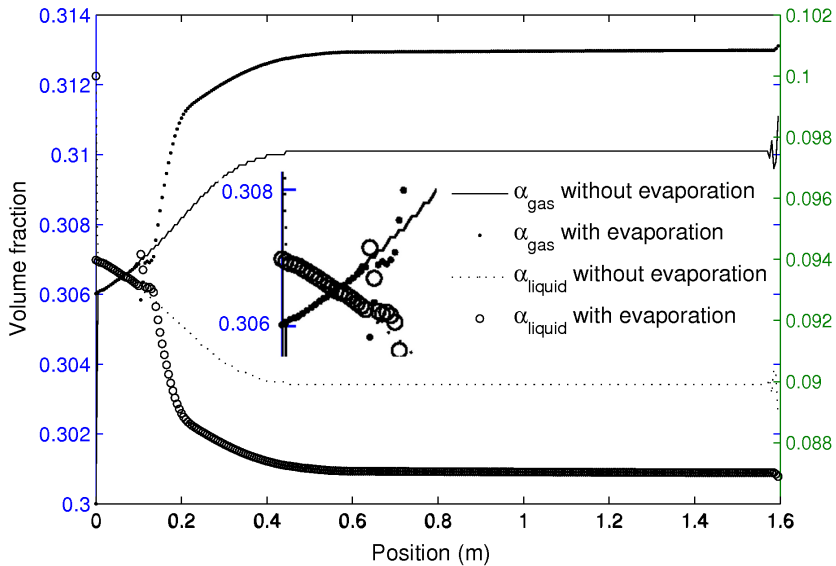


Figure 8.2: Volume fraction of the liquid and gas phases along the trickle bed reactor with and without evaporation.

For the trickle bed reactor with evaporation, when the temperature increases along the reactor and reaches to the saturation temperature, Benzene starts to evaporate. Evaporation starts about 0.15 m downstream the inlet. Evaporation is an endothermic phenomenon and consumes the heat produced with the exothermic reaction. As a consequence, the temperature increases very little (less than the normal flow reactor without evaporation) and consequently the gas phase does not expand too much. On the other hand, we have mass transfer from gas to liquid. Therefore, the volume fraction of the gas phase decreases (mass transfer from gas to liquid dominates over expansion). This behavior of the volume fraction of the gas phase at the beginning of the evaporation is because of the lack of gas expansion for a short time. The evaporation rate increases due to the high temperature (reaction is still happening) and then the volume fraction changes follow the expected behavior which is the increase of the volume fraction of the gas phase. In addition, when there is evaporation in the system the rate of changes in the volume fraction of both phases is larger than the normal system without evaporation. This is because of the mass transfer from the liquid to the gas phase due to the evaporation.

8.4.2 Distribution of Benzene in the liquid and gas phases

Figure 8.3 shows the molar flow rate of C_6H_6 in both liquid and gas phases. As mentioned before when we start up the reactor there is no C_6H_6 in the gas phase. So, near the inlet of the reactor where evaporation has not started yet (about 0.15 m from the inlet), the molar flow rate of C_6H_6 in the gas phase is zero. In this part of the reactor, the molar flow rate of C_6H_6 in the liquid phase is constant. At about 0.15 m downstream the inlet, the evaporation starts and C_6H_6 transfers from the liquid to the gas phase. At about 0.2 m downstream the inlet, the evaporation is finished due to the lack of C_6H_6 in the liquid phase. So, the molar flow rate of C_6H_6 in the gas phase is constant and in the liquid phase is zero.

The molar flow rates of other species in the both gas and liquid phases of the normal flow reactor have been discussed in chapter 7. The trend of the consumption and production of all other species for both normal flow and the reactor with evaporation are the same. So, this is not discussed here.

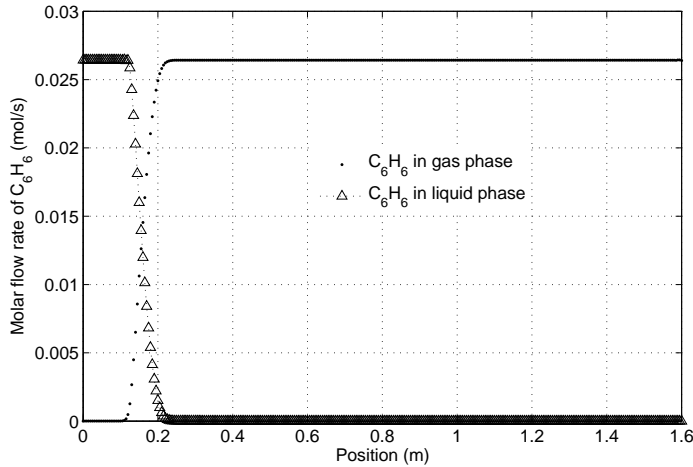


Figure 8.3: Molar flow rate of C_6H_6 along the reactor in both liquid and gas phases.

8.4.3 Temperature distribution in the trickle bed reactor

Figure 8.4 shows the temperature profile for the reactor with normal flow condition, the reactor with evaporation and the plug flow model. For the reactor with normal flow condition, the temperature is increasing from the inlet of the reactor due to the heat of reaction. Then it is constant after a distance of about 0.5 m downstream the inlet because there is no reaction in the reactor due to the lack of reactant (C_6H_{12}), see chapter 7. A simple 1-D plug flow model is used to validate the simulations. In the plug flow model we considered one phase flow with constant velocity. We assumed that there is enough Hydrogen and all C_6H_{12} will be consumed in the reaction. In addition, all properties of the fluid such as density and specific heat are constant. Figure 8.4 shows that the results of the CFD simulations and 1-D plug flow model are in agreement.

In the case of evaporation, the thermal behavior of the reactor is different. Figure 8.4 shows that the evaporation starts about 0.15 m downstream the inlet. Between 0.15 m to 0.2 m downstream the inlet the temperature increases slightly in comparison with the reactor without evaporation. This slight increase is because of the consumption of part of the energy produced due to the reaction. Then the temperature increases and when the reaction is finished the temperature is constant. The temperature of the reactor at the end of the reaction (0.5 m downstream the inlet)

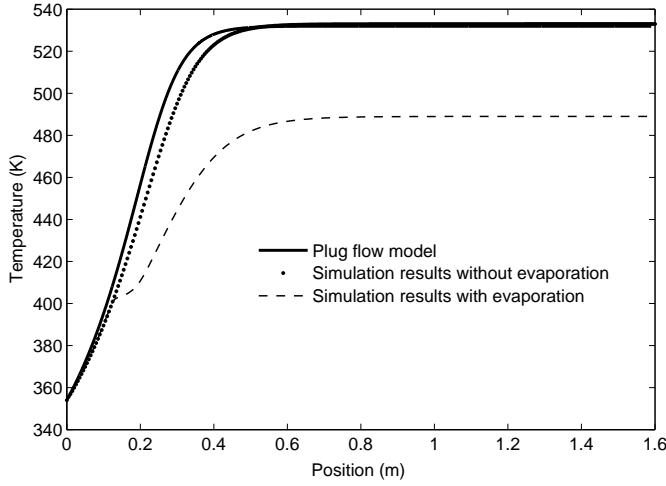


Figure 8.4: Temperature profile along the trickle bed reactor.

in case of evaporation is about 50 K less than the reactor without evaporation. The effect of evaporation on the temperature profile is very important in the investigation of hot spot formation because it consumes a lot of energy and can help reactor to stay away from formation of hot spots.

To estimate the temperature increase in the region where evaporation happens (0.15-0.20 m downstream the inlet of the reactor) we write an energy balance for the liquid phase in this region:

$$\dot{m}_l C_{p,l} (T_{l,0.2m} - T_{l,0.15m}) = \dot{m}_{C_6H_6} \Delta H_{evap} + \dot{m}_{C_6H_{14}} \Delta H_r \quad (8.23)$$

The mass flow rate of the liquid phase at the beginning of evaporation ($\dot{m}_{l,0.15m}$), mass flow rate of Benzene ($\dot{m}_{C_6H_6}$) in the liquid phase, mass flow rate of n-Hexane ($\dot{m}_{C_6H_{14}}$) in the liquid phase, the specific heat of liquid, the latent heat, the heat of reaction and $T_{l,0.15m}$ are 0.075 kg/s, 1.95×10^{-3} kg/s, 8.6×10^{-4} kg/s, 2030 J/kg K, 394164 J/kg, -145800 J/mol and 400 K, respectively. According to the equation 8.23, the temperature increases due to the reaction downstream the inlet (0.15-0.20 m) with about 4.5 K. The simulation results show a temperature increase of about 5 K.

8.4.4 Grid independence

We tested the grid dependency of our CFD simulations by using four different meshes. The meshes contain 2400, 9600, 38400 and 153600 (1 : 4 : 16 : 64) grid cells, respectively. Figure 8.5 shows the pressure drop of the bed at four different mesh resolutions. It can be seen that the difference of the calculated pressure drops from the last three meshes is rather small. So, the results are independent from the grid size. For our simulations we selected the mesh size of 9600 and we used this grid size for the research presented in this paper [10], [19].

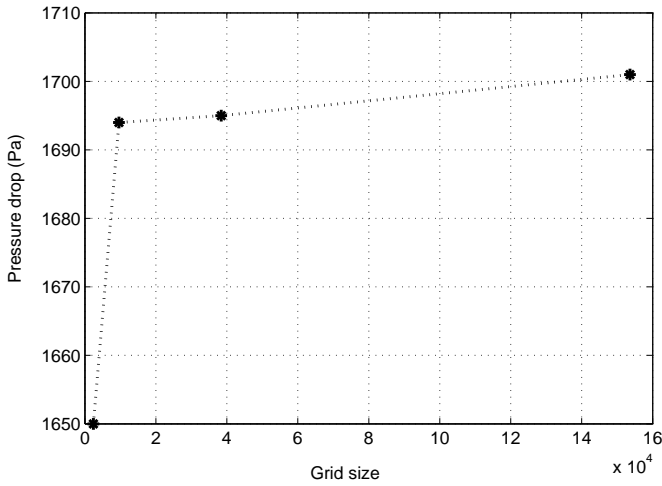


Figure 8.5: Pressure drop of the trickle bed reactor for various meshes.

8.5 CONCLUSIONS

In this work the operation of a trickle bed reactor with evaporation is studied using CFD. Evaporation affects the volume fraction and temperature profile along the reactor. The results show that the volume fraction of gas can increase very fast in the evaporative reactor. This increase of volume of the gas may result to an unsafe situation. In addition, when the volume fraction changes the concentration of species in the liquid and gas phase will change. These changes can affect the production rate of desired and undesired products.

The effect of evaporation on the temperature profile is very important in the investigation of formation of hot spots in trickle bed reactors. Evaporation is an endothermic process and can prevent hot spots formation due to the consumption of heat of reaction. On the other hand, evaporation can affect the production rate of desired or undesired products due to the temperature effect on reaction rate. The results show that for a trickle bed reactor the temperature of the reactor at the outlet can decrease too much in comparison with a normal condition without evaporation (in our case about 50K). For our case the evaporation rate is assumed to be very small. In case of higher evaporation rates the temperature and volume fraction changes would be much higher than the case with small evaporation rate. The developed CFD-based model provides knowledge that is often difficult to obtain with experiments. These CFD simulations provide very useful data of the temperature and volume fraction profile in trickle bed reactors with evaporation which can be used to improve the design and operation of trickle bed reactors. In addition, we are able to estimate the temperature changes due to the evaporation using the results of this work.

Acknowledgement

The authors would like to thank Shell Global Solutions International B.V, Amsterdam for the scientific and financial support.

NOMENCLATURE

ρ	density	kg/m^3
t	time	s
\vec{v}	velocity vector	m/s
P	pressure	Pa
τ	stress tensor	N/m^2
\vec{g}	gravitational acceleration vector	m/s^2
\vec{F}	force	N
μ	molecular viscosity	kg/ms
$\nabla \cdot \vec{v}_q$	effect of volume dilation	$1/s$
S_m	mass source	kg/m^3s
I	unit tensor	—
k	conductivity	W/mK
S_q	heat source	J/m^3s
Y_i	mass fraction of species i	—
\vec{J}_i	diffusion flux of species i	kg/m^2s
R_i	mass reaction rate of production of species i	kg/m^3s
$D_{i,mix}$	mass diffusion coefficient of species i	m^2/s
$D_{T,i}$	thermal diffusion coefficient of species i	m^2/s
$\hat{R}_{i,r}$	molar rate of reaction	mol/m^3s
M_W	molecular weight	gr/mol
\dot{m}	mass transfer rate	kg/m^3s
K	interphase momentum exchange coefficient	Ns/m
α	volume fraction	—
R	universal gas constant	$J/molK$
Q_{pq}	energy transfer between the phases	J/m^3s
\vec{v}_{pq}	interphase velocity	m/s
$Y_{p,i}$	mass fraction of species i in phase p	—
C	concentration	mol/m^3
f	drag function	—
τ_{par}	particulate relaxation time	s
L	latent heat	J/kg
d_p	particle diameter	m
C_D	drag coefficient	—
H	enthalpy	J/kg
\vec{q}_q	heat flux	W/m^2s

8. Normal operation and evaporation in a trickle bed

\mathbb{R}	heterogeneous reaction rate	$\text{mol}/\text{m}^3\text{s}$
T	temperature	K
$h_{c,pq}$	heat transfer coefficient between the phases	$\text{W}/\text{m}^2\text{K}$
d_s	solid phase diameter	m
τ_s	particulate relaxation time	s
Re	Reynolds number	—
Nu	Nusselt number	—
Pr	Prandtl number	—
Re_{sf}	Relative Reynolds of solid and fluid (gas or liquid)	—
Re_{gl}	Relative Reynolds of gas and liquid	—
β	accommodation coefficient	—
$coeff$	evaporation coefficient	$1/s$
$\dot{m}_{e \rightarrow v}$	evaporation rate	$\text{kg}/\text{m}^3\text{s}$
\dot{m}	mass flow rate	kg/s
C_p	specific heat	$\text{J}/\text{kg}\cdot\text{K}$

INDICES

p	phase p
q	phase q
pq	interaction between phase p and q
l	liquid phase
g	gas phase
s	solid phase
f	fluid
v	vapor
vm	virtual mass force
$lift$	lift force
m	mass source
h	heat source
i	species i
j	species j
mix	mixture
W	weight
H_2	Hydrogen
C_6H_{12}	Hexene
C_6H_{14}	Hexane
C_6H_6	Benzene
n	number of phases
exp	exponential factor
par	particulate relaxation time
dr	drag force
op	operating condition
cte	constant
sat	saturation temperature
r	reaction
$evap$	evaporation

8.6 Bibliography

- [1] Muthanna H. Al-Dahhan, Faical Larachi, Milorad P. Dudukovic, and Andre Laurent. High pressure trickle bed reactors : A review. *Ind. Eng. Chem. Res.*, 36:3292–3314, 1997.
- [2] Y. Jiang, M. Khadilkar, M. Al-Dahan, and M. Dudukovic. CFD modeling of multi-phase flow distribution in catalytic packed bed reactors: scale down issues. *Catalysis Today*, 66:209–218, 2001.
- [3] Y. Jiang, M. Khadilkar, M. Al-Dahan, and M. Dudukovic. CFD of multi-phase flow in packed-bed reactors: I. k-fluid modeling issues. *AIChE Journal*, 48:701–715, 2002.
- [4] R. Lopes and R. Quinta-Ferreira. Evaluation of multiphase CFD models in gas-liquid packed-bed reactors for water pollution abatement. *Chemical Engineering Science*, 65:291–297, 2010.
- [5] R. Lopes and R. Quinta-Ferreira. Trickle-bed CFD studies in the catalytic wet oxidation of phenolic acids. *Chemical Engineering Science*, 62:7045–7052, 2007.
- [6] R. Lopes and R. Quinta-Ferreira. Turbulence modeling of multiphase flow in high-pressure trickle-bed reactors. *Chemical Engineering Science*, 65:291–297, 2009.
- [7] P.R. Gunjal and V.V. Ranade. Modeling of laboratory and commercial scale hydro-processing reactors using CFD. *Chemical Engineering Science*, 62:5512–5526, 2007.
- [8] K. Lappalainen, M. Manninen, and V. Alopaeus. CFD modeling of radial spreading of flow in trickle-bed reactors due to mechanical and capillary dispersion. *Chemical Engineering Science*, 64:207–218, 2009.
- [9] F. Mousazadeh, H.E.A. van den Akker, and R.F. Mudde. Normal operation and hot spots formation in a trickle bed reactor. *Chemical Engineering Journal*, Submitted.
- [10] F. Mousazadeh, H.E.A. van den Akker, and R.F. Mudde. Eulerian simulation of heat transfer in a trickle bed reactor with constant wall temperature. *Chemical Engineering Journal*, 207-208:675–682, 2012.

- [11] FLUENT Incorporate, Natick, MA. *Fluent 12.06.016 Theory Guide*, 2009.
- [12] L. Schiller and Z. Naumann. A drag coefficient correlation. *Verein Deutscher Ingenieure*, 77:318, 1935.
- [13] D. Gidaspow, R. Bezburuah, and J. Ding. Hydrodynamics of circulating fluidized beds, kinetic theory approach. In *fluidization VII, Proceeding 7th Engineering foundation conference on fluidization*, 7:75–82, 1992.
- [14] C.Y. Wen and Y.H. Yu. Mechanics of fluidization. *Chemical engineering Progress Symposium Series*, 62:100–111, 1966.
- [15] S. Ergun. Fluid flow through packed columns. *Chem. Eng. Prog.*, 42:89–94, 1952.
- [16] T.B. Anderson and R. Jackson. A fluid mechanical description of fluidized beds. *I and EC Fundam*, 6:527–534, 1967.
- [17] R.M. Bowen. *Theory of mixtures*. 1976.
- [18] W.H. Lee. A pressure iteration scheme for two-phase modeling. *Technical Report, Los Alamos Scientific Laboratory, Los Alamos, New Mexico*, 79:975, 1979.
- [19] F. Mousazadeh, H.E.A. van den Akker, and R.F. Mudde. Direct numerical simulation of an exothermic gas-phase reaction in a packed bed with random particle distribution. *Chemical Engineering Science*, 100:259–265, 2013.

CONCLUSION

9.1 Review of the work

This thesis presents a Computational Fluid Dynamics (CFD) study of two-phase (gas-solid) packed bed reactors and three-phase (gas, liquid and solid) trickle bed reactors. We studied hot spots formation and important issues in the formation of hot spots such as radial heat transfer and evaporation in trickle beds using CFD. Two different methods, Direct Numerical Simulation (DNS) and the Eulerian-Eulerian multi-phase method were used in this research.

A two-phase packed bed reactor with a volumetric reaction in the gas phase was modeled. Fluid flow, the effect of the wall on the pressure drop, channeling and radial convection in two-phase packed bed reactors were investigated. We used two different configurations. This part of the project was performed using the DNS method.

A three-phase trickle flow reactor was modeled under normal flow condition with mass transfer from the gas to the liquid phase, an exothermic reaction in the liquid phase and heat transfer between the phases. Next, the performance of a trickle bed reactor with a local mal-distribution was investigated. Two different mal-distributed reactors were used for this purpose: a reactor with a local blockage and a reactor with diagonal barriers against flow. In addition, we investigated the operation of the modeled trickle bed reactor under normal flow condition with evaporation. This part of the project was performed using the Eulerian-Eulerian method.

To perform the above mentioned simulations, a commercial CFD code, Ansys Fluent, was used. All simulations were performed in a 2-D Cartesian or a 2-D Axi-symmetric geometry.

The thesis includes the following topics:

- Analysis of the fluid flow, pressure drop and channeling in 2-D packed bed reactors;
- Analysis of the radial convection in a two-phase packed bed reactor with an exothermic gas-phase reaction;
- Radial heat transfer in two-phase packed bed reactors and three-phase trickle bed reactors;
- Formation of hot spots in a trickle bed reactor with local mal-distribution;
- Effects of evaporation on the performance of a trickle bed reactor.

Chapters 1, 2 and 3 include the theoretical part of the project: Introduction, Multi-phase flow concepts and the Ansys Fluent model.

Chapter 4 reports DNS analysis of the fluid flow in 2-D packed bed reactors with cylindrical particles. The effects of particle distribution on the flow field, radial convection and channeling were investigated. In addition, the effects of the wall on the pressure drop and velocity distribution were investigated.

We used two different configurations of particles. The first one is a (almost) linear configuration of non-overlapping cylindrical particles arranged on a regular square lattice with random position perturbation. The second one is a configuration with more random distribution of particles than the first one. The axial velocity profile inside the packed bed shows that the velocity distribution is a function of the porosity and arrangement of particles. In the regions where the porosity is higher, the local velocity is also higher in comparison with the regions with lower porosity. In the regions with low porosity, velocities lower than the inlet velocity were observed. In the regions with high porosity, velocities even 2-10 times larger than the inlet velocity were observed because of the channeling in the reactor. Channeling may exist in packed beds near the wall as well as in the bulk, depending on the arrangement of the particles and the porosity distribution. The length of channels are very different in these two configurations. For a packed bed with more random configuration of particles, channels are 20-30% of the length of the reactor. For a packed bed with (almost) linear configuration of particles the length of channels are 2-3 times larger than the packed bed with more random configuration of particles. Wall effects are important in the design and optimization of packed beds. They have a significant effect on the pressure drop of the bed. According to the results of the simulations, for our geometry, walls increase the pressure drop of packed beds by about 20-25%. Therefore, in the investigation of the hydrodynamics of packed

beds, walls should be taken into account.

Chapter 5 focuses on the simulation of an exothermic gas phase reaction in a two-phase (gas-solid) packed bed reactor to investigate the effects of particle distribution on the radial heat transfer. We used the DNS method in this part of the research. In the case we have investigated, there is a region in the reactor with high reaction rate where basically all heat is produced. A large temperature gradient was observed in this region in the radial direction. The temperature difference between the wall and the bulk of the bed in this region is about 100 K . Such a temperature gradient is quite large for a small length (width of the reactor is 38 mm). In the other parts of the reactor there is no temperature gradient in the radial direction. The high temperature gradient in the radial direction shows that convection in the radial direction is rather small in the modeled packed bed. This rather small convection in the radial direction is the result of the (almost) linear arrangement of the particles. The fluid mainly flows in channels and does not convect very well in the radial direction. This arrangement is not an ideal particle distribution for a packed bed. According to our results, more random distribution of particles shows higher radial convection. Radial convection is an important issue in the design and performance of packed beds. So, the particles should be distributed randomly in DNS simulations to have results closer to the real packed beds in the industry.

Chapter 6 reports a CFD study of steady-state heat transfer of gas and liquid flowing through a two-phase (gas-solid) packed bed and three-phase (gas, liquid and solid) trickle bed reactor. Spherical particles of 2.06 mm are used and the temperatures of the walls are constant. We focused on the radial heat transfer of two-phase packed bed reactors and three-phase trickle bed reactors. The effects of gas and liquid flow rates on the radial heat transfer were investigated. We used the Eulerian-Eulerian multi-phase approach in this part of the research.

The mechanism of heat transfer inside trickle beds are: conduction through the particles, conduction through contact surfaces of two particles, conduction through the fluid film near the contact surface of two particles, convection in fluids and radial mixing of fluids. Heat transfer in trickle beds can be conventionally expressed by the concept of an effective radial bed conductivity which is based on the assumption that on a macroscale, the bed can be described as a continuum. This parameter comprises of all above mentioned heat transfer mechanisms. Heat transfer in the radial direction in two-phase packed beds increases if we increase the mass flux of the gas. In case of a trickle bed, the effective radial bed conductivity is a function of both gas and liquid mass fluxes but the effect of the liquid flow is much more significant than the gas flow because of the higher conductivity of the liquid than of the gas. To increase the radial conductivity of the bed in a plug flow trickle bed we

considered the conductivity of the flowing gas and liquid as a function of Reynolds and Prandtl number according to the equation $k_{fluid} = k_f + 0.10k_f Re_p Pr_f$. As mentioned, we used the Eulerian-Eulerian multi-phase approach in this part. In this method, the mass, momentum and energy conservation equations are solved based on an averaging method. So, we added $0.10k_f Re_p Pr_f$ as the dynamic part of the conductivity for both gas and liquid phases to increase the conductivity in the radial direction to have more realistic results. According to the simulation results the effective radial bed conductivities for two-phase (gas-solid) and three-phase (gas, liquid and solid) flow reactors are in the range of 0.3-1.2 and 1.5-4.0 $W/m.K$ depending on the velocity of the liquid and gas phases. In trickle flow regime, the effective radial conductivity of the bed is 2-5 times higher than the dry gas flow system and if the superficial velocity of the liquid is higher the effective radial bed conductivity is larger. In the trickle flow regime an increase of the liquid flow rate is an effective way to increase the heat transfer rate in the radial direction.

The results help us to have the radial heat transfer of trickle beds as plug flow reactors from the modelings closer to the real industrial trickle beds. So, the results are applicable for a full model of a trickle bed reactor. These results were validated with experiments and they are quite reliable.

In chapter 7, the performance of a trickle bed reactor under normal flow condition (plug flow regime) and with local mal-distribution was discussed. We investigated the thermal performance of a trickle bed reactor under both normal flow condition and with a local mal-distribution. We used two different configurations to make a local mal-distribution in the reactor: a reactor with a blocked cup-like region and a reactor with diagonal barriers against flow.

A hot spot is observed in the trickle flow reactor with a local blockage which prevents fluid from flowing downstream the reactor. The hot spot is located at the top of the blocked area. The size of the hot spot is not more than the size of several particles. Liquid is trapped in this area (the density of the liquid is much higher than of the gas) and cannot convect along the reactor nor in the radial direction. The only way through which heat can transfer out of the blocked area is conduction through all phases. But the rate of heat production is very high and the heat cannot transfer easily out of this area with only conduction. Hence, a hot spot is formed. We estimated the temperature difference between the hot spot and surrounding regions by the assumption that the heat transfers out of the hot area via conduction in the solid and liquid phases. We do not take into account the gas phase because of the much lower conductivity of the gas than the liquid and solid. In addition, there is no gas in the blocked area in the modeled trickle bed. A simple energy balance for the blocked area can be written by using parallel or serial channel models (see

chapter 7). The temperature difference between the hot spot and surrounding regions according to the energy balance for parallel and serial models is 117 K and 136 K , respectively. From the simulation results the temperature difference between the hot spot and surrounding regions is 120 K .

In the other case with diagonal barriers against flow, hot spots are not observed. In this case, the gas phase fills the back of the barriers (the density of gas is lower than the liquid and it can move easier in the radial direction). So, there is no liquid in this area and therefore no reaction. Consequently, there is no hot spot in the mal-distributed area.

In the reactor with the diagonal barriers beside the walls, gas fills the area in the back of barriers and beside the walls. Therefore, diagonal barriers can be used in trickle beds to prevent channeling of the liquid beside the walls. This is an advantage of using these barriers in trickle beds. In addition, these barriers can improve radial dispersion in trickle beds because they force liquid and gas to move in the radial direction. Using these barriers inside the trickle beds may help to prevent formation of hot spots.

The final conclusion is that when the liquid is trapped in a blockage we observe hot spots. If the liquid can convect in the radial and axial direction hot spots are not expected to form. In general, we think that trickle bed reactors have the potential of hot spots formation in the case of local blockage against flow. For the formation of local hot spots, liquid needs to be trapped. Figure 9.1 shows a hot spot in a trickle bed reactor with a local blockage.

Performance of a trickle bed reactor with evaporation is discussed in chapter 8. The effect of evaporation on the temperature and volume fraction profile along the reactor is discussed in detail. From the simulation results, we find that the temperature at the outlet of the normal reactor is about 50 K higher than that of the reactor with evaporation. Evaporation is an endothermic process and can help to prevent formation of hot spots in trickle beds due to the consumption of heat of reaction. On the other hand, it can affect the production rate of desired and undesired species due to the effect on the volume fraction of the liquid and gas phases and consequently the concentration of species in these phases. Production of a specific species and rate of production of that are important in the operation of trickle bed reactors. The effect of evaporation on the concentration of species can be as important as the effect on the temperature profile depending on what the target is: production or temperature control. Therefore, it is recommended to use the evaporation process as a tool in trickle beds to protect them from formation of hot spots if the temperature control is more important than the production.

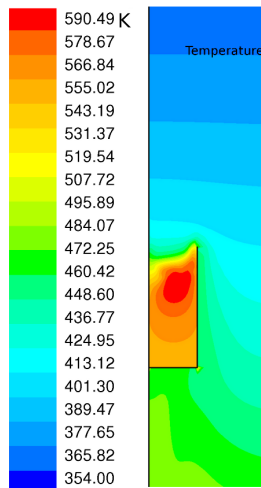


Figure 9.1: A hot spot in a trickle bed reactor with a local blockage.

9.2 Recommendations for future work

Considering the limitations and capability of the numerical code used in this project, computation time, mesh generation and complexity of the modeling of trickle beds some works are recommended.

For the case of the DNS research, it is recommended to perform two-phase (gas-solid) simulations with a catalytic reaction on the surface of the solid instead of a reaction in the gas phase. In the case of a catalytic reaction, the results of the CFD simulations will be much closer to the real industrial gas-solid packed bed reactors. In addition, we recommend to perform a three-phase (gas, liquid and solid) trickle bed reactor modeling with reaction using the real geometry of a trickle bed and DNS method. In this case, it is also recommended to model a catalytic reaction instead of a reaction in the bulk of the gas phase. It can be challenging but the results can be very valuable and useful for understanding of trickle beds.

In addition, we recommend to perform simulations with the DNS method focusing on the heat transfer between the fluid or fluids (in case of gas-liquid flow) and the particles. In this case, we can learn more about the heat transfer process in these beds.

For the case of the Eulerian-Eulerian simulations, it is highly recommended to model a trickle bed reactor with mal-distribution by implementing evaporation in

the regions where hot spots were observed. In this case, the effect of evaporation on the formation of hot spots can be investigated. In addition, we may understand how evaporation can help to control hot spots.

In the trickle bed model with evaporation, a constant boiling point was defined for the evaporation and only one species evaporates. We recommend to perform new simulations with more than one evaporative species and variable boiling point (for example, boiling point as a function of pressure) to make the model closer to the trickle bed reactors which are in operation in the industry.

In general, in trickle bed reactors, there is more than one reaction in the system. It is computationally expensive to model a lot of reactions running in a trickle bed reactor. It is recommended to perform modeling with more than one reaction with different rates of reaction. In this case, it will be possible to investigate the effects of evaporation on the species distribution in the reactor.

List of Publications

F. Mousazadeh and H. E. A. van den Akker and R. F. Mudde. Eulerian simulation of heat transfer in a trickle bed reactor with constant wall temperature. Published in *Chemical Engineering Journal*, 207-208: 675–682, 2012.

F. Mousazadeh and H. E. A. van den Akker and R. F. Mudde. Direct numerical simulation of an exothermic gas-phase reaction in a packed bed with random particle distribution. Published in *Chemical Engineering Science*, 100: 259-265, 2013.

F. Mousazadeh and H. E. A. van den Akker and D. Ambesi and R. F. Mudde. CFD-based analysis of fluid flow in a 2-D packed bed reactor with random particle distribution. In: *Proceedings of the 8th International Conference on Multi-phase Flow*, 26-31 May 2013, Jeju, Korea.

F. Mousazadeh and H. E. A. van den Akker and R. F. Mudde. Normal operation and hot spots formation in a trickle bed reactor. Submitted to *Chemical Engineering Journal*.

F. Mousazadeh and H. E. A. van den Akker and R. F. Mudde. Normal operation and evaporation in a trickle bed reactor. Submitted to *Chemical Engineering Journal*.

Acknowledgement

I would like to thank the members of the thesis committee Prof.dr.ir. Jos Derksen, Prof.dr.ir. Sankaran Sundaresan, Prof.dr.D.J.E.M. Roekaerts, Dr.B.I.M. ten Bosch and Prof.dr.ir.M.T. Kreutzer.

I would like to thank my supervisors Rob and Harry. Rob, thank you very much for giving me the opportunity to do my PhD research at Delft University of Technology under your supervision. Thank you for all support during my PhD. I learned a lot from you as a teacher of Physics and English language. You really helped me to improve my writing skills in English. I learned step by step from you how to do research in a proper and effective way. Moreover, your criticism on making presentations and writing articles was helpful for me. I really appreciate your help. I improved my presentation skills under your supervision. Harry, you helped me with planning for the PhD period step by step. In addition, you made me familiar with the projects running in Shell and the way of dealing with that. Thank you very much for useful recommendations and advice.

I am thankful to Dr. Ed Ouwerkerk, Dr.B.I.M. ten Bosch and Dr. Sami Sapmaz from Shell Global Solutions, Amsterdam for their insightful ideas and recommendations. I would like to thank Dr. Benoit Witkamp in particular, for all time that we spent together discussing about the project.

I also thank all the members of Transport Phenomena Group of the Department of Chemical Engineering, Delft University of Technology. Davide, thank you very much for helping me in learning software such as Fluent, Gambit and LaTeX. Federico, thanks a lot for making the office happier and much more efficient. I would like to thank Mohammad, Usama, Anton, Duong, Xiaogang, Dries, Bernhard, Laurens, Wenjie, David, Rudi, Galileu, Hamid, Niels, Rajat, Milos, Reza, Annekatrien, Michiel, Heleen, Ozgur and Adrian. My special thanks goes for Koen for the translation of the 'Summary' of my thesis into Dutch. I would like to thank the secretaries of MSP and TP Groups, Amanda, Angela, Anita and Fiona.

I would like also to thank my professors at Amirkabir University of Technology (Tehran Polytechnic) specially Prof. dr. T. Kaghazchi, Prof. dr. M. Sohrabi and my M.Sc supervisor Prof. dr. Rashidi. I would like to thank all my teachers at high school specially Mr Asgharifar and Abolhasanian.

I am thankful to my friends from high school, Taher, Mehrdad and Yousef. Many thanks goes to Elham, Milad, Mohsen and Bahareh, Ali and Elaheh, Sepideh and Ammar, Goodarz and Semiramis, Kathy, Hanieh, Farid, Naghmeh and Babak, Sepideh and Hamed, Sogol and Stephan, Ayleen and Peter, Stephan and Veronica,

Mahnoush and Mojtaba, Mojgan and Mehrdad, Negar and Roozbeh, Seyran and Nader, Sadegh and Sanaz, Ali, Sepideh Babayi and Sina. In addition, my special thanks goes to Farzad Farshbaf and Rouhi for all supports during my PhD.

At the end, I would like to thank my family and in-laws for all their supports. My dear dad, thank you for teaching me all the time during school time and after that. Thanks for all supports during my study and living far from family. Mom, I really love you and I would like to thank you for all supports and helps. My bigger brother, Farrokh, thank you very much for encouraging and pushing me to do a PhD. My baby brother, Hamed, thanks a lot for love and also introduction of old fashioned cars to me. My lovely Nasim thank you very much for all supports during my PhD. You are my love and will be my love forever.

My lovely grandmother! I lived with you for almost eight years. You left me when I was a M.Sc student. You could not even read and write but you encouraged me and supported me to study more and more. I learned a lot from you. You will be in my heart forever.

Curriculum Vitae

Farzad Mousazadeh was born on 21st April, 1979 in Ardebil, Azerbaijan province, Iran. He got his high school diploma in mathematics and physics in the Sama high School in Ardebil. Then he moved to Tehran. He got his B.Sc and M.Sc in Chemical Engineering from Amirkabir University of Technology (Tehran Polytechnic). He got his M.Sc in 2005. He worked for couple of years as a technical engineer and process engineer in Petrochemical Down Stream Industries Development Company (PDSID) and Hirbodan EPC Company in Tehran. Then he moved to the Netherlands in October 2008. He started his Ph.D in April 2009, in Transport Phenomena Group, Department of Chemical Engineering, Delft University of Technology. He started his new career in March 2013 at Yokogawa Europe Solutions B.V. in the Netherlands.

